Marine and Petroleum Geology 159 (2024) 106566

Contents lists available at ScienceDirect

Marine and Petroleum Geology

journal homepage: www.elsevier.com/locate/marpetgeo

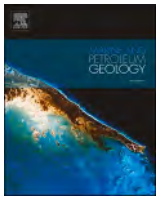

Detrital zircon geochronology and provenance of Cenozoic deposits in the Qaidam basin, northern Tibetan plateau: An overview with new data, implications and perspectives

Xing Jian [a,*], Ping Guan [b], Ling Fu [c], Wei Zhang [a], Xiaotian Shen [a], Hanjing Fu [a], Ling Wang [a]

[a] State Key Laboratory of Marine Environmental Science, College of Ocean and Earth Sciences, Xiamen University, Xiamen, 361102, PR China
[b] MOE Key Laboratory of Orogenic Belts and Crustal Evolution, School of Earth and Space Sciences, Peking University, Beijing, 100871, PR China
[c] Research Institute of Petroleum Exploration and Development (RIPED), PetroChina, Beijing, 100083, PR China

ARTICLE INFO

Keywords:
Detrital zircon geochronology
Sedimentary provenance analysis
Qaidam basin
Tibetan plateau
Tectonic and climatic controls

ABSTRACT

An increasing number of detrital zircon U–Pb geochronological data have been reported to trace sediment provenance for the Cenozoic Qaidam basin, which is crucial to understanding crustal deformation, paleoclimate change and basin development in northern Tibetan Plateau and to assessing geodynamic models of plateau growth. However, the existing provenance interpretations are highly diverse and how the northern Tibet has evolved remains controversial. This contribution presents new detrital zircon dating results from Cenozoic outcrop and borehole samples and compiles published data from the whole Qaidam basin, adjacent small Cenozoic basins and the surrounding mountains. Our new synthesis indicates that, Paleoproterozoic signals (1800–2000 Ma and 2350–2500 Ma), rather than the Permian–Triassic ages, can be applied effectively to distinguish the Qilian, Altun and Eastern Kunlun-sourced detrital zircons. The Cenozoic Qaidam basin exhibits spatiotemporally variable detrital zircon age populations. Most sandstones from the western and southern basin are characterized by Phanerozoic bimodal age spectra (i.e., 400–480 Ma and 220–280 Ma) with minor Precambrian signals, indicating major contributions from the neighboring Altun and Eastern Kunlun ranges. By contrast, almost all the northern and eastern basin sandstones display prominent early Paleozoic detrital zircon ages; but Paleoproterozoic, Neoproterozoic (750–950 Ma) and Permian–Triassic signals only appear as dominant age clusters in some samples. Different temporal variation trends are observed from the investigated sections in this region, revealing variable zircon supply from different micro-terranes in the Qilian Mountains. This implies that using detrital zircon provenance data from a single section or from a local area of the Qaidam basin to address regional tectonic and climatic issues of the northern Tibetan Plateau unlikely provide useful results. We propose that the Cenozoic Qaidam basin deposits were derived from localized, adjacent source regions, rather than cross-basinal, distant mountains. Our conclusions support models with synchronous deformation throughout most of northern Tibet in the Cenozoic. The observed spatiotemporal variations in detrital zircon populations are not only attributed to tectonic deformation-induced source changes, but can also be due to heterogeneity of the source terranes (e.g., durability and zircon fertility) and variable factors (e.g., hydrodynamic sorting, recycling and sedimentary microenvironment) in transport-deposition processes. This study also highlights the importance of involving detrital zircon textural and sedimentological parameters to zircon provenance interpretations. An integrated provenance analysis combining other detritus components is helpful to comprehensively characterize source-to-sink systems for sedimentary basins.

1. Introduction

Zircon is highly refractory at the Earth's surface and occurs in virtually all clastic sedimentary systems. Detrital zircon grains from sedimentary records have proven to preserve crucial information about a wide range of geological processes and thus serve as an essential mineral in geoscience research (e.g., Fedo et al., 2003; Perri et al., 2008; Cawood et al., 2013; Gehrels, 2014; McKenzie et al., 2016; Tang et al.,

* Corresponding author.
E-mail address: xjian@xmu.edu.cn (X. Jian).

https://doi.org/10.1016/j.marpetgeo.2023.106566
Received 22 August 2023; Received in revised form 16 October 2023; Accepted 19 October 2023
Available online 23 October 2023

2021; Fornelli et al., 2022). The developed in-situ mass-spectrometric techniques, such as secondary ion mass spectrometry (SIMS) and laser-ablation inductively coupled plasma mass spectrometry (LA-ICP-MS), provide powerful analysis platforms to obtain single detrital zircon ages with reasonable precision, accuracy and efficiency (Košler et al., 2002; Ireland and Williams, 2003; Gehrels et al., 2006). In general, detrital zircon U–Pb ages may provide valuable clues on source history of a deposit and, in many cases, also provide crucial clues on their depositional ages, which must be always younger than the age of the youngest zircon grain. As a result, detrital zircon geochronology has become a potent tool in sediment provenance studies and in maximum depositional age estimation for ancient sedimentary strata (Dickinson and Gehrels, 2009; Thomas, 2011; Cawood et al., 2012; Coutts et al., 2019; Copeland, 2020; Jian et al., 2020). Furthermore, detrital zircon U–Pb ages, in combination with element geochemical tracers (e.g., rare earth elements or other trace elements), isotopic tracers (e.g., Hf and O isotopes) or thermochronology (e.g., fission track and (U–Th)/He dating), can also be used to address a variety of other geoscience issues, for example, sediment dispersal patterns and paleogeography (Sharman et al., 2015; Xu et al., 2017; Stalder et al., 2018; Jian et al., 2019a), tectonic evolution of mountain belts and sedimentary basins (Lease et al., 2007; Carrapa, 2010; Saylor et al., 2012), paleoclimatic history (Soreghan et al., 2002; Pullen et al., 2011; McKenzie et al., 2016) and crustal evolution processes (Griffin et al., 2006; Cawood et al., 2013; Lancaster et al., 2011; Tang et al., 2021).

The detrital zircon geochronological technique has been widely applied in Tibetan Plateau geological studies. The Tibetan Plateau (Fig. 1), as the world's highest and most extensive plateau, has long been considered as an ideal test ground for understanding the geodynamic processes of continental convergence, collision and deformation, and the interactions between plateau topography and global climate change (Molnar et al., 1993; Tapponnier et al., 2001; Kapp and DeCelles, 2019; Ding et al., 2022). Vast amounts of detrital zircon age data from modern sediments, sedimentary rocks and metasedimentary rocks in this region have been published over the past few decades. Those data are mainly involved in discussing the following topics, 1) origin and early evolution of the continental blocks (Fig. 1B), which made up the plateau (e.g., Gehrels et al., 2003; Leier et al., 2007; Dong et al., 2011; Zhu et al., 2011; Jian et al., 2020); 2) assembly processes of the blocks and related tectono-magmatic evolution of the orogenic belts among the blocks (e.g., Pullen et al., 2008; Gehrels et al., 2011; Zuza et al., 2018; Wu et al., 2019a; Zhang et al., 2021); and 3) sediment provenance and infilling processes of Mesozoic–Cenozoic sedimentary basins on the plateau and associated tectonic deformation and unroofing history of these detritus source terranes (Weislogel et al., 2006; Kapp et al., 2007; Ding et al., 2013; Decelles et al., 2014; Orme et al., 2015; Jian et al., 2019a; Cheng et al., 2021).

However, how the Tibetan plateau deformed and grew remains controversial and several models have been proposed to interpret the geodynamic mechanism of plateau growth. These models mainly include simple crustal thickening (Argand, 1922), convective removal of mantle lithosphere (Houseman and England, 1993), lower crustal flow (Royden et al., 1997), northward stepwise development (Tapponnier et al., 2001) and outward growth of a central "proto-Tibetan Plateau" (Wang et al., 2008a). Although the India-Eurasia collision at 50–55 Ma (and subsequent convergence) was probably not the only forcing for Tibetan crust deformation (Kapp and DeCelles, 2019 and reference therein), it created the south boundary of the plateau and played an important role in forming the current tectonic framework and high topography. The northern Tibet is 1500–2000 km away from the collisional zone (Fig. 1B). Since these proposed geodynamic mechanisms predict distinct growth patterns for the northern Tibet, this region acts as a critical research target to test these models. Numerous Cenozoic intermontane basins have developed in the northern Tibetan Plateau (Fig. 1C). Sedimentary successions in these basins are thought to preserve records of geological evolution for both the basins and the high-relief mountains (Zhuang et al., 2011; Yuan et al., 2013; Wang et al., 2016; Wu et al., 2019b; Cheng et al., 2021). Detrital zircon geochronological studies on siliciclastic sedimentary strata from those intermontane basins are expected to be helpful for better understanding of the basin-range systems and thus allow reconstructing crustal deformation and uplift history of the northern Tibetan Plateau.

2. Detrital zircon U–Pb age data-based provenance of the Cenozoic Qaidam basin: under debate

The Qaidam basin is the largest intermontane basin in northern Tibet and is currently bounded by the Qilian Mountains, Altun and Eastern Kunlun Ranges (Fig. 1). The extensive clastic sedimentary rocks within the basin may serve as pivotal, effective targets to unravel uplift and unroofing processes of the surrounding ranges (Zhuang et al., 2011; Guan and Jian, 2013; Cheng et al., 2021). Extensive detrital zircon U–Pb age data have been reported for the Cenozoic Qaidam basin in recent years (Pullen et al., 2011; Bush et al., 2016; Cheng et al., 2016a, 2016b, 2019a,b; Wang et al., 2017, 2020, 2022; Zhu et al., 2017; Zhou et al., 2018; McRivette et al., 2019; Song et al., 2019; Wu et al., 2019b; Zhuang et al., 2019; Li et al., 2021b; Xia et al., 2021; Lu et al., 2022). However, these research groups provided dissimilar provenance interpretations based on their own detrital zircon age data and proposed distinct models for uplift and growth processes of the ranges. Even for samples from the same outcrop section (e.g., the Huaitoutala section, Fig. 1C; Bush et al., 2016; Zhuang et al., 2019; Li et al., 2021b) or sections that are close to each other (e.g., the Honggou section; Bush et al., 2016; Wang et al., 2017; and the Dahonggou section; Song et al., 2019; about 5 km apart), the obtained detrital zircon age data were distinct and diverse explanations were provided.

One of the popular viewpoints advocates that the Qilian Mountains are characterized as an early Paleozoic orogenic belt, whereas the Eastern Kunlun Range successively experienced early Paleozoic and Permian–Triassic tectono-magmatic processes. Under the circumstances, comparatively high proportions of Permian–Triassic ages in the detrital zircon age populations were thus considered to represent detritus contributions by the unroofing of the Eastern Kunlun Range (e.g., Bush et al., 2016; Wang et al., 2017). Another viewpoint favors that the Permian–Triassic age signatures cannot be ignored for the Qilian Mountains and for the crystalline basement of the Qaidam basin (Cheng et al., 2017; Song et al., 2019; Zhang et al., 2021). Thus, the occurrence of abundant detrital zircon grains with Permian–Triassic ages in the Cenozoic Qaidam basin was not necessary to be interpreted as major contributions from the Eastern Kunlun Range (Cheng et al., 2019b; Song et al., 2019; Zhuang et al., 2019; Jian et al., 2023). Furthermore, recycling of pre-Cenozoic sedimentary strata was also considered as a non-negligible source for detrital zircons in the basin (Lu et al., 2018, 2022). Therefore, we suggest that more detailed, elaborative work is required to better understand the tectono-magmatic history and zircon U–Pb age signatures of the potential source terranes. Basin-wide detrital zircon comparative analysis and more deeper explanations are also important to unravel sediment provenance of the Cenozoic Qaidam basin and to rationally evaluate plateau growth models.

We note that the major controversy occurs in sediment provenance interpretations for the northern and eastern Qaidam basin and the reported detrital zircon samples therein are mainly collected from outcrop sections along the north margin of the basin. Here, we report new detrital zircon U–Pb age data for both outcrop and borehole samples (12 sandstone samples in total) from the northern and eastern Qaidam basin and compile published age data of the Cenozoic strata from the entire basin (119 samples). The aims are 1) to have an overview of Cenozoic spatial and temporal distributions of detrital zircon records in the Qaidam basin, 2) to discuss potential controls on detrital zircon populations and related influences on provenance interpretations, and 3) to better understand provenance implications for the Cenozoic tectonic and climatic evolution of the northern Tibetan Plateau.

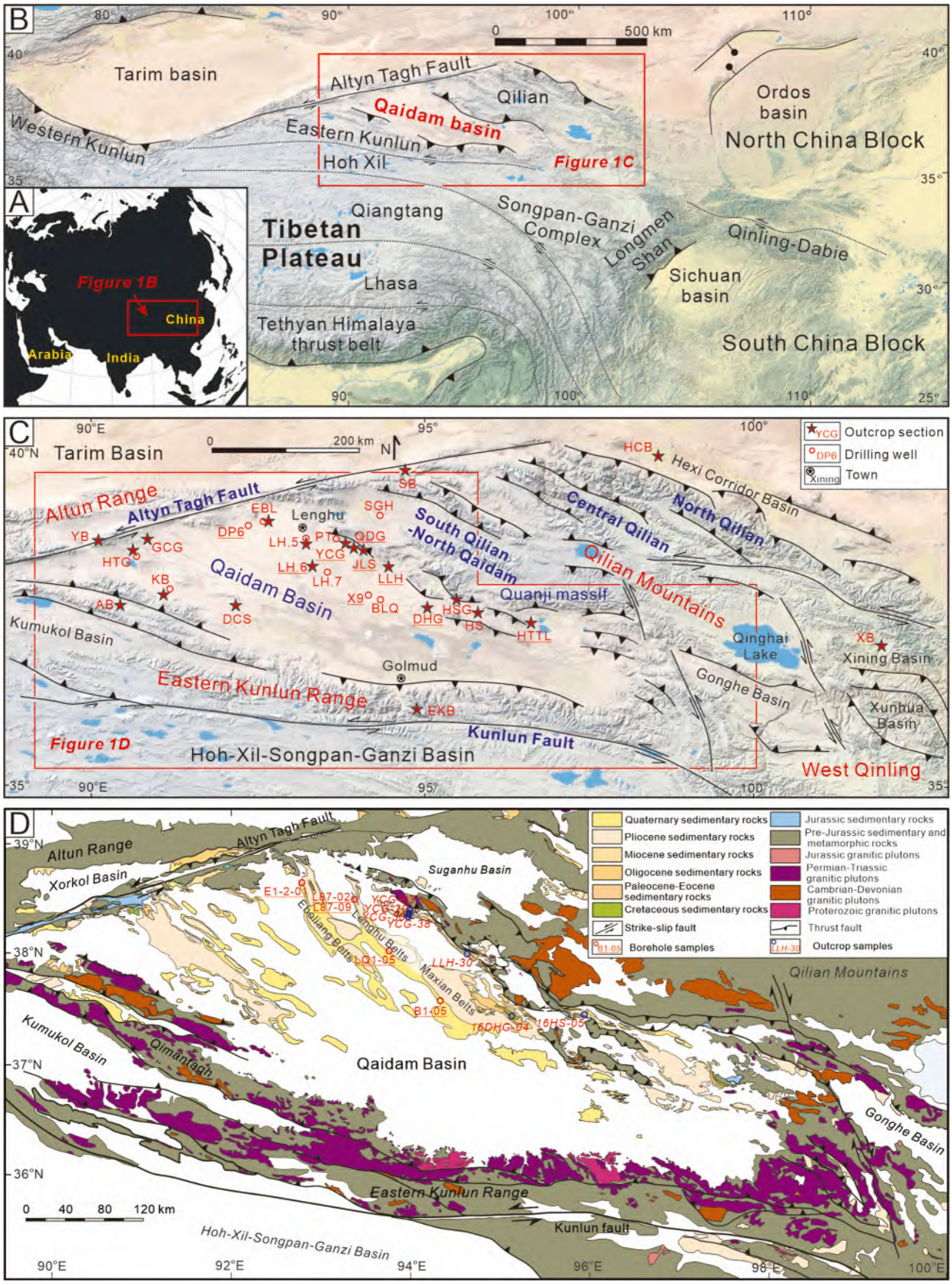

(caption on next page)

Fig. 1. (A) Location of the Tibetan Plateau on the Asia continent. (B) Background of the Tibetan Plateau and its surrounding regions. (C) A map of the northern Tibetan Plateau showing locations of the Qaidam basin and surrounding tectonic elements (modified from Jian et al. (2018, 2019b)). The red circles (borehole) and stars (outcrop) indicate the locations of previously reported and new detrital zircon samples (Cenozoic, including the Qaidam basin and the surrounding intermountain basins) and the locations of photos in Figs. 3 and 4 (underlined). (D) A geologic map of the Qaidam basin and the surrounding mountains (modified from Lu et al. (2018)) and sample locations in this study. HTTL: Huaitoutala section; HS: Hongshan section; HSG: Hongshangou section; DHG: Dahonggou section; BLQ: Beilingqiu region; *X*9: well *X*9; LLH: Lulehe section; JLS: Jielvsu section; QDG: Quandonggou section; YCG: Yingchaogou section; PT: Pingtai region; LH.5: No. 5 Lenghu; LH.6: No. 6 Lenghu; LH.7: No. 7 Lenghu; EBL: Eboliang region; DP6: well DP6; GCG: Ganchaigou region; HTG: Huatugou region; KB: Kunbei region; DCS: Dongchaishan region; EKB: a Neogene intermountain basin within the Eastern Kunlun Range; AB: Adatan basin; YB: Yitunbulake basin; SB: Subei basin; HCB: Hexi Corridor basin; XB: Xining basin.

3. Geological setting

3.1. Major tectonic elements in the northern Tibetan plateau

The Tibetan Plateau has extremely high elevation (~5 km above sea level), exceptional crustal thickness (~70 km) and wide lateral extent (~3 million km^2). Although formation and uplift of the plateau is thought to be closely related to the Cenozoic India-Eurasia collision, its geological framework and initial growth were fundamentally a result of multiple, previous ocean closure and intercontinental suturing events (Yin and Harrison, 2000; Gehrels et al., 2011; Kapp and DeCelles, 2019). The northern Tibetan Plateau has a unique, complex range-basin system which includes Qilian Mountains, Altun, Eastern Kunlun and West Qinling ranges, Hoh-Xil-Songpan-Ganzi basin, Qaidam basin and other mesoscale–small intermontane basins (Fig. 1C).

The Qilian Mountains represent as a ca. 300 km-wide fold-thrust belt (Zuza et al., 2018; Zhang et al., 2021) that forms the northernmost high topography of the Tibetan Plateau. From north to south, the Qilian Mountains involve the following tectonic domains: 1) southern margin of the North China Block, including Neoproterozoic passive-margin sedimentary strata; 2) the North Qilian suture, as a belt with discontinuously exposed ophiolitic materials that locally experienced blue schist-facies metamorphism; 3) the Central Qilian basement, with widespread Proterozoic metasedimentary sequences (mainly including quartzite, marble and schist); 4) the South Qilian-North Qaidam metamorphic belts, including the South Qilian suture, a belt of variably exposed ophiolite fragments that do not record high-grade metamorphism, a wide zone of arc volcanic and plutonic rocks associated with the Qilian arc which respectively overlie and intrude amphibolite-grade metamorphic rocks and the North Qaidam ultrahigh pressure metamorphic belt, with associated ophiolite complex (Gehrels et al., 2003; Zuza et al., 2018 and references therein). The Qilian orogen has an early–mid Neoproterozoic age-dominated basement, which was likely involved in the Grenvillian orogenesis during the assembly and subsequent breakup process of the Rodinia supercontinent (Song et al., 2012; Yu et al., 2013; Jian et al., 2020). The Qilian Mountains are thought to document the tectonic history of the Paleo-Qilian Ocean (as a part of the Proto-Tethys Ocean) and the ultimate collision and amalgamation processes of related micro-continents (e.g., the Central Qilian, Quanji and Kunlun-Qaidam blocks) during the Cambrian to Devonian (400–520 Ma) (Zuza et al., 2018; Zhang et al., 2021 and references therein). Some Permian–Triassic (230–280 Ma) plutons are exposed in South Qilian and North Qaidam regions and these rocks are interpreted to be related to the low-angle, northward Paleo-Tethys subduction during that time (e.g., Wu et al., 2016; Cheng et al., 2017; Jian et al., 2020; Zhang et al., 2021).

The Altun Range is mainly created by the Altyn Tagh Fault, which is an active left-lateral strike-slip fault with a cumulative offset of ca. 375 km (Gehrels et al., 2003; Yue et al., 2004). This fault cuts the Kunlun orogen into the Western Kunlun and Eastern Kunlun ranges and separates the Qaidam basin from the Tarim basin (Fig. 1). The strike-slip movement was accommodated out of the Tibetan Plateau, rather than within the plateau (Gehrels et al., 2003; Yue et al., 2004; Jian et al., 2018; Zhuang et al., 2018). The north part of the Altyn Tagh Fault is thought to have rock assemblages that are similar to those in the Qilian Mountains (Gehrels et al., 2003). Pre-Cenozoic bedrocks in the south part of the fault are relatively rare, discontinuously exposed and can be considered as basement rocks of the west margin of the Cenozoic Qaidam basin.

The Eastern Kunlun Range appears as a ca. 1000 km-long, latitudinally-trending and granitoid-rich belt (Fig. 1; Wu et al., 2019a; Jian et al., 2020). The Eastern Kunlun orogenic belt contains a highly metamorphosed and deformed Precambrian basement (similar Precambrian tectonic history to the Central Qilian block) and is dominantly composed of Ordovician–Devonian plutons, Permian to Triassic arc sequences, Paleozoic marine sedimentary successions and sporadically distributed Jurassic and Cenozoic non-marine rocks (Li et al., 2013; Wu et al., 2019a; Jian et al., 2020). It subsequently experienced tectono-magmatic events and sedimentary filling history related to the successive closure of the Proto-Tethys and Paleo-Tethys Oceans during the Cambrian–Triassic (Li et al., 2013; Wu et al., 2016, 2019a; Jian et al., 2020). An active left-lateral strike-slip fault, i.e. the Kunlun Fault system (Fig. 1), is present in the Eastern Kunlun Range as one of the major intracontinental strike-slip faults in the Tibetan Plateau that developed in response to the India-Eurasia collision (Wu et al., 2019a).

The Hoh-Xil-Songpan-Ganzi basin (also named as Songpan-Ganzi Complex) is located to the south of the Eastern Kunlun Range (Fig. 1) and is mainly composed of Triassic highly-deformed, slightly-metamorphosed deep-water marine calciclastic and siliciclastic rocks and Late Triassic–Early Jurassic (190–220 Ma) intermediate-acid igneous intrusions (Weislogel et al., 2010; Ding et al., 2013; Jian et al., 2019a).

The West Qinling Range is located to the east of the Eastern Kunlun Range and the Qilian Mountains, as the westernmost part of the Qinling-Dabie orogen. This orogen was finally formed during the middle–late Triassic collision between the North China and South China blocks and currently trends E-W in central China (Weislogel et al., 2010; Dong et al., 2021).

In addition to the Qaidam basin, there are several Cenozoic sedimentary basins within or along with those mountains. These mainly include Hexi Corridor, Subei, Suganhu, Kumukol, Gonghe, Xunhua, Xining, Lanzhou and Linxia basins (Fig. 1C; Yuan et al., 2013). The current basin-range system in northern Tibet is commonly thought as a result of far-field effects of the India-Eurasia collision and the on-going convergence between the two plates (Yin and Harrison, 2000; Zhuang et al., 2011; Yuan et al., 2013; Wang et al., 2014).

3.2. Cenozoic tectonics, climate, stratigraphy, lithology and depositional environments of the Qaidam basin

A comprehensive investigation on available borehole pre-Mesozoic basement crystalline rocks within the Qaidam basin reveals that the Qaidam region was involved into at least three tectono-magmatic episodes (i.e., early Neoproterozoic, early Paleozoic and late Paleozoic–earliest Mesozoic) and shows as a tectono-magmatic rejuvenated terrane, rather than a rigid and mechanically-strong craton (different from the adjacent Tarim basin) (Cheng et al., 2017). Although most structures in the north margin of the Tibetan Plateau have proven to initiate since the middle Miocene, a growing dataset indicates that widespread deformation and exhumation occurred in the early Cenozoic, even in the late Mesozoic, i.e., prior to the India-Eurasia collision (Jian et al., 2018; Li et al., 2020; Wu et al., 2021a). The Cenozoic Qaidam basin was created by development of a large synclinorium (Yin

et al., 2008b) and is thought to have developed under a contractional tectonic regime (Cheng et al., 2019a; Jian et al., 2023). In addition to the deformation in the surrounding ranges, the Qaidam basin has also experienced intensive deformation (e.g., strata shortening), after or coeval with the Cenozoic depositional process. Specifically, interpretations of regional seismic-reflection profiles indicate that the Cenozoic upper-crustal shortening decreases eastward across the basin from >48% in the west to <1% in the east (Yin et al., 2008b). As a result, a series of thrust fold belts with NW-SE directions are present inside the basin and reverse faults have developed along the basin-range margins (Fig. 1D).

The Qaidam basin, as a part of NW China, was successively controlled by the Paleogene planetary wind-dominated climate system and the Neogene and Quaternary monsoon-dominated climate system (Sun and Wang, 2005). Although the current Qaidam basin is extremely arid, this region overall had semiarid to arid climatic conditions with relatively humid intervals during the Cenozoic (Wang et al., 1999; Jian et al., 2013b, 2014, 2019b; Miao et al., 2019; Nie et al., 2020; Sun et al., 2020; Liang et al., 2021).

The Cenozoic sedimentary succession of the Qaidam basin is commonly divided into 7 stratigraphic units (Fig. 2), (in ascending order) including 1) Lulehe Formation (E_{1+2}); 2) Xia Ganchaigou Formation (E_3); 3) Shang Ganchaigou Formation (N_1); 4) Xia Youshashan Formation (N_2^1); 5) Shang Youshashan Formation (N_2^2); 6) Shizigou Formation (N_2^3); and 7) Qigequan Formation (Q_{1+2}). These Cenozoic deposits are thick and lithologically diverse (Figs. 3 and 4) and are thought to accumulate in fluvial-lacustrine depositional environments (Zhuang et al., 2011; Guan and Jian, 2013; Jian et al., 2014, 2018; Fu et al., 2022). Previous investigations demonstrate that the Qaidam sedimentary depocenters shifted east-ward during the Cenozoic (Yin et al., 2008b; Bao et al., 2017), resulting in highly spatial and stratigraphic variations in lithology (Fig. 2). The northern and eastern Qaidam basin regions are dominated by siliciclastic sedimentary rocks (Zhuang et al., 2011; Jian et al., 2013a; Fu et al., 2022), whereas carbonate rocks, evaporite rocks and mixed carbonate-siliciclastic deposits are common in the western Qaidam basin (Fig. 2; Jian et al., 2014; Guo et al., 2017; Wang et al., 2023). Stratigraphically, the Cenozoic sedimentary succession generally indicates from oldest to youngest coarse-grained (Fig. 3, E_{1+2}) then relatively fine-grained (Fig. 4, E_3, N_1, N_2^1 and N_2^2), before reverting to coarse-grained again (Fig. 3, N_2^3 and Q_{1+2}) (Fig. 2).

3.3. Depositional ages of the Cenozoic sedimentary strata in the Qaidam basin

Two depositional age models have been proposed for the Cenozoic Qaidam basin. A traditional age model suggests that the Cenozoic basin filling initiated in the early Eocene (ca. 54 Ma), based on magnetostratigraphic and biostratigraphical data from several outcrop sections in the western, northern and eastern Qaidam basin (Sun et al., 2005; Ji et al., 2017; Fang et al., 2019b). By contrast, a younger age model, which relies on magnetostratigraphy and a middle Miocene mammalian fauna from the Honggou section in the eastern Qaidam basin, claims for a late Oligocene–early Miocene initial deposition (ca. 20–25 Ma) of the

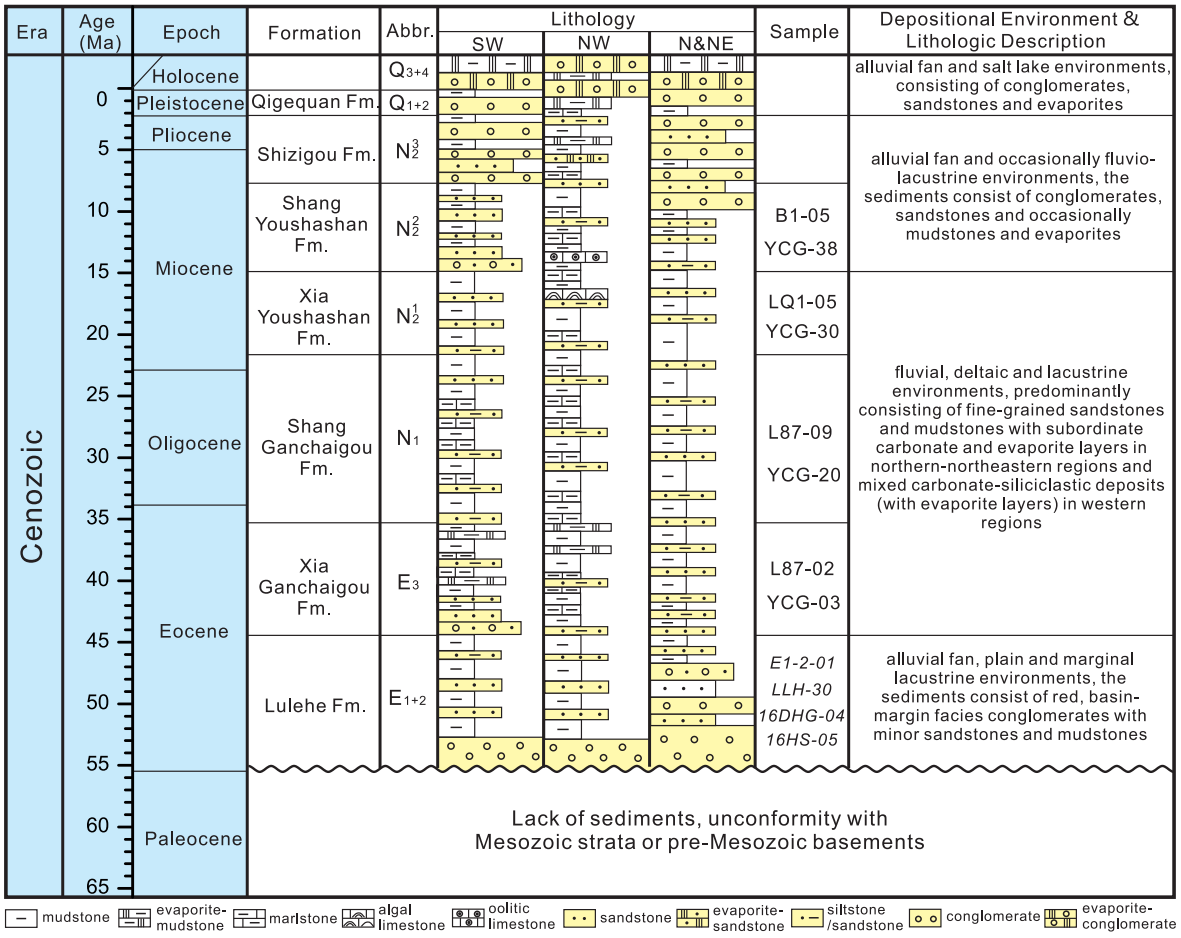

Fig. 2. Cenozoic stratigraphic framework, depositional environment, lithological description of the Qaidam basin, modified from Jian et al. (2013b), Wang et al. (2023) and references therein. The lithologic columns of SW, NW and N&NE Qaidam basin are modified from Cheng et al. (2021), Zhang et al., and Jian et al. (2013a), respectively. The depositional age constrains of these stratigraphic units are from previous magnetostratigraphic studies on those representative outcrop sections in the margins of the basin (e.g., Sun et al., 2005; Fang et al., 2007, 2019b; Lu and Xiong, 2009; Chang et al., 2015; Ji et al., 2017).

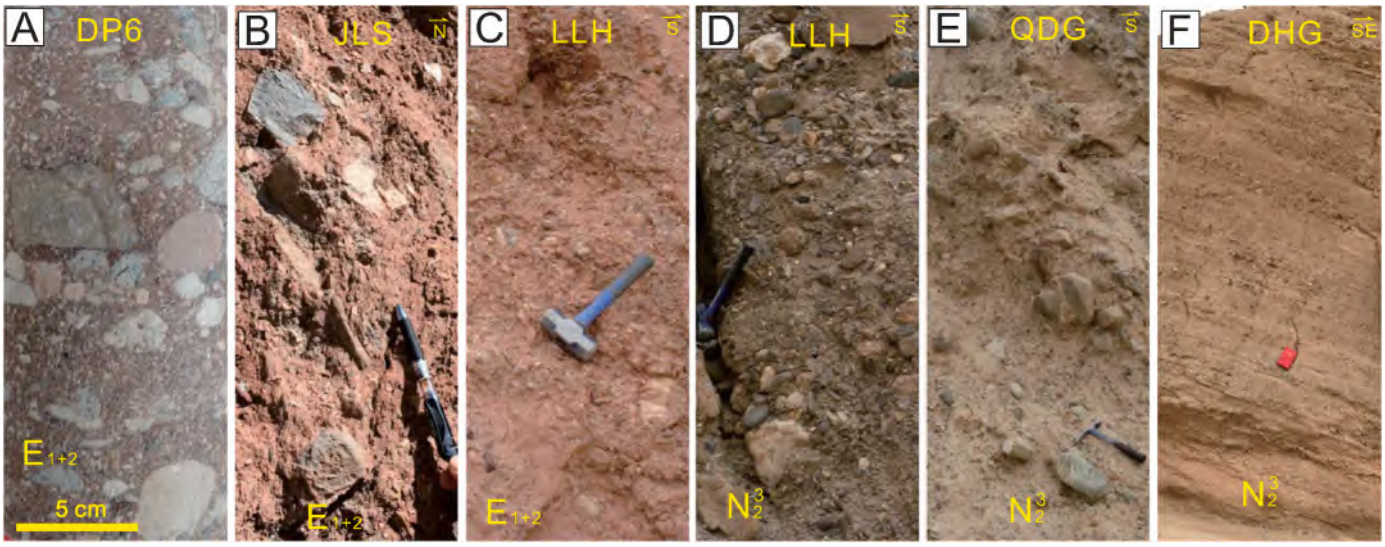

Fig. 3. Representative coarse-grained sedimentary rocks of the Lulehe (E_{1+2}) and Shizigou (N_2^3) Formations from northern and eastern Qaidam basin. (A): Drilling well DP6; (B): JLS section; (C–D): LLH section; (E): QDG section; (F): DHG section. For locations of these sections, see Fig. 1C. Refer to Jian et al. (2023) for more E_{1+2} sedimentary strata photos and descriptions. Most of these E_{1+2} and N_2^3 coarse-grained strata are matrix-supported and poorly sorted. These strata can be interpreted as products from high-gradient depositional systems with proximal sources (Zhuang et al., 2011; Guan and Jian, 2013).

Cenozoic strata (Wang et al., 2017; Nie et al., 2020).

Detailed reviews and comparison analyses of these two age models were recently reported by several research groups (Sun et al., 2020; Cheng et al., 2021; Jian et al., 2023) and this study does not add to the age models. We prefer the traditional older age model for the whole Qaidam basin because of the following regional observations and interpretations. Numerous paleoclimatic records (such as sedimentary carbonate stable isotopes, biomarkers and facies) indicate that, in the case of Eocene-onset deposition, climatic fluctuations in the Qaidam basin correspond well with regional climatic conditions in the northern Tibetan Plateau and with the global climate history (e.g., Guo et al., 2017; Sun et al., 2020; Liang et al., 2021; Wu et al., 2021b). Widespread Eocene exhumation in the surrounding Qilian Mountains, Eastern Kunlun and Altun ranges, which has been well recognized (Jian et al., 2018; An et al., 2020; Li et al., 2020 and references therein), may result in detritus accumulation in adjacent sedimentary basins. Furthermore, early shortening in the Qilian Mountains may generate more reasonable crustal thickening rates (Zuza et al., 2018, 2019) than proposed Miocene-initiated shortening.

4. Samples and methods

Twelve Cenozoic sandstone samples (Figs. 1 and 2) were selected for detrital zircon U–Pb geochronological analysis. All the samples were previously analyzed for petrographic and heavy mineral compositions (Jian et al., 2013a) and some of them were also applied in detrital garnet and tourmaline geochemistry and detrital apatite fission track analyses (Jian et al., 2013a, 2018; Hong et al., 2020) (Figs. 5 and 6). Most samples are medium-to fine-grained litharenites (e.g., samples YCG-03 and L87-02) or lithic wackes (e.g., samples YCG-38 and DHG-04), with high contents of quartz and metasedimentary lithic fragments (Fig. 5; Table A1 in Appendix A). Detrital framework grains are texturally poorly sorted and angular to subangular in roundness (Fig. 5). The transparent heavy minerals in these samples are mostly dominated by epidote, garnet, titanite and zircon (Fig. 6).

In preparation for U–Pb isotopic analysis, detrital zircon grains were separated from ~1 to 2 kg samples and were then mounted in epoxy. The mounts were sanded down to a depth of ~20–30 μm, polished and imaged. Cathode luminescence (CL) images were taken for inspecting internal structures of individual zircons and for selecting spot positions for laser ablation. LA-ICP-MS U–Pb analyses were performed using an Agilent 7500a equipped with a 193-nm laser. Each analysis incorporated a background acquisition of approximately 15–20 s (gas blank) followed by 50 s data acquisition from the analyzed grain, using 32 μm diameter laser spot, 10 Hz frequency and Helium as a carrier gas. Unknown zircon grains were selected randomly, leaving out grains with apparent inclusions or cracks. The U–Pb dating was monitored using standard-sample bracketing with the Plesovice (337 Ma) and 91,500 (1062 Ma) zircon reference materials. Common lead was corrected for using the correction function (Andersen, 2002). Zircon U–Pb ages with poor precision (>±10%) and high discordance (>±15%) were omitted from the kernel density estimation plots and from interpretation. Ages <1000 Ma were based on common Pb corrected $^{206}Pb/^{238}U$ ratios, whereas ages >1000 Ma were based on common Pb corrected $^{206}Pb/^{207}Pb$ ratios.

Furthermore, grain sizes of the analyzed detrital zircons were obtained by using equivalent spherical diameter calculation method (Garzanti et al., 2008; Shen et al., 2021), based on transmitted-light photomicrographs of the grains after mounting and polishing. The equivalent spherical diameter therein is the cube root of the product of the three grain axis lengths (assuming that the third axis (Y) is approximately equivalent to the Z axis (width)).

5. Results

We report a total of 1124 new detrital zircon U–Pb ages from the Cenozoic sandstone samples (the results of four E_{1+2} samples were also present in Jian et al. (2023)). The analyzed detrital zircon grains range from 40 to 200 μm. Most grains are characterized by oscillatory zoning textures (Fig. 7) and have high Th/U ratios (>0.1). Detrital zircon U–Pb age populations of the 4 samples from the YCG section are dominated by early Paleozoic (420–500 Ma) ages, with subordinate Neoproterozoic (750–950 Ma) and Permian (250–270 Ma) ages (Fig. 8). Sample YCG-38 therein indicates predominant Phanerozoic zircon ages (70 in 78). The 2 borehole samples from drilling well L87 (i.e., samples L87–02 and L87-09) show similar detrital zircon age spectra with the YCG section samples (Fig. 8). However, drilling well samples LQ1-05 and B1-05 have more diverse detrital zircon age populations than other samples. These two samples are characterized by Triassic–Permian (210–290 Ma), early Paleozoic (420–510 Ma), Neoproterozoic (750–1000 Ma), Paleoproterozoic (1650–1950 Ma and 2300–2500 Ma) zircon ages (Fig. 8). In

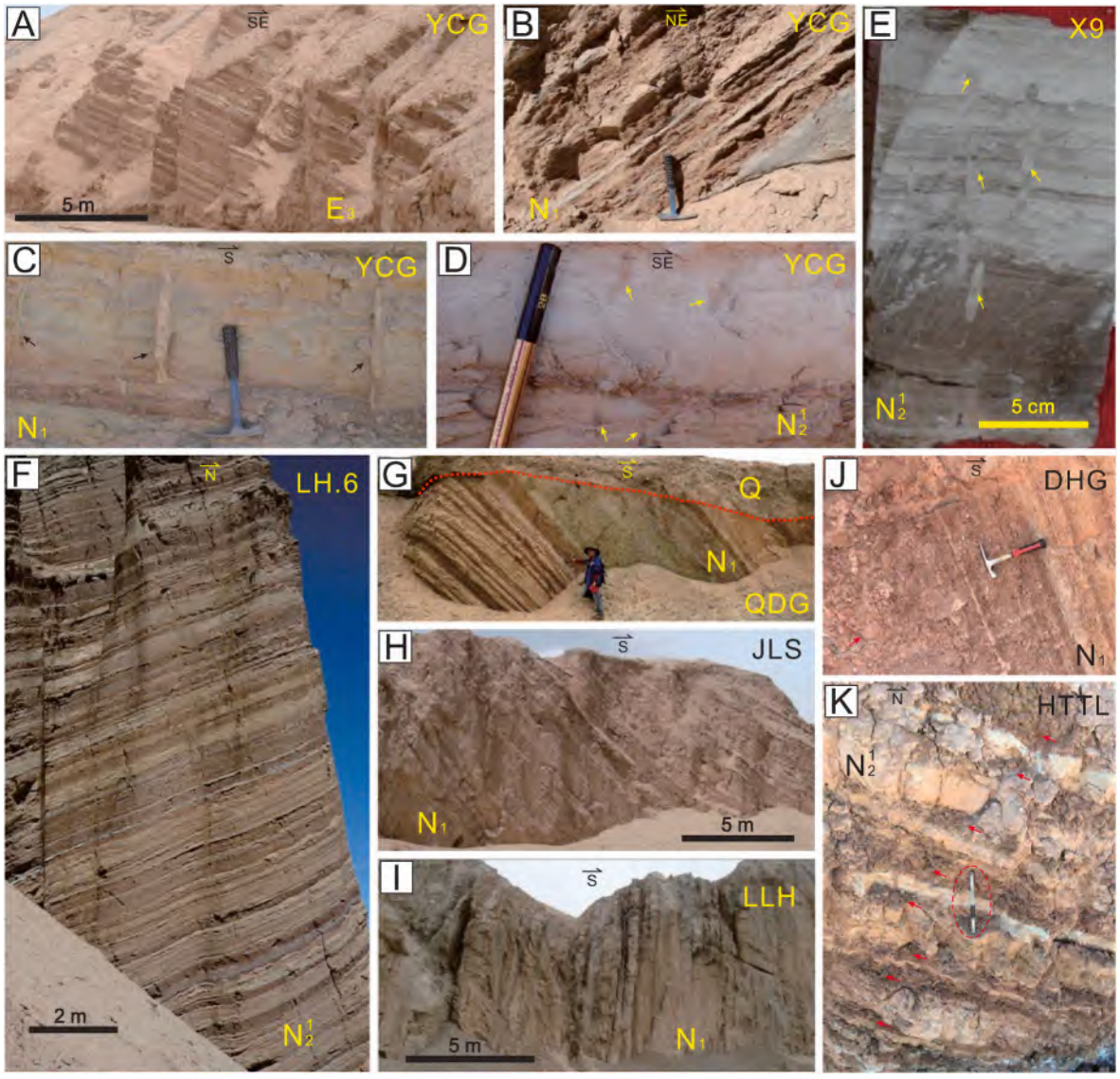

Fig. 4. Representative outcrop and borehole fine-grained sedimentary rock features of the Shang Ganchaigou (N_1) and Xia Youshashan (N_2^1) Formations in the northern Qaidam basin. (A–D): YCG section; (E): drilling well *X*9; (F): LH.6 section; (G): QDG section; (H): JLS section; (I): LLH section; (J): DHG section; (K): HTTL section. For locations, see Fig. 1C. Note that these strata in the western region are characterized by marginal lacustrine thin interbedded sand-mud successions with common mud cracks (black arrows in Fig. 4C) and vertical biological burrows (yellow arrows in Fig. 4D and E), whereas the fine-grained strata in the eastern region are featured by well-developed paleosols (red arrows in Fig. 4J and K).

addition, these two samples also have Carboniferous and Late Devonian (300–380 Ma) zircon grains (Fig. 8), which are quite different from other analyzed samples.

The relations between detrital zircon grain sizes and U–Pb ages indicate that most relatively coarse-grained, elongated zircon grains, e.g., fine-grained sand size (125–250 μm) or zircons with length/width ratios >2, are dominated by Phanerozoic ages (with minor Neoproterozoic ages), whereas most Precambrian ages, especially the ages prior to the Mesoproterozoic (1600–2800 Ma), are present in those relatively small grains, such as very fine-grained sand (63–125 μm) and coarse silt-grained (32–63 μm) size detrital zircons (Fig. 9). The details about the grain sizes, length/width ratios, U–Th–Pb isotopic ratios and ages of all the analyzed detrital zircons are shown in Table A2. The U–Pb age Concordia diagrams are shown in Fig. S1 in Appendix B. Furthermore, we also compile all the available detrital zircon age data (119 published and 12 new samples, 11,744 ages in total) from the Cenozoic sedimentary rocks in the Qaidam basin (Table A3). The collected detrital zircon U–Pb age data of the mentioned Cenozoic intermountain basins (28 samples, 2568 ages) and modern river sands (50 samples, 4836 ages) are shown in Table A4.

6. Bedrock lithology and zircon U–Pb age signatures of the potential source regions for the Cenozoic Qaidam basin

We compile reported zircon ages of granitic rocks (Fig. 10) and detrital zircon age data from Precambrian metasedimentary rocks, modern river sands and representative small Cenozoic intermountain basins in northern Tibet (Fig. 11) to characterize zircon age signatures for the potential sediment source regions. Note that we do not advocate compiling detrital zircon age data from Paleozoic–Mesozoic sedimentary rocks to reflect the Cenozoic sediment source age signatures, due to the complex, to some extent uncertain paleogeographic environments and sediment routes (i.e., paleo-drainage networks) for accumulating those successions. We also do not advocate combining all the available zircon age data as source signatures for a complex orogen or for a large tectonic domain. We instead plot the ages separately for different areas

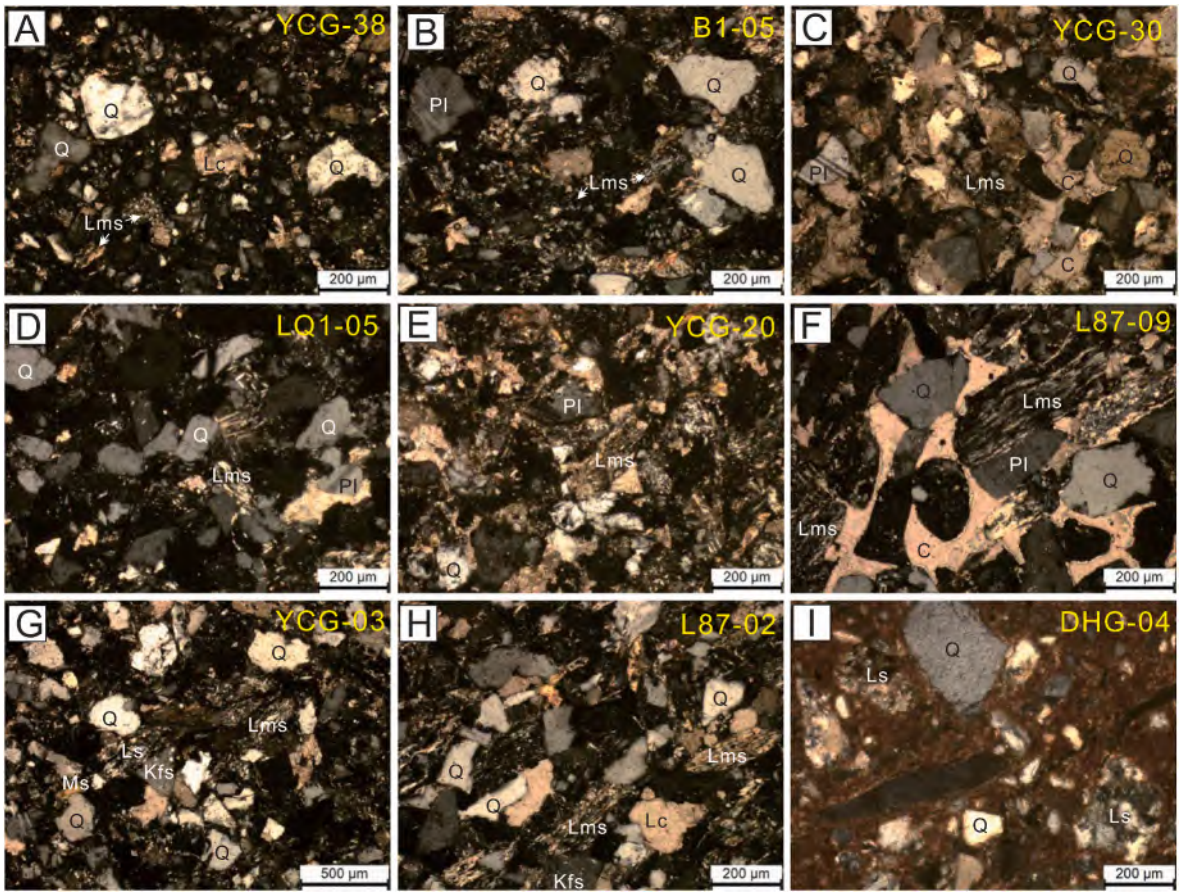

Fig. 5. Representative photomicrographs of the analyzed sandstone samples from the study area. Note that the Cenozoic sandstones from the northern and eastern Qaidam basin show significant compositional and textural variability, although most of these rocks are lithic sandstones and the framework grains are dominated by sedimentary and metasedimentary lithic fragments. Data of the E_{1+2} sample DHG-04 were reported in Jian et al. (2023). Q: quartz; Pl: plagioclase; Kfs: K-feldspar; Ls: sedimentary lithic fragment; Lms: metasedimentary lithic fragment; Lc: carbonate lithic fragment; C: carbonate cement; Ms: muscovite.

in those potential source orogens (Figs. 10 and 11).

6.1. Qilian Mountains

The Qilian Mountains are mainly composed of Precambrian and Paleozoic metamorphic strata and early Paleozoic granitic rocks (Gehrels et al., 2003, Fig. 1D). The Precambrian zircon age signals are characterized by early–mid Neoproterozoic ages (750–1000 Ma, Fig. 11D). Note that a nearly latitudinally-trending massif with Paleoproterozoic (1800–2000 Ma and 2350–2500 Ma) crystalline rocks, i.e., the Quanji massif (also named as Oulongbuluke block in some literatures), has been recognized as a part of the South Qilian and North Qaidam metamorphic belts (Chen et al., 2009, 2012, 2013; Yu et al., 2017; Zhang et al., 2021). These two Paleoproterozoic zircon age clusters are also reflected by detrital zircon dating data from several modern river sand samples and the Cenozoic intermountain basin sedimentary strata in the Qilian Mountains (Fig. 11B and C). Both magmatic and detrital records indicate that the 400–520 Ma age cluster is a notable Phanerozoic zircon age signature for most areas of the Qilian Mountains (Fig. 11). Although the currently exposed granitic rocks in the Central and North Qilian regions mainly show Cambrian–Devonian U–Pb ages (Fig. 10), both modern river sands and Cenozoic intermountain basin sedimentary rocks related to these regions indicate obvious Permian–-Triassic zircon age populations (Fig. 11). Explaining these young ages remains challenging, but the Permian–Triassic zircon age signals deserve more attention when considering the Qilian Mountains as a possible Mesozoic–Cenozoic sediment source terrane.

6.2. Eastern Kunlun range and pre-Cenozoic basement of the Qaidam basin

Most studies suggest that the Qaidam basin basement and the Eastern Kunlun Range had similar pre-Mesozoic history and can be considered as a single terrane (so-called Kunlun-Qaidam terrane) for characterizing early tectonic evolution (e.g., Yin and Harrison, 2000; Gehrels et al., 2011; Cheng et al., 2017; Wu et al., 2019a; Jian et al., 2020; Zhang et al., 2021). Thus, these two regions are expected to have similar pre-Mesozoic bedrock lithology and zircon U–Pb age signatures. As most areas of the Qaidam basin are solidly filled by Mesozoic and Cenozoic sedimentary rocks, geology of the Kunlun-Qaidam terrane is best exposed in the Eastern Kunlun Range along the south margin of the terrane. Available data demonstrate that the Precambrian basement is featured by early–mid Neoproterozoic zircon age signals (Fig. 10; Fig. 11D) and the Phanerozoic signals display prominent 400–500 Ma and 220–290 Ma zircon ages (Figs. 10 and 11). Note that detrital zircon U–Pb dating data from the modern river sands and the Cenozoic intermountain basin sedimentary rocks in the Eastern Kunlun Range indicate dominant Phanerozoic ages (i.e., those two prominent age clusters), which are quite different from those in the Qilian Mountains (Fig. 11).

6.3. Altun Range

Zircon age signatures of the north regions of the Altyn Tagh Fault are similar to the west part of the North and Central Qilian regions (Fig. 10), whereas the south regions of the fault have similar zircon ages to the Eastern Kunlun and pre-Cenozoic basement of the Qaidam basin

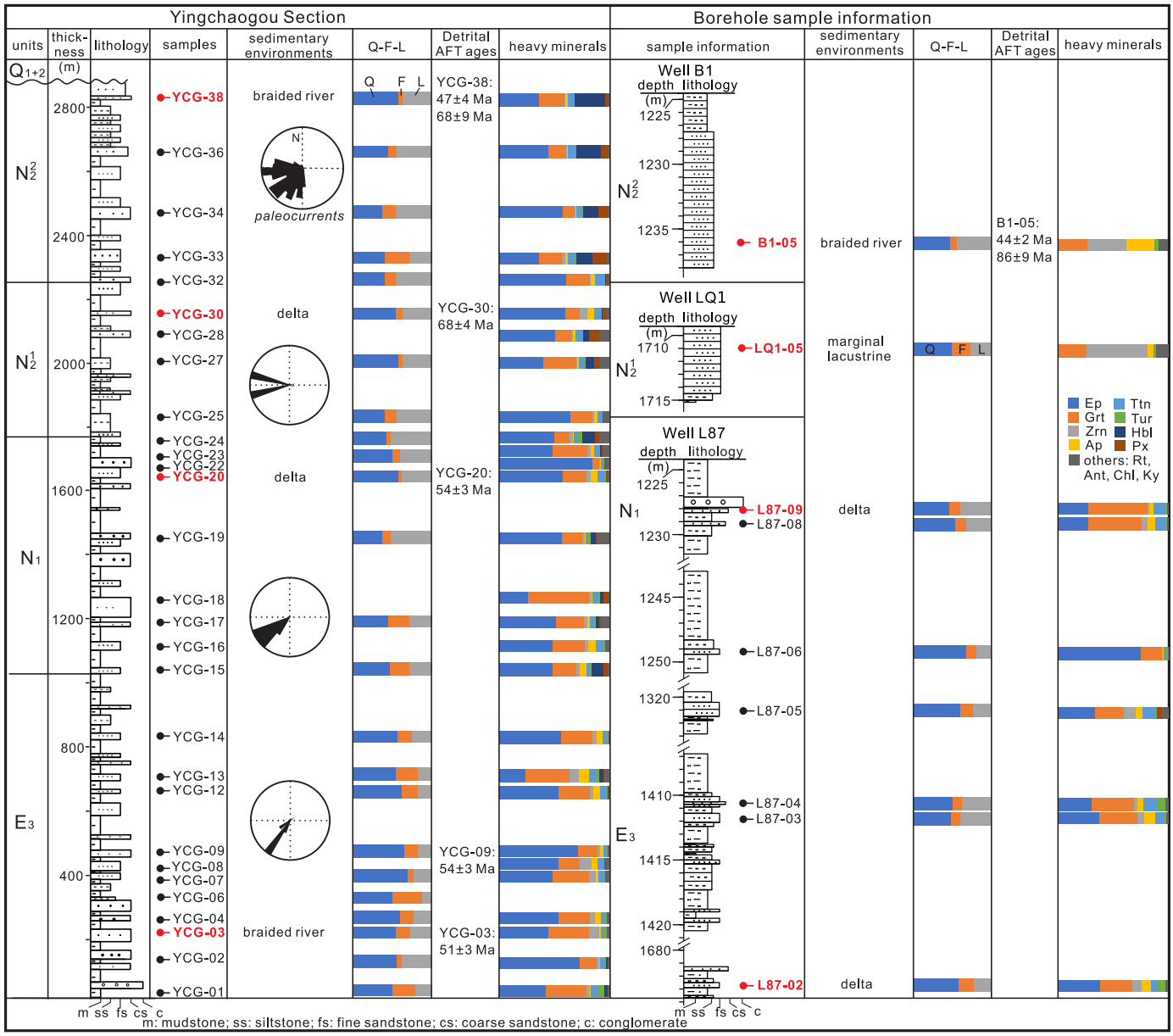

Fig. 6. Stratigraphic columns of the analyzed outcrop section and drilling cores and previously published data. The samples marked as red names were selected for detrital zircon U–Pb geochronology in this study. Framework petrography and heavy mineral analysis results are from Jian et al. (2013a). Paleocurrent data and detrital apatite fission track results are from Jian et al. (2018). Q: quartz; F: feldspar; L: lithic fragment; Ep: epidote; Grt: garnet; Zrn: zircon; Ap: apatite; Ttn: titanite; Tur: tourmaline; Hbl: hornblende; Px: pyroxene; Rt: rutile; Ant: anatase; Chl: chlorite; Ky: kyanite.

(Fig. 11B). Specifically, the Precambrian basement of the Altun Range features early–mid Neoproterozoic zircon ages (850–1000 Ma, Figs. 10 and 11). Phanerozoic rocks in the northern Altun Range are dominated by early Paleozoic zircon ages, whereas those in the southern Altun Range indicate both early Paleozoic and Permian–Triassic zircon age clusters (Figs. 10 and 11). Although Paleoproterozoic crystalline rocks were found to be sporadically distributed in the Altun Range regions (Yu et al., 2017 and reference therein), Paleoproterozoic age signals are not prominent in the reported detrital zircon age data of related modern river sands and Cenozoic sandstones (Fig. 11), which are different from those in the Qilian Mountains but is similar to the Eastern Kunlun Range.

6.4. Songpan-Ganzi Complex

The Songpan-Ganzi Complex is proposed to act as a possible detritus source for the Cenozoic Qaidam basin when the Eastern Kunlun had a relatively low relief (e.g., McRivette et al., 2019; Wu et al., 2019b). Detrital zircon U–Pb ages of the Triassic turbidites (the most important sedimentary records in the Songpan-Ganzi Complex) mainly comprise five populations: 240–310 Ma, 400–480 Ma, 750–1000 Ma, 1700–2000 Ma and 2300–2600 Ma (Weislogel et al., 2010; Ding et al., 2013; Jian et al., 2019a). These zircon age signals are also well indicated by the available modern river sand data (e.g., the fountainhead of the Yellow River, Fig. 11B).

6.5. West Qinling Range

As a part of the Qinling-Dabie orogen, the West Qinling Range is thought to have Neoproterozoic basement (Jian et al., 2019a; Dong et al., 2021). Phanerozoic granitoid rocks in the West Qinling Range mainly display Triassic (210–250 Ma) ages, with subordinate Late Ordovician–Early Devonian (400–460 Ma) ages (Dong et al., 2011). This

Fig. 7. Representative CL images, Th/U values and U–Pb ages of the analyzed detrital zircon grains in the Cenozoic sandstone samples from the northern Qaidam basin. The white bars represent 50 μm.

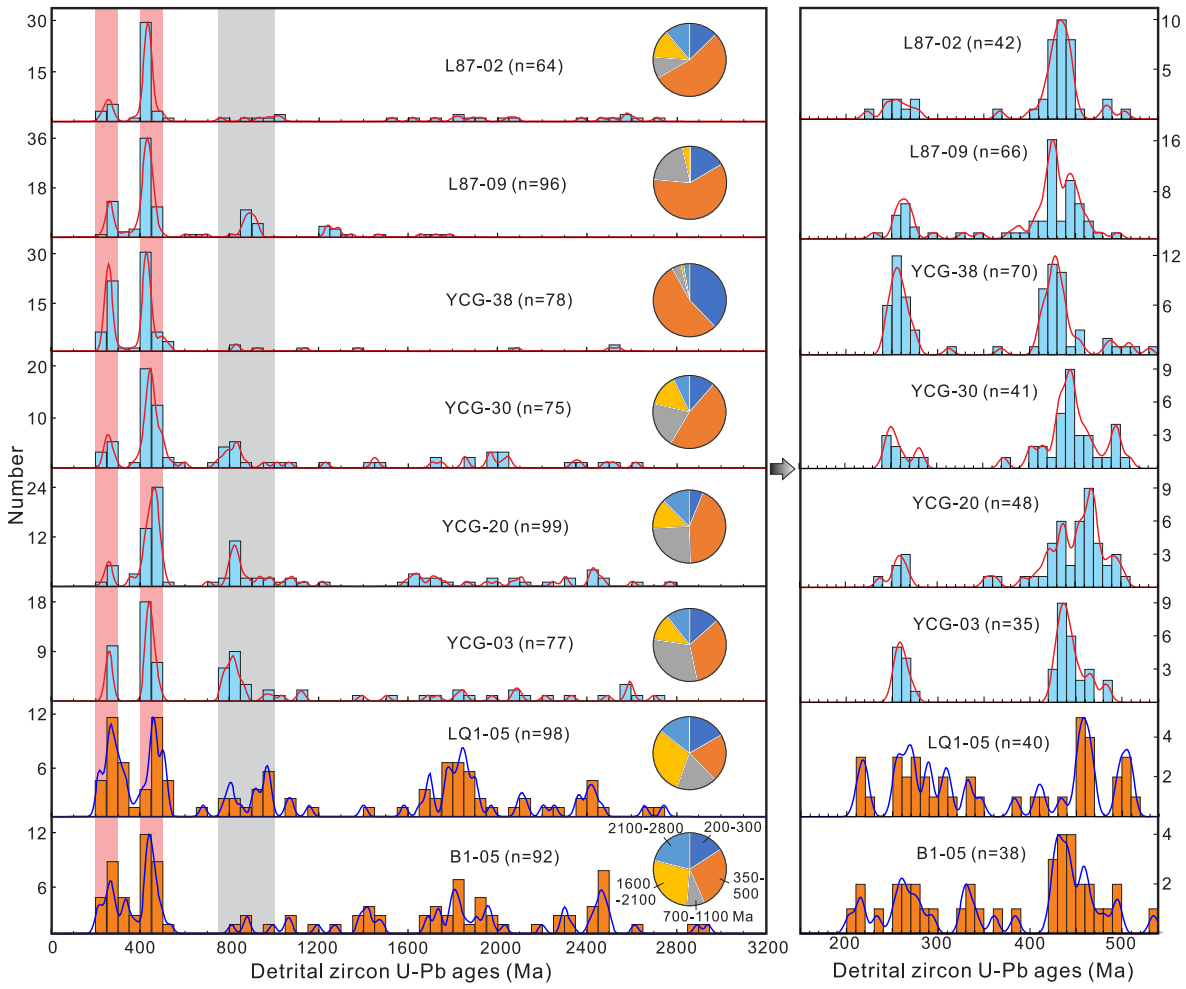

Fig. 8. Detrital zircon U–Pb age distributions of the analyzed Cenozoic sandstone samples in this study. All-age plots were drawn by using bandwidth = 15 in the DensityPlotter Program (Vermeesch, 2012), while the Phanerozoic-age plots were drawn by using bandwidth = 5.

is consistent with the available detrital zircon data of the modern sands from small mountainous rivers within the north part of this range (Lease et al., 2007) which indicate prominent Triassic U–Pb ages (Fig. 11). Pre-Cenozoic sedimentary covers in the West Qinling Range are dominated by upper Permian–Triassic deep-water marine deposits (detrital zircon age signatures are similar to those in the Songpan-Ganzi Complex as mentioned above, Jian et al. (2019a)) with minor Silurian–Carboniferous sedimentary successions (J. Li et al., 2014). Furthermore, Late Jurassic–Early Cretaceous granitoid rocks (110–150 Ma) are also widely distributed in the Qinling-Dabie orogen (Dong et al., 2011), particularly in the central and east segments of the orogen.

7. Spatial and temporal variations in detrital zircon U–Pb ages and provenance interpretation of the Cenozoic deposits in the Qaidam basin

Previously reported and new data (Figs. 12–20) indicate that the detrital zircon U–Pb age populations of the Cenozoic sedimentary rocks from the Qaidam basin have obvious spatial and temporal diversity. This implies spatiotemporally variable sediment sources or fluctuant sediment routing systems for the detrital zircon records. The following are specific spatial and temporal variations in detrital zircon ages and corresponding provenance interpretations.

7.1. Spatial variations of each stratigraphic unit

Most dated E_{1+2} sandstones (21 samples) are located along the current margins of the Qaidam basin (Fig. 12). Both KDE and MDS illustrations of these E_{1+2} samples indicate remarkable spatial differences in detrital zircon U–Pb ages (Fig. 12), revealing different sources for the Cenozoic basal deposits. Specifically, Precambrian zircon grains are relatively predominant in those samples from the regions close to the Qilian Mountains, such as the HS, LLH and SGH regions (Fig. 12). The 750–1000 Ma ages are abundant in the analyzed zircon grains from LLH and SGH samples (Fig. 12), indicating the prominent contributions of the Neoproterozoic basement rocks from the Qilian orogen. By contrast, the E_{1+2} sedimentary rocks from the regions close to the Altun and Eastern Kunlun ranges are dominated by Phanerozoic zircon age populations, with few Precambrian ages (Fig. 12). These features correspond well with zircon age signatures of the adjacent regions in the two ranges. Furthermore, the PT sample and some DHG samples are featured by 400–480 Ma zircon ages (Fig. 12), suggesting that these detrital zircons were most likely sourced from granitoid rocks related to the Ordovician to Devonian subduction-closure process of the Proto-Tethys Ocean. Given that the E_{1+2} sandstones are mainly present as interlayers in conglomerate-dominated red beds deposited in high-gradient depositional systems (Fig. 3; Zhuang et al., 2011; Guan and Jian, 2013; Cheng et al., 2019a; Lu et al., 2022; Jian et al., 2023), we favor that the detrital zircon grains in the E_{1+2} sedimentary strata were derived from various, adjacent high-relief regions (Fig. 21A), rather than distal sources. For example, the E_{1+2} deposits in the northern and eastern Qaidam basin were most likely fed by parent-rocks from the local paleo-highs in the Qilian Mountains and by the pre-Cenozoic basement rocks within the Qaidam terrane interior (Fig. 21A; Jian et al., 2023), rather than the

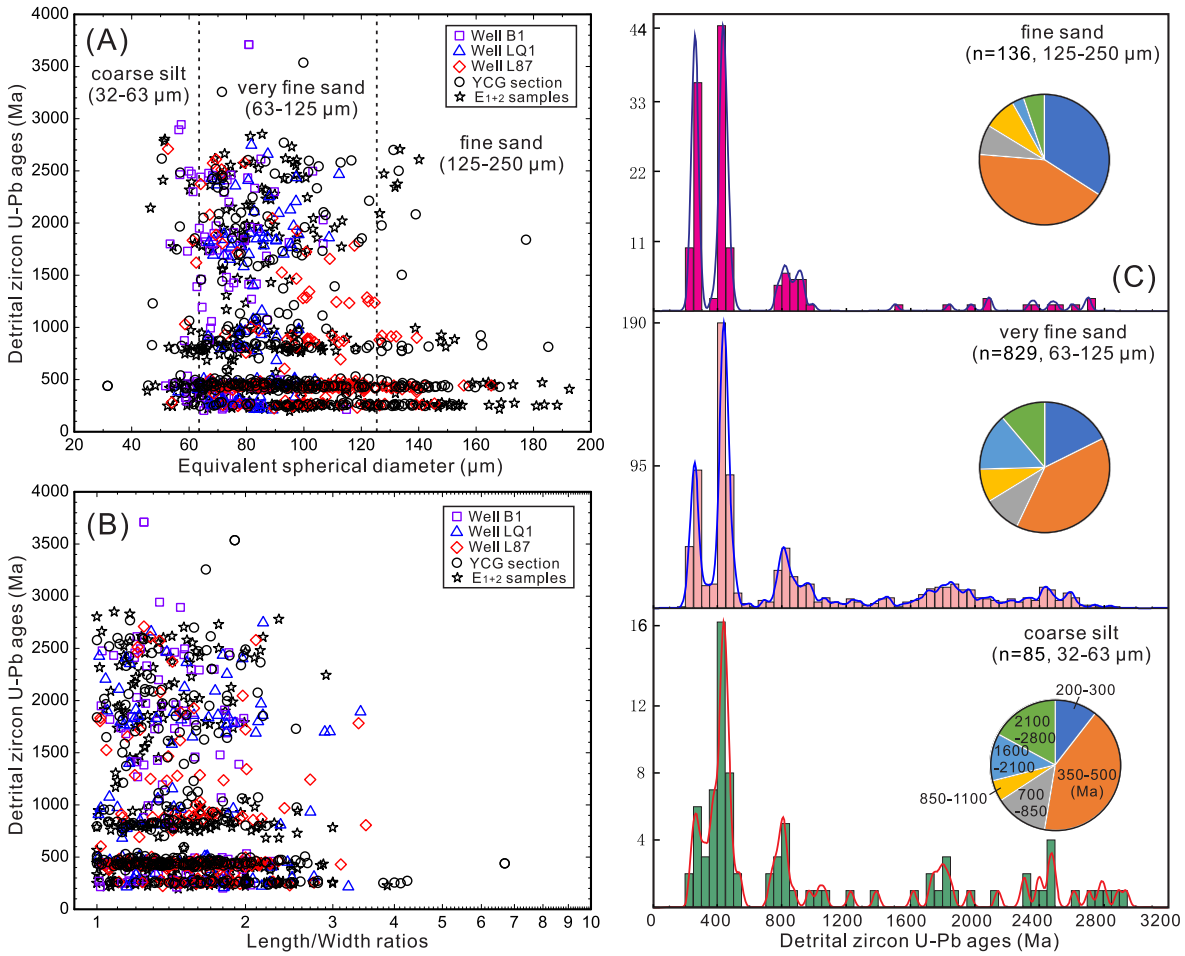

Fig. 9. Relationships between detrital zircon U–Pb ages and grain sizes (A) and length/width ratios (B). The detrital zircon grain length (X axis) and width (Z axis) were measured directly from microscopic images. Data of the E_{1+2} samples are from Jian et al. (2023).

distant Eastern Kunlun regions. Combining other provenance indicators (such as paleocurrent orientations, conglomerate clast composition, sandstone petrography and heavy mineral data) and stratigraphic and seismic data, we suggest that the Qaidam terrane showed as several isolated depocenters, rather than a coherent basin, in the early stage of the Cenozoic deposition (Jian et al., 2023). As mentioned above, the traditional age model suggests that the Cenozoic sediment accumulation initiated in the early Eocene (Ji et al., 2017; Fang et al., 2019b), if it is true, the E_{1+2} sediment provenance interpretation supports the proposition that early Eocene deformation was widespread in northern Tibet. The tectonic domains therein, e.g. the Qilian, Altun and Eastern Kunlun orogens and the Qaidam basin interior, synchronously deformed, shortly after the India-Eurasia collision (e.g., Clark, 2012; Yuan et al., 2013; Jian et al., 2018; Cheng et al., 2019a; Li et al., 2020; He et al., 2021).

Different from the evident variations in the E_{1+2} detrital zircon age data, the overlying E_3 sandstones (26 samples) from different locations of the Qaidam basin (except the SGH samples) show relatively similar detrital zircon age populations, indicated by both KDE and MDS plots (Fig. 13). The U–Pb age clusters are dominated by 400–480 Ma and 220–280 Ma, with minor Precambrian ages. Note that the E_3 strata in different locations indicate quite different paleocurrent orientations (Fig. 13A) and mainly accumulated in relatively low-gradient fluvio-lacustrine depositional systems (Zhuang et al., 2011; Guan and Jian, 2013). Therefore, the similar age signals do not mean that all the E_3 deposits were fed by the same source regions, instead reveal that these detrital zircon grains were derived from the surrounding different mountains with relatively well-mixed U–Pb age populations. The well-mixed detrital zircon age signals probably imply relatively large drainage basin for the paleo-Qaidam lake during that time (Fig. 21B), which carried abundant, blended detritus from different source terranes. This is consistent with the widely-accepted lake basin expansion that initiated in the depositional period of the E_3 strata (Zhuang et al., 2011; Guan and Jian, 2013; Cheng et al., 2019b; Wu et al., 2021b). Some E_3 samples from the eastern and northern Qaidam basin regions (e.g., the DHG, YCG, PT and LH.5 samples) indicate slightly stronger Precambrian zircon age signals than samples from other regions (Fig. 13), reflecting comparatively higher contributions of old source terranes (e.g., the Quanji massif) in the Qilian Mountains.

The N_1 and N_2^1 detrital zircon dating samples to some extent inherit the age signatures of the E_3 samples but indicate more pronounced spatial differences. Specifically, detrital zircon records from the eastern and northern Qaidam basin regions are featured by high proportions of Precambrian ages (e.g., HTTL, LH.7 and some DHG samples), in particular the Paleoproterozoic zircon age populations (Figs. 14 and 15), or dominated by early Paleozoic ages (e.g., LH.5, YCG and some DHG samples). These age signals imply predominant contributions from source terranes in the Qilian Mountains, especially in the South Qilian and North Qaidam belts (Figs. 10 and 11). Most N_2^2 and N_2^3 samples from these northern and eastern regions have similar detrital zircon U–Pb age populations to those N_1 and N_2^1 samples (Figs. 16 and 17). By contrast, the western Qaidam basin samples collected from these stratigraphic units are overwhelmingly dominated by Phanerozoic detrital zircons, with dominant 400–480 Ma and 220–280 Ma clusters and minor Neoproterozoic age populations (Figs. 12–18). Combining the available paleocurrent orientation data (Figs. 12–18), these deposits are favored to be derived from the adjacent Altun and Eastern Kunlun ranges

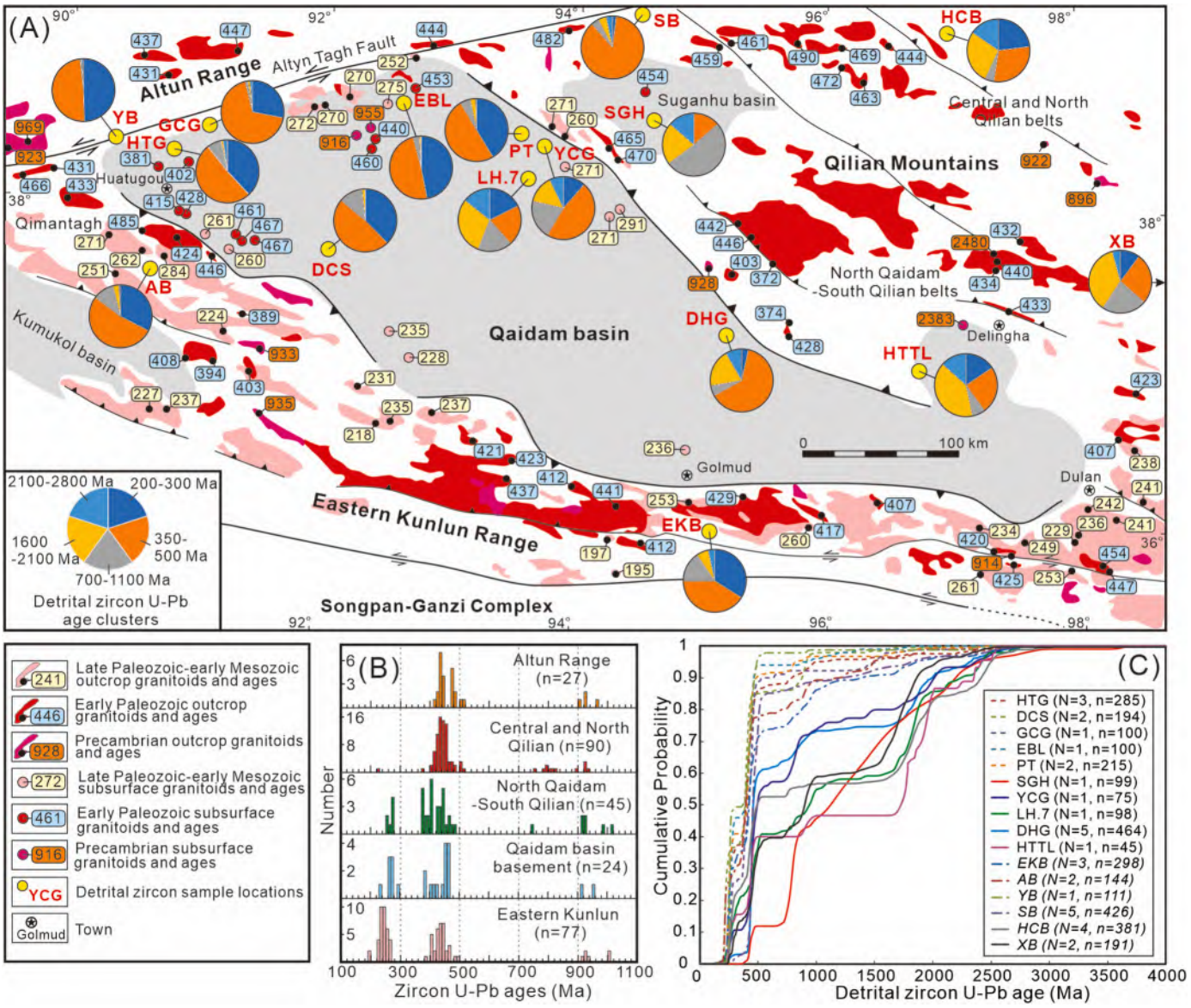

Fig. 10. (A) Published zircon U–Pb ages of granitoid rocks in northern Tibetan Plateau (modified from Jian et al. (2023)). Black and colored spots indicate outcrop and borehole data, respectively. For sources of the data, see Jian et al. (2023) and references therein. Similar compilations were also shown in Cheng et al. (2017); Lu et al. (2018) and Jian et al. (2020). (B) Histograms of the collected granitoid rock zircon U–Pb age data. Note that the data of the Altun Range are from the north regions of the Altyn Tagh Fault and the ages from the south regions of the fault are included in the age plots of the Qaidam basin basement. (C) Detrital zircon age cumulative probability curves of the N_2^1 sandstones from the Qaidam basin and Miocene sandstones from the surrounding Cenozoic basins. EKB: a Neogene inter-mountain basin within the Eastern Kunlun Range (McRivette et al., 2019; Wu et al., 2019b); AB: Adatan basin (data from Cheng et al., 2016a), in the Qimantagh area, west margin of the Eastern Kunlun Range; YB: Yitunbulake basin (data from Zhang et al., 2017), along the Altyn Tagh Fault; SB: Subei basin (data from L. Li et al., 2014), along the Altyn Tagh Fault; HCB: Hexi Corridor basin (data from Wang et al., 2016; An et al., 2018), as a foreland basin close to the Qilian Mountains to the north; XB: Xining basin (data from Zhang et al., 2016), within the Qilian Mountains to the east. For locations and corresponding pie charts of the detrital zircon age populations, see Fig. 10A.

(Fig. 21B). For example, most sandstones from the KB and DCS regions indicate prominent 380–480 Ma zircon age populations and subordinate 220–280 Ma ages. This matches well with the zircon age signals of the modern river sands (Fig. 11), revealing major contributions from the nearby northern Qimantagh regions (Fig. 10). Note that almost all the sedimentary rocks from these stratigraphic units have detrital zircons with 380–480 Ma ages, whereas the proportions of the 220–280 Ma cluster vary obviously among analyzed samples. This implies variable contributions of the Permian–Triassic terranes in the surrounding mountains.

Most Quaternary Q_{1+2} samples mainly have Phanerozoic detrital zircons and Precambrian ages are comparatively minor, except the SGH sample (Fig. 18). These samples also indicate relatively marked spatial differences in detrital zircon ages (Fig. 18). For instance, the HTTL and PT samples from the eastern and northern Qaidam basin are featured by Permian–Triassic detrital zircon ages, whereas the adjacent LH.5 sample indicates predominant early Paleozoic zircon age populations (Fig. 18). The EBL and HTG samples show both 220–280 Ma and 380–480 Ma age clusters, whereas the KB and DCS samples are characterized by the 380–480 Ma cluster. In addition, Paleoproterozoic age signals are also relatively prominent in HTTL and LH.5 samples, probably revealing the contributions from the adjacent Quanji massif. All the detrital zircon age features demonstrate localized, diverse sediment source terranes for the Qaidam basin Q_{1+2} deposits (Fig. 21C). This interpretation is consistent with the intense lake contraction and depositional area segmentation in the Qaidam basin during the Quaternary time (Owen et al., 2006;

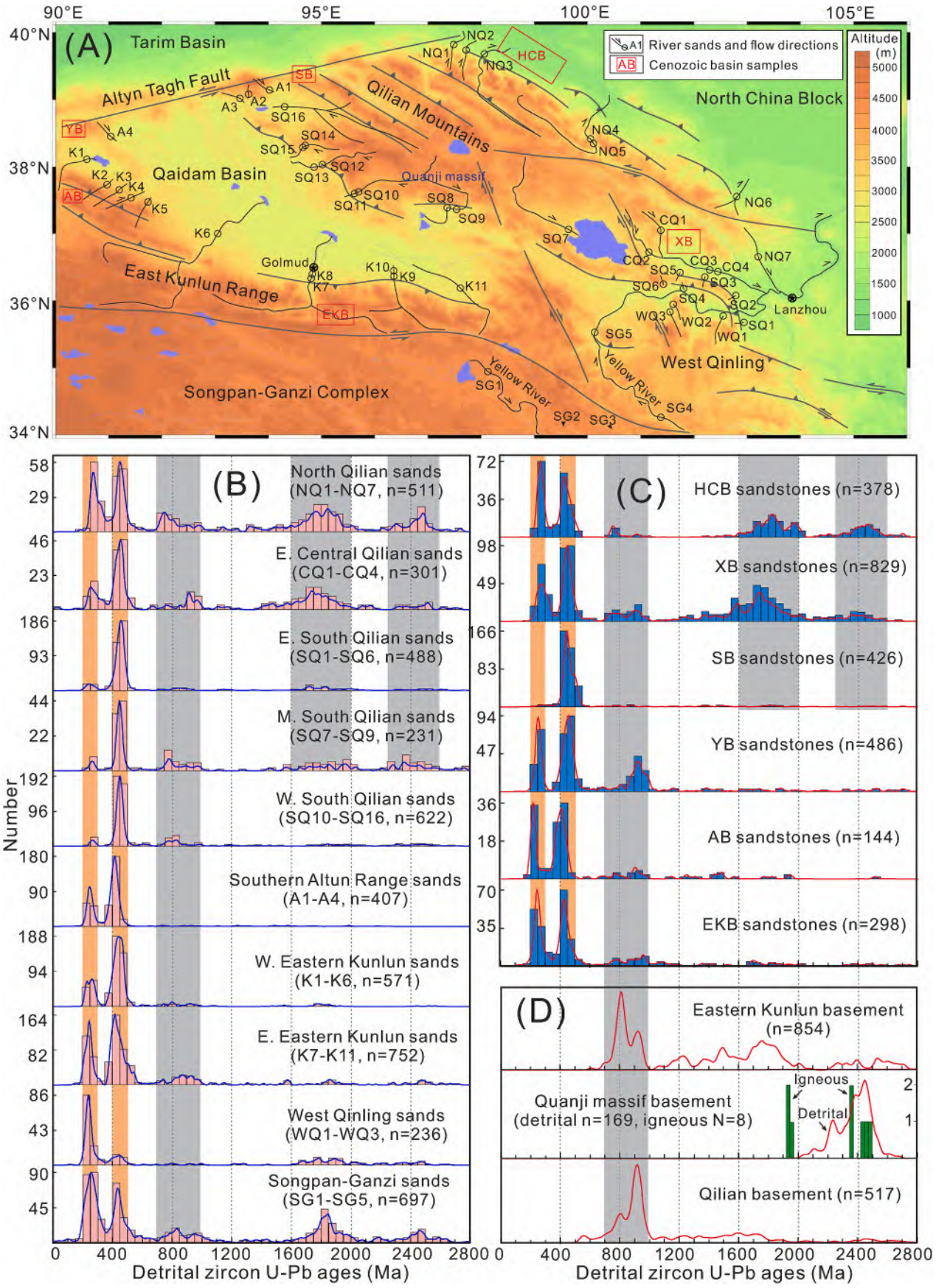

(caption on next page)

Fig. 11. (A) The locations of modern river sands and representative Cenozoic intermountain basins with reported detrital zircon age data in northern Tibetan Plateau. (B) Detrital zircon age KDE plots for the river sands. The detrital zircon U–Pb age data of modern river sands are from Lease et al. (2007); Liu et al. (2012); Li et al. (2013); Nie et al. (2015); Wang et al. (2016); Gong et al. (2017); Song et al. (2019); Kang et al. (2018, 2019, 2020); Zhang et al. (2021); Zhang et al. (in press) and Feng et al. (2023). Note that the rivers have different drainage ranges. For example, the data of Lease et al. (2007) are from very small rivers in the east part of South Qilian belt (SQ1–SQ6) and in the West Qinling belt (WQ1–WQ3). The Songpan-Ganzi Complex zircon age signatures involve samples SG1–SG5 (SG2 and SG3 are not shown in the map), from the most upper reaches of the Yellow River (Nie et al., 2015). (C) Detrital zircon age KDE plots of Cenozoic strata from representative intermountain basins (for the basin full names and detrital zircon data sources, see the captions of Fig. 10) in the northern Tibet. (D) Zircon age signatures of the Qilian and Eastern Kunlun orogens and the Quanji massif. Note that the Quanji massif, which is a part of the southern Qilian metamorphic belt, has basement rocks with obvious 1700–2000 Ma and 2300–2600 Ma zircon age signatures. The detrital zircon U–Pb age data of Precambrian basements of the surrounding ranges are from Gehrels et al. (2003, 2011), Xu et al. (2007), Wang et al. (2008b), Chen et al. (2009, 2012), Yu et al. (2017, 2019) and Jian et al. (2019a, 2020).

Zhuang et al., 2011; Guan and Jian, 2013; Heermance et al., 2013). Both source terrane tectonic deformation-induced variations and depositional environment changes could contribute the Q_{1+2} detrital zircon age diversity.

7.2. Temporal variations of the major depositional areas

We note that the detrital zircon U–Pb age populations of samples from different locations indicate diverse temporal variation trends (Figs. 19 and 20; Figs. S2–S3). For example, the 25 samples from the DHG section in the eastern Qaidam basin display complicated variations in detrital zircon age populations. Three lower E_{1+2} samples therein are dominated by 400–480 Ma detrital zircon age populations, whereas Permian–Triassic and Precambrian (particularly Paleoproterozoic) age populations are commonly present in those upper E_{1+2}, E_3 and N_1 samples (Fig. 19). Ordovician–Devonian ages are dominant in the age clusters of all the N_2^1 samples and some N_2^2 samples, while other N_2^2 samples and the N_2^3 samples are characterized by Permian–Triassic and Paleoproterozoic age populations again (Fig. 19). We advocate that the Qilian Mountains had been the major source area for the deposits in the DHG area since the period of the initiated lake basin expansion (i.e., the mid–late Eocene) and the variations in the Permian–Triassic and Precambrian age populations most likely reveal varied contributions of related parent-rocks in the South Qilian and North Qaidam belts. The compilation results of the PT and YCG samples (these two sections are close to each other) indicate that the Permian–Triassic age signals are comparatively minor in the E_{1+2}, E_3 and N_1 strata but are dominant in most N_2^1, N_2^2, N_2^3 and Q_{1+2} strata (Fig. S2). Precambrian ages are generally minor in these samples and indicate relatively higher in the lower stratigraphic units, compared to the upper units (Fig. S2). Samples from the easternmost part of the basin, i.e., the HTTL samples, also reveal temporal variations in detrital zircon age populations but have quite different variation trends from the DHG, PT and YCG samples mentioned above. The major changes are from the abundances of the Ordovician–Devonian and Paleoproterozoic ages (Fig. S3). Given the overwhelming south- and southwest-directed paleocurrent orientations (Figs. 12–18) and the complex tectono-magmatic history of the Qilian Mountains (Figs. 10 and 11; Zuza et al., 2018; Zhang et al., 2021), we contend that all the detrital zircon age temporal variations in these sections from E_3 strata to Q_{1+2} strata are due to variable contributions of the different micro-terranes in the Qilian Mountains (Fig. 21), rather than detritus supply from the Altun and Eastern Kunlun ranges.

By contrast, the detrital zircon age populations of the western Qaidam basin samples only exhibit slight variations over time. Take the Huatugou region (involving HTG and GCG sections) as an example, all the published 18 sandstone samples are featured by dominant 400–480 Ma and 220–280 Ma age clusters, with subordinate 750–1000 Ma ages and few Paleoproterozoic ages (Fig. 20). We favor that the detrital zircon grains in the western Qaidam basin were relatively stably fed by terranes in the surrounding Altun and Eastern Kunlun ranges during the whole Cenozoic (Fig. 21), consistent with previous propositions (e.g., Cheng et al., 2016a, 2019b; Zhu et al., 2017; Wang et al., 2020; Xia et al., 2021). Note that the detrital zircons of the Songpan-Ganzi Complex are characterized by Paleoproterozoic ages (Fig. 11; Weislogel et al., 2010; Ding et al., 2013; Jian et al., 2019a), which are different from the ones in the Cenozoic western and southern Qaidam basin sandstones (e.g., KB and DCS samples) and in Cenozoic samples from the intermountain basin (e.g., EKB) within the Eastern Kunlun Range (Fig. 11C). Therefore, we contend that the Eastern Kunlun Range has uplifted since the initiation of Cenozoic Qaidam basin deposition (Fig. 21) and acted as a topographic barrier against detritus supply from the Songpan-Ganzi regions to the south.

8. Bias in detrital zircon provenance interpretations for the Cenozoic Qaidam basin

Most previous detrital zircon-based provenance studies on the Cenozoic Qaidam basin usually attribute the age pattern variations to source terrane changes that are related to regionally variable tectonic and/or climatic processes (e.g., Bush et al., 2016; Cheng et al., 2016a, 2016b, 2019b; Wang et al., 2017; Song et al., 2019; Zhuang et al., 2019; Wu et al., 2019b; Xia et al., 2021). However, there are a range of biases that may influence detrital zircon age signals and thus confuse the provenance interpretations, as detailed in the following sections. These include lithologic erodibility (or durability) and zircon fertility of sediment parent-rocks, depositional settings, hydrodynamic sorting, zircon recycling and selective sampling and analysis (e.g., Fedo et al., 2003; Lawrence et al., 2011; Sláma and Košler, 2012; Malusà et al., 2013; Zimmermann et al., 2015; Capaldi et al., 2017; Muhlbauer et al., 2017; Ibañez-Mejia et al., 2018; Chew et al., 2020; Anders et al., 2022; Dröllner et al., 2022; Sylvester et al., 2022).

8.1. Grain size and morphology of the analyzed detrital zircons

Our data demonstrate that the Paleoproterozoic zircon grains are relatively small (most <125 μm) in size, whereas the large zircon grains are dominated by Phanerozoic ages (Fig. 9A). Specifically, the proportions of Permian–Triassic and Paleoproterozoic ages are influenced by detrital zircon grain sizes (Fig. 9C). This might be due to more sedimentary cycles for some of the older zircon grains that were supplied by metasedimentary parent-rocks, such as the Precambrian metamorphic basement rocks in the surrounding mountains (Fig. 1D; Yu et al., 2017). Similar phenomena that older grains are smaller on average and younger zircons have coarser and more variable sizes have also been observed by several other detrital zircon geochronological studies on both modern and deep-time records (e.g., Lawrence et al., 2011; Yang et al., 2012). Therefore, hydrodynamic fractionation of age populations can't be ignored when interpreting detrital zircon provenance. Furthermore, we note that most of the elongated zircon grains (i.e., length/width ratios >2) are dominated by Phanerozoic ages (Fig. 9B). Previous studies have also found that rounded grains are statistically older than euhedral grains in some cases (e.g., Malusà et al., 2013). These results reveal that dating detrital zircon grains with different morphological features to some extent may result in intra- and inter-sample diversity in age populations and thus should be concerned in detrital zircon provenance analysis. Several recent case studies demonstrate that detrital zircon grain shape and surface microtexture analyses in combination with U–Pb data permit more robust provenance interpretations (Finzel, 2017; Makuluni et al., 2019; Bónová et al., 2020; Armstrong-Altrin et al., 2021; Zeh and Cabral, 2021). In addition,

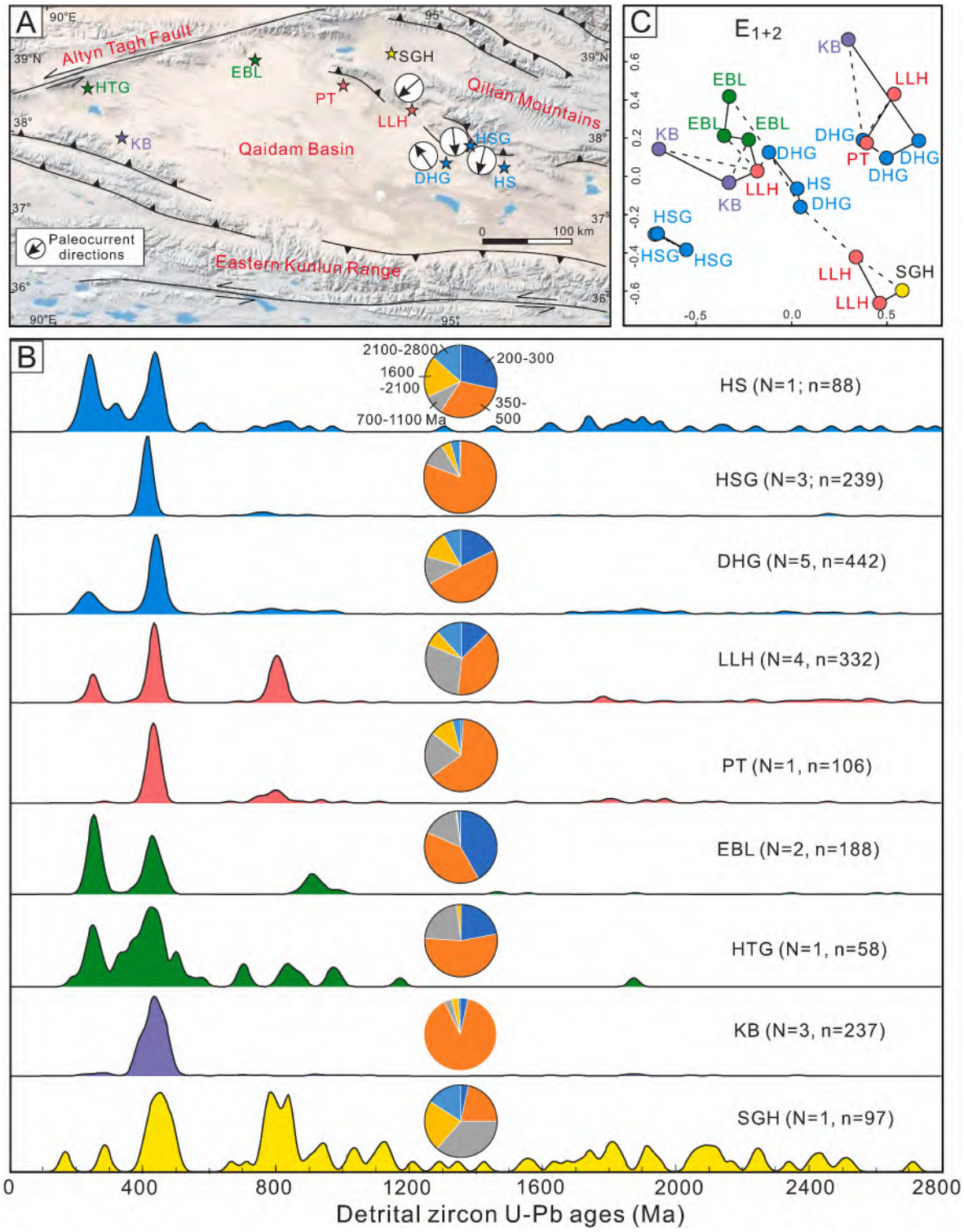

Fig. 12. Detrital zircon sample locations and paleocurrent orientations (A), U–Pb age distributions (B) and age non-metric multi-dimensional scaling (MDS) plots (C) for E_{1+2} sandstone samples. The R programming language-based Provenance software (Vermeesch et al., 2016) was employed for the MDS illustration. Each paleocurrent symbol shows dominant paleocurrent orientation and covers published data and new data in this study. For detrital zircon age data sources, see Table A3 in Appendix A.

human-induced methodological bias (e.g., sampling, mineral separation and selection) have been widely recognized (Sircombe and Stern, 2002; Sláma and Košler, 2012; Dröllner et al., 2021; Zutterkirch et al., 2022) and deserve more attention in detrital zircon age-based provenance studies.

8.2. *Sedimentary facies of the analyzed sandstones*

Variations in depositional settings or microenvironments where the analyzed sediments accumulate may influence detrital zircon populations, even for those sediments with the same routes or sediments from the same source regions (Lawrence et al., 2011; Ibañez-Mejia et al.,

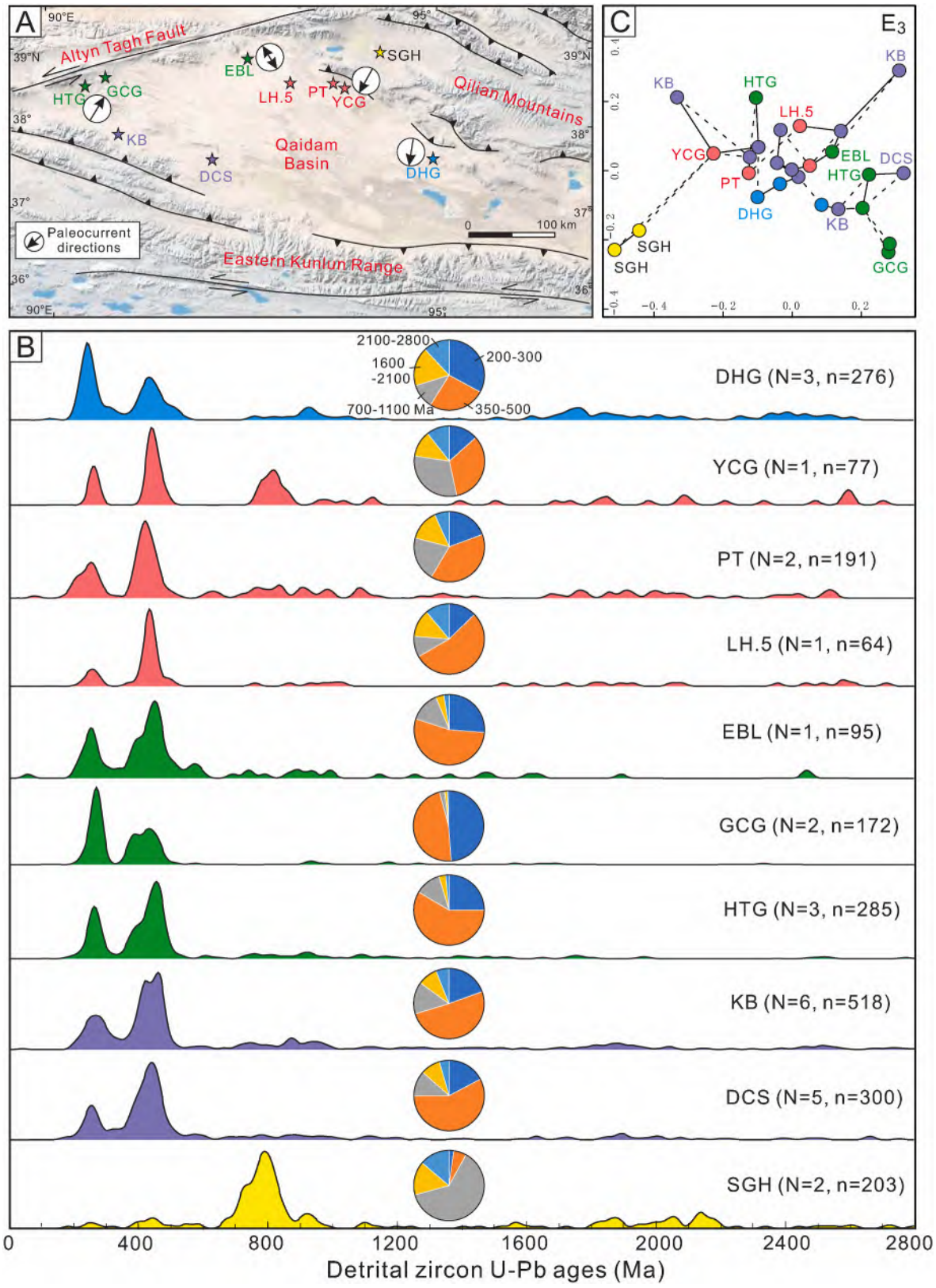

Fig. 13. Detrital zircon sample locations and paleocurrent orientations (A), U–Pb age distributions (B) and age MDS plots (C) for E_3 sandstone samples.

2018). Sediments from distal settings (such as marginal sea or lake environments) generally contain mixed detrital zircon grains from diverse source terranes and thus exhibit a wider spread of detrital zircon ages than those proximal (such as alluvial fan or fluvial environments) deposits in a sediment source-to-sink system (Avigad et al., 2015). This means that, unless a sedimentary system is extremely well mixed and homogenized, the provenance signal should be retained, but will vary within a basin depending on depositional environments and facies (e.g., Anders et al., 2022). A great number of case studies have realized the facies-related bias in detrital zircon U–Pb geochronological data and

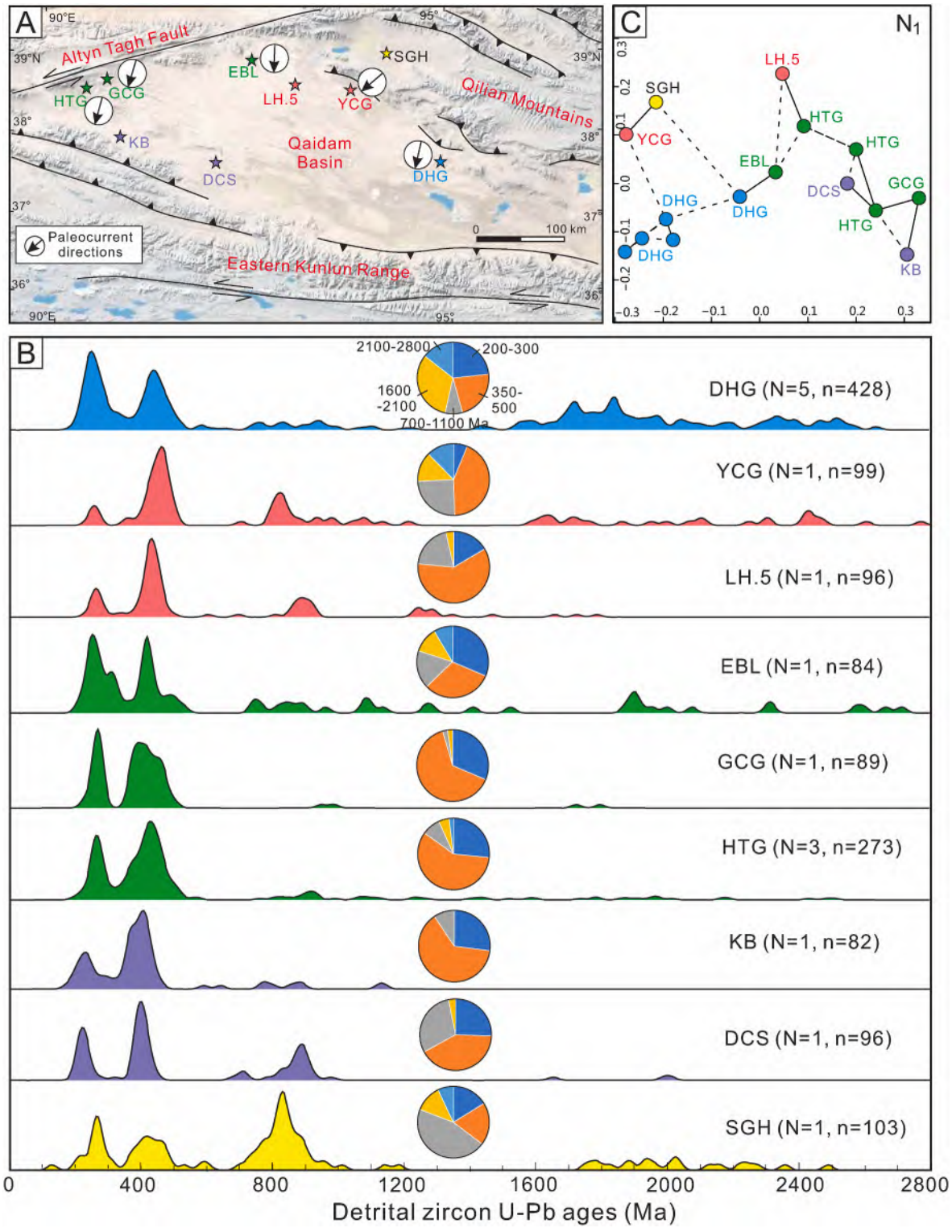

Fig. 14. Detrital zircon sample locations and paleocurrent orientations (A), U–Pb age distributions (B) and age MDS plots (C) for N_1 sandstone samples.

highlighted the importance of sedimentological parameters in zircon provenance analysis (e.g., DeGraaff-Surpless et al., 2003; Avigad et al., 2015; Zimmermann et al., 2015; Leary et al., 2020; Anders et al., 2022; Sylvester et al., 2022). For instance, a case study on the Cretaceous Methow basin, southern Canadian Cordillera indicates that deep-water turbidite deposits have comparatively systematic and predictable detrital zircon age heterogeneity, whereas fluvial deposits have heterogeneous detrital zircon age distributions that vary unpredictably from sample to sample (DeGraaff-Surpless et al., 2003). The Upper Cretaceous interbedded mudstone and sandstone strata from the Raton basin, Colorado (USA), revealing prodelta and delta-front facies, respectively, were found to have significantly different detrital zircon age populations (Sylvester et al., 2022).

As mentioned above, the Qaidam basin has temporally and spatially varied rock associations and sedimentary facies (Figs. 2–4). The dated sandstone samples in this study accumulated in different depositional

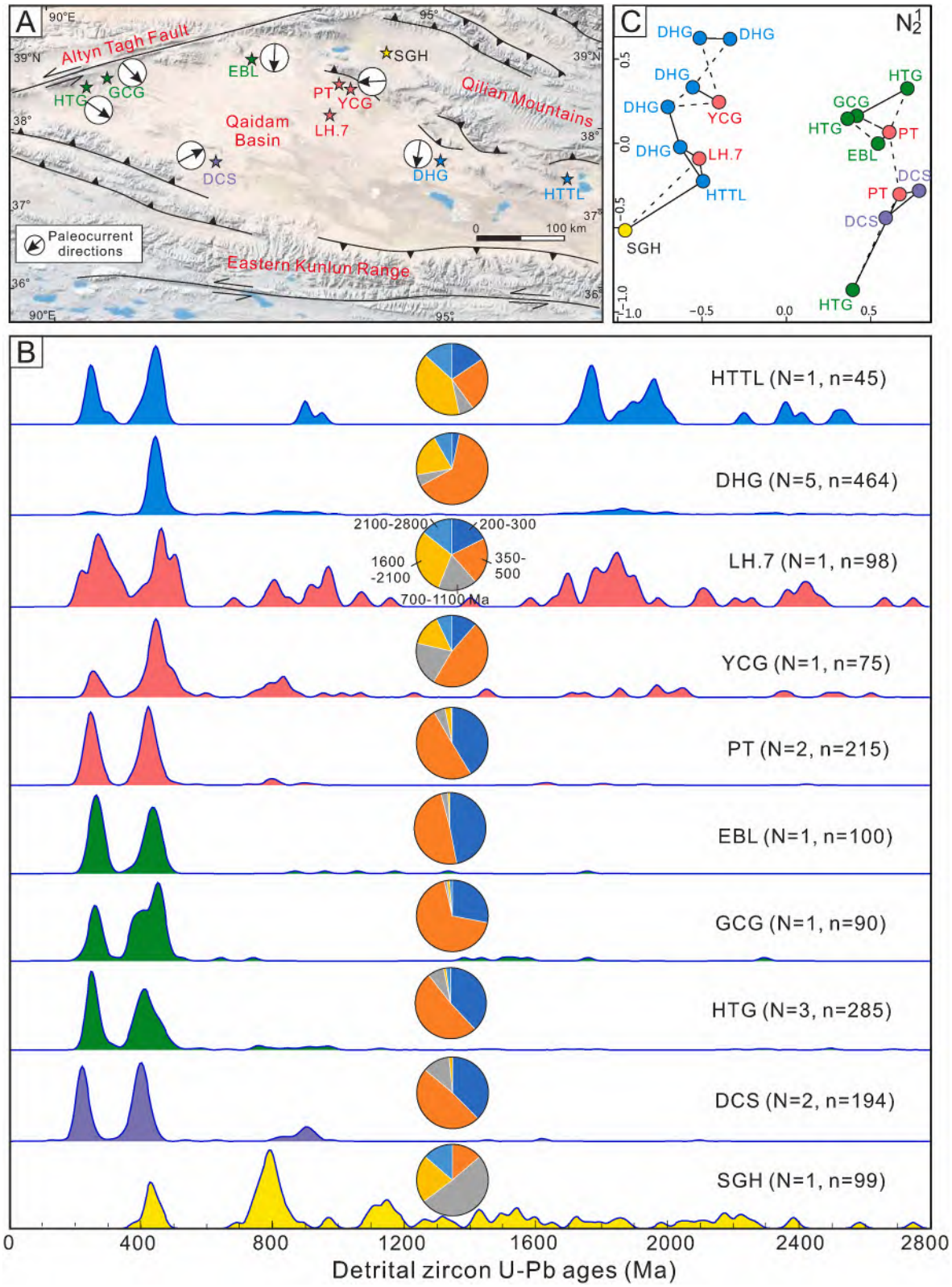

Fig. 15. Detrital zircon sample locations and paleocurrent orientations (A), U–Pb age distributions (B) and age MDS plots (C) for N_2^1 sandstone samples.

environments (Table A1). The Cenozoic basal E_{1+2} strata are composed of distal fluvial to marginal lacustrine deposits and proximal fluvial deposits along the southern margin of the basin whereas proximal alluvial fan deposits occur in the northern and eastern parts of the basin (Zhuang et al., 2011; Guan and Jian, 2013; Cheng et al., 2019a; Jian et al., 2023). In this case, the analyzed detrital zircon grains in sandstone interlayers within massive conglomerate beds (Fig. 3) from the northern and eastern Qaidam basin were most likely derived from localized, spatially diverse sources with small drainage networks (Fig. 21A; Jian et al., 2023), rather than the southern distant Qimantagh and Eastern

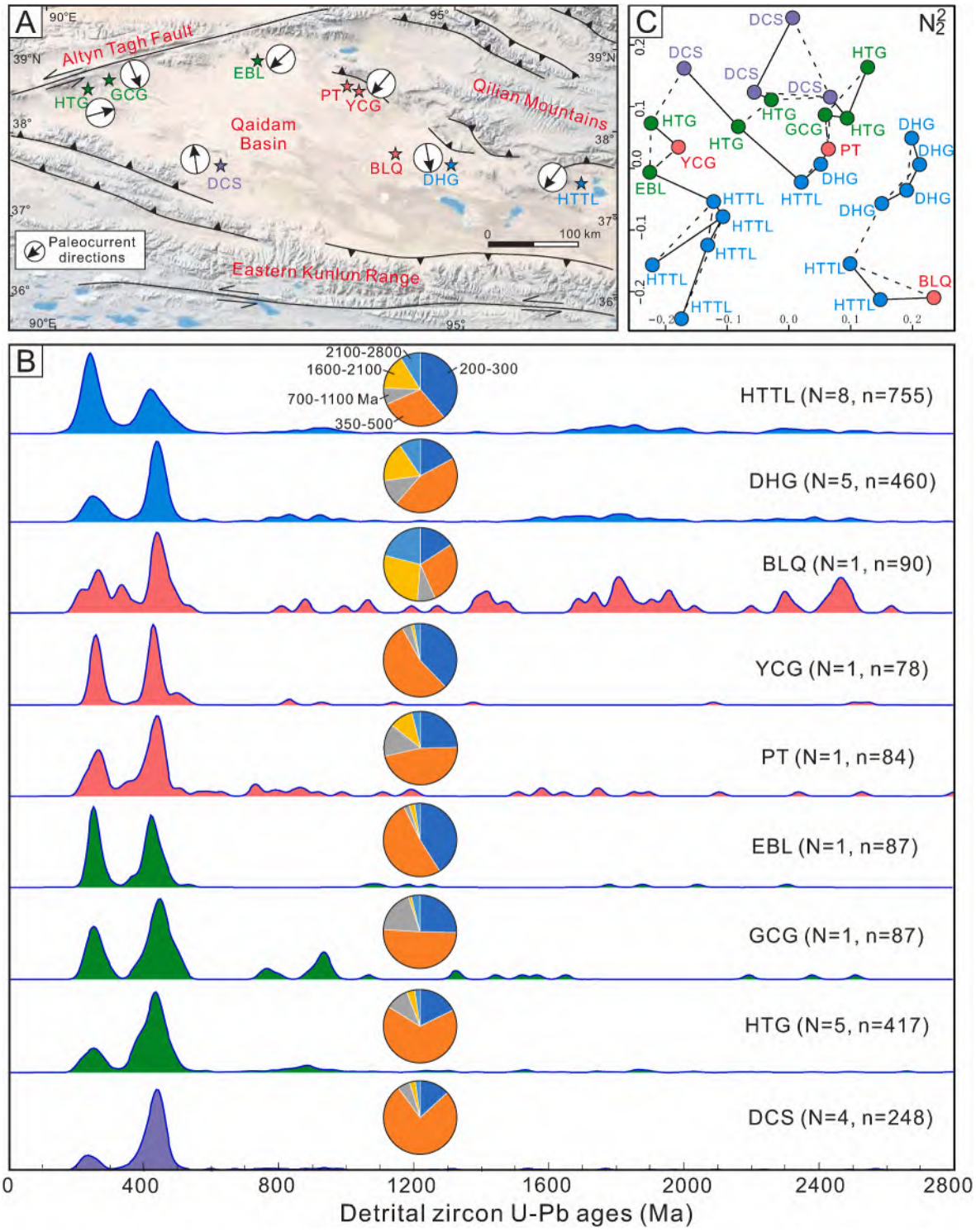

Fig. 16. Detrital zircon sample locations and paleocurrent orientations (A), U–Pb age distributions (B) and age MDS plots (C) for N_2^2 sandstone samples.

Kunlun regions. The overlying E_3, N_1, N_2^1 and N_2^2 strata in most regions of the Qaidam basin are dominated by fine-grained deposits (siliciclastic deposits for the northern and eastern regions and mixed carbonate-siliciclastic deposits for the western regions; Fig. 2; Fig. 4). These sedimentary strata were deposited in fluvial, deltaic and lacustrine environments (Fig. 22; Zhuang et al., 2011; Guan and Jian, 2013; Jian et al., 2018; Fu et al., 2022) and a relatively unified megalake is inferred to have existed during this depositional stage (Liang et al., 2021; Wu et al., 2021b). Furthermore, we note that the E_3–N_2^2 strata in the wide northern and eastern Qaidam basin regions are characterized by thin interbedded sandstone and mudstone assemblages, various fine-grained siliciclastic lithofacies associations and intermittent exposure-caused sedimentary structures or records (such as mud cracks, vertical biological burrows and paleosols, Fig. 4), revealing dominant marginal lacustrine and shallow-water delta environments with high-frequency variations in microenvironments in a low-gradient depositional system (Fig. 22; Zhuang et al., 2011; Song et al., 2022a, 2022b). The current Poyang Lake (Fig. 22), which is a large, ephemeral

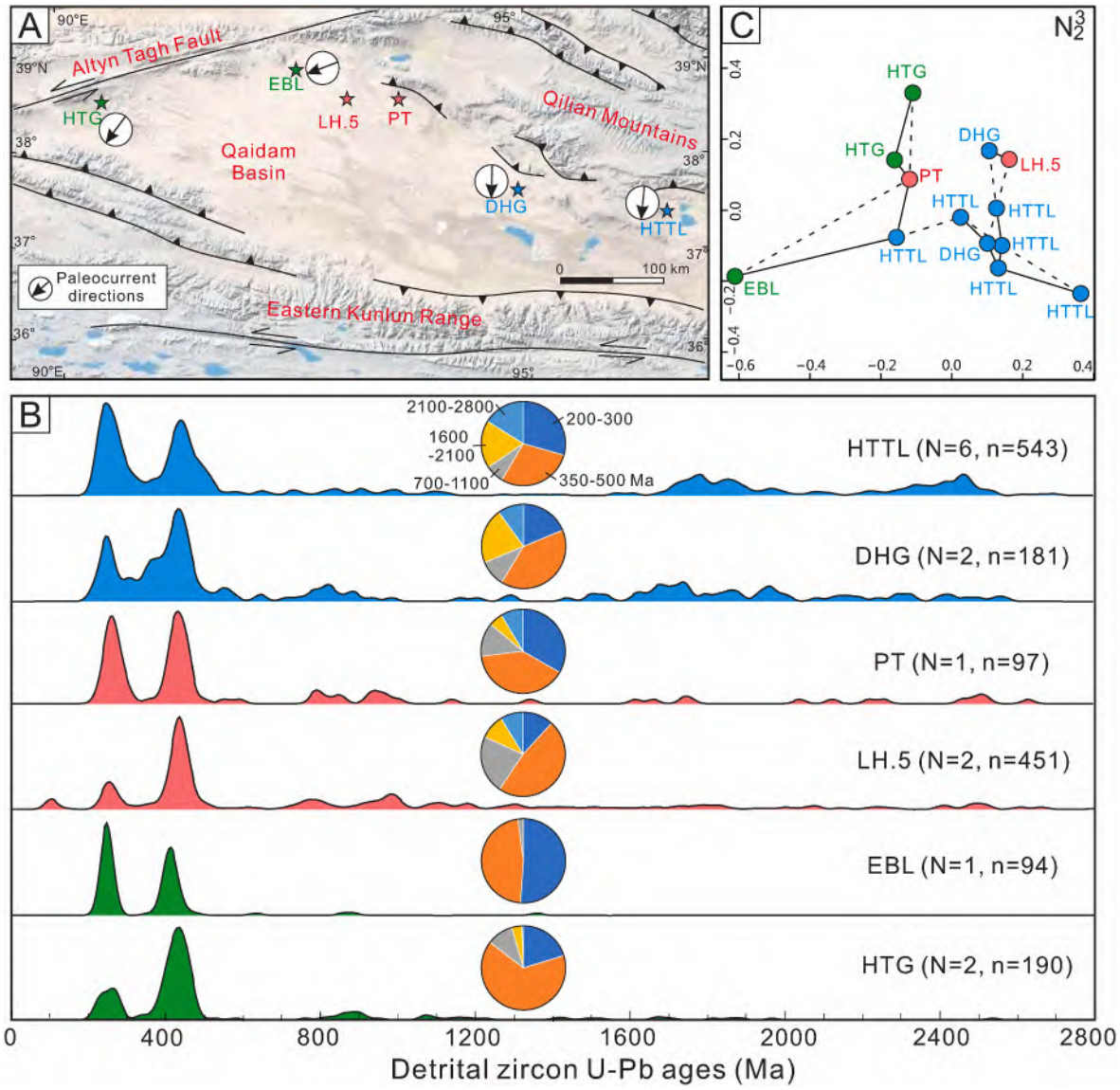

Fig. 17. Detrital zircon sample locations and paleocurrent orientations (A), U–Pb age distributions (B) and age MDS plots (C) for N_2^3 sandstone samples.

lake in Jiangxi Province, south China (Feng et al., 2012) and covers more than 4000 km^2 (mean lake water level > ca. 20 m) in flood seasons and less than 500 km^2 (mean lake water level < ca. 12 m) in dry seasons, can be regarded as a modern analogue for the Qaidam paleo-megalake during the Miocene time. Although tectonic and climatic settings and the size of the Poyang Lake differ significantly from those of the Miocene Qaidam megalake, these two lake systems have flat floors, shallow water and fine-grained sediment fill and exhibit evident short-timescale variations in lake water body areas and sedimentary microenvironments (Fig. 22). We suggest that these sedimentary microenvironment variations may result in different detrital zircon populations under unchanging source region conditions (i.e., without tectonic deformation in source terranes).

Here, conceptual models (Fig. 23) are built to illustrate how the potential depositional environment changes during flood-dry cycles (i.e., lake level fluctuations) alter detrital zircon U–Pb age signals in sandstone samples. These models provide possible explanations for the above-mentioned, various temporal and spatial variations in E_3–N_2^2 detrital zircon age populations of the investigated sections in the northern and eastern Qaidam basin. Although million-year-scale climate changes have been highlighted to play crucial roles in mountain erosion and thus in the varied detrital zircon records (Cheng et al., 2019b), we favor that the short-term fluctuant microenvironments can be either climate-controlled or non-climate-controlled. In other words, the observed detrital zircon age variations among samples from a sedimentary section or from different regions may be sedimentological parameter-related, rather than due to mountain tectonic deformation events or regional climate changes. The N_2^3 and Q_{1+2} strata in the Qaidam basin also indicate spatially various lithofacies associations, with massive conglomerate-dominated proximal deposits (Fig. 3) in some regions and mixed carbonate-evaporite-siliciclastic fine-grained brackish lake deposits in other regions (e.g., Heermance et al., 2013; Jian et al., 2014; Fu et al., 2022; Wang et al., 2023). Sedimentary depocenters shifted eastward (Yin et al., 2008b; Bao et al., 2017) and the paleo-Qaidam lake was separated into several small lakes during this stage (Fig. 21C). We contend that detrital zircons grains in these N_2^3 and Q_{1+2} deposits were derived from local sources under restricted routing systems and the facies diversity should be also concerned in provenance interpretations.

8.3. Zircon fertility of the potential parent-rocks

Different types of rocks on the Earth have variable zircon contents. Specifically, granitic plutons and granitoid gneisses for which granitic

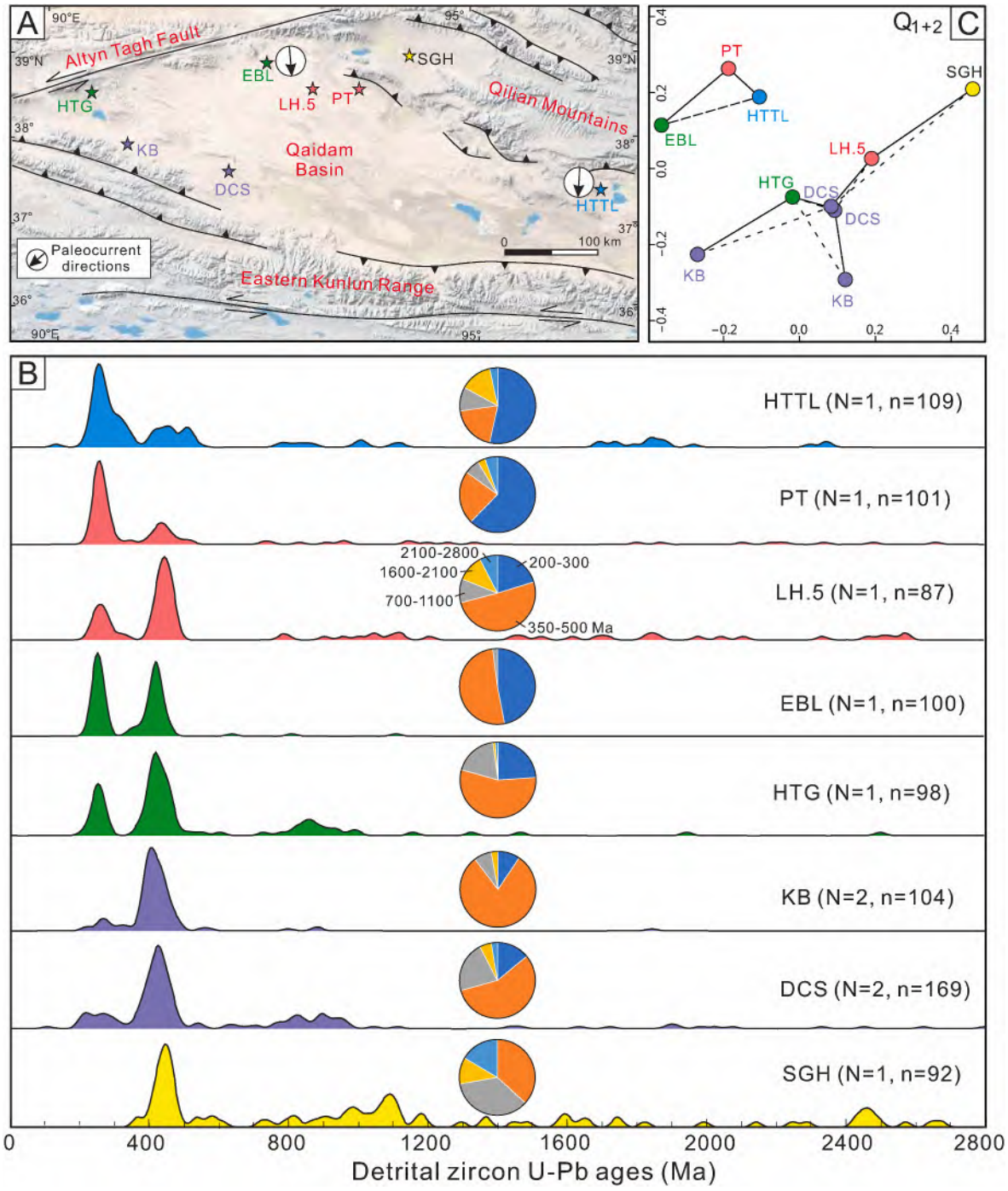

Fig. 18. Detrital zircon sample locations and paleocurrent orientations (A), U–Pb age distributions (B) and age MDS plots (C) for Q_{1+2} sandstone samples.

rocks were the protolith are commonly richer in zircon than mafic plutonic and metaplutonic rocks (Lee et al., 2016 and references therein). Among sedimentary rocks, the mature, polycyclic sandstones are generally expected to have more zircon grains than mudstones, carbonate rocks and relatively immature sandstones. Even granitic rocks might not be expected to be equally fertile for zircon production when serving as sediment parent-rocks (Moecher and Samson, 2006; Dickinson, 2008). In view of these scenarios, heterogeneous zircon fertility of detrital source terranes has been highlighted as a non-ignorable bias in detrital zircon record in many cases (e.g., Sláma and Košler, 2012; Cawood et al., 2013; Spencer et al., 2018; Chew et al., 2020; Flowerdew et al., 2020).

The zircon fertility of source terranes can be determined by measuring zircon contents in related river (draining source terranes) sediments that are not significantly affected by hydraulic-sorting processes (Malusà et al., 2016). This is a direct, quantitative approach that is quite practicable for modern settings and for those ancient catchments that were not markedly different from their present-day configurations (Malusà et al., 2016). However, this approach might not be applicable to the Cenozoic Qaidam basin, since the past surrounding mountain catchments and paleogeographic environments are highly enigmatic (Fig. 21). Although the element Zr enters the lattices of some other rock-forming minerals sparingly, zircon abundances in potential parent-rocks generally vary with Zr contents (Dickinson, 2008).

Here, we compile published bulk-rock Zr content data of crystalline rocks (mostly felsic igneous rocks) from the Qilian, Eastern Kunlun and

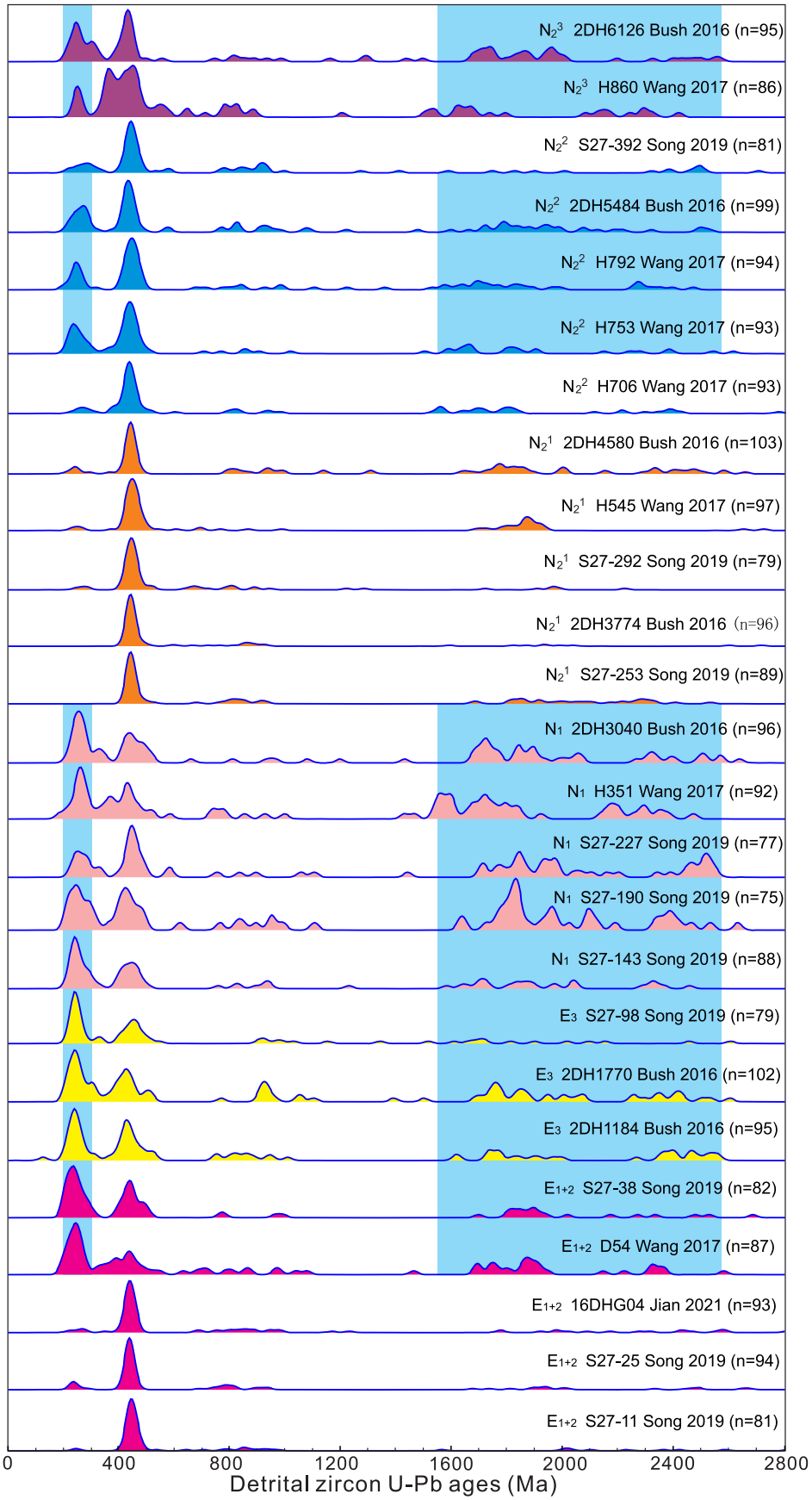

Fig. 19. Detrital zircon U–Pb age distributions of the Cenozoic sandstone samples from the DHG area in eastern Qaidam basin. The Data are from Bush et al. (2016); Wang et al. (2017); Song et al. (2019) and Jian et al. (2023). Note that stratigraphic information of the samples from Bush et al. (2016) was corrected based on Lu et al. (2018).

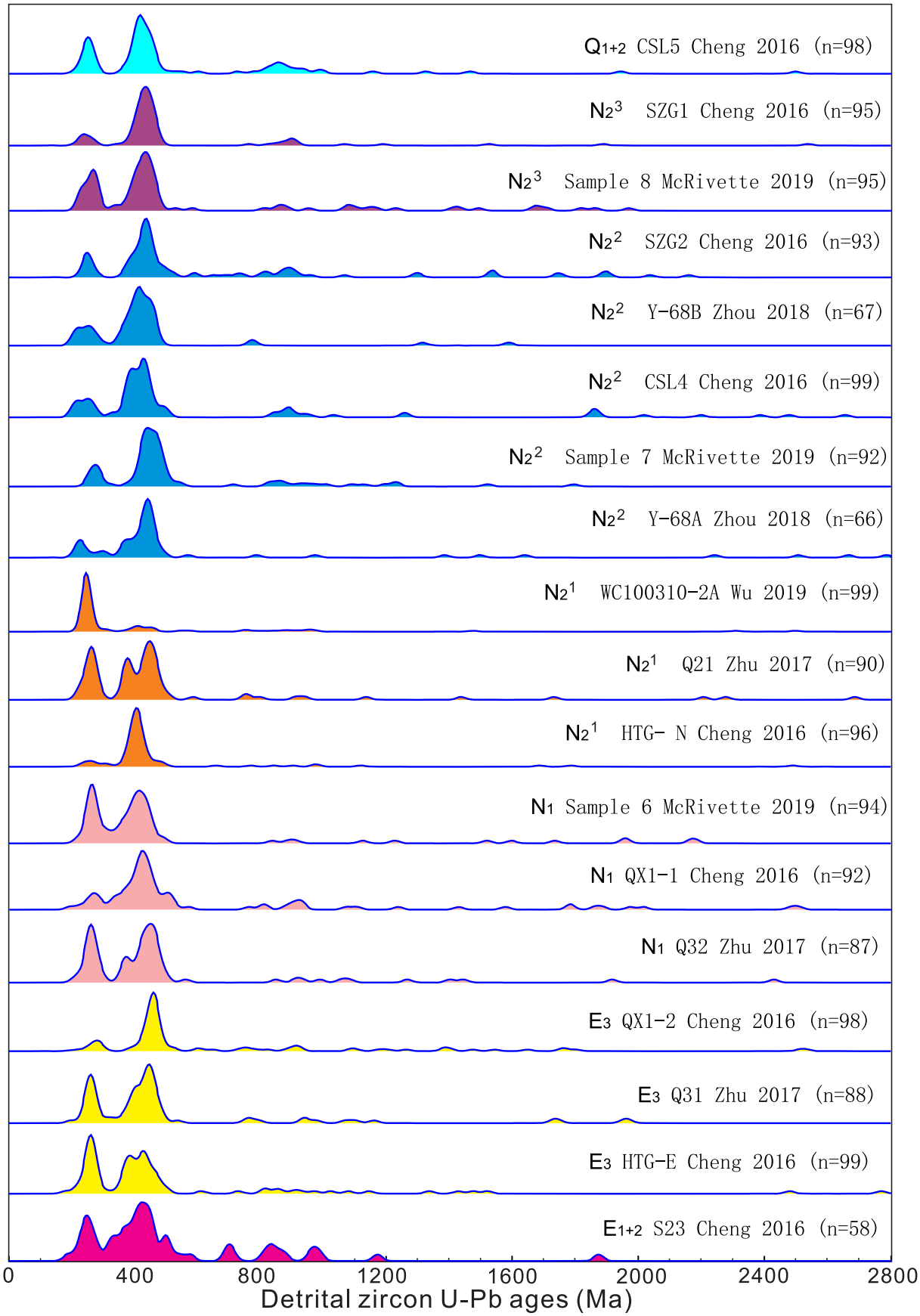

Fig. 20. Detrital zircon U–Pb age distributions of the Cenozoic sandstone samples from the HTG area in the western Qaidam basin. Data are from Cheng et al. (2016a, 2016b), Zhu et al. (2017), Zhou et al. (2018), McRivette et al. (2019) and Wu et al. (2019a).

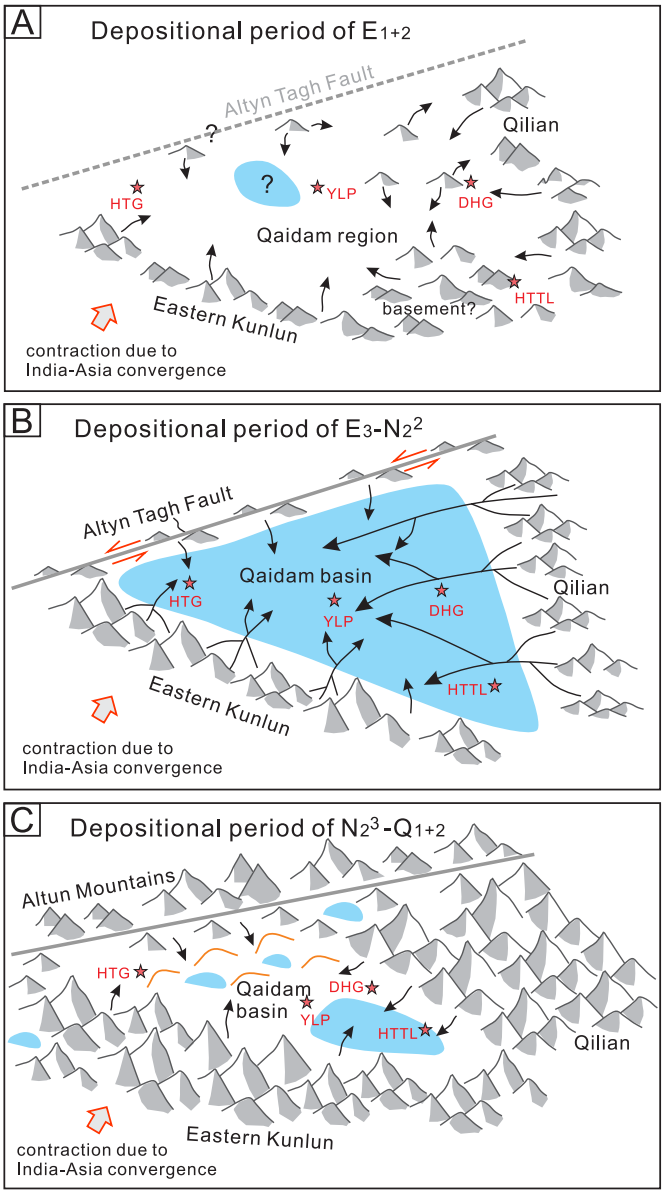

Fig. 21. Simple models for the basin-range relations and sediment routing systems for the Cenozoic Qaidam basin. (A) The Qaidam region was most likely present as isolated depocenters at the beginning of the Cenozoic deposition. Most E_{1+2} strata were preferred to be fed by localized, spatially diverse sources with small drainage networks; (B) In the lake basin expansion stage, the Qaidam basin received detritus from the surrounding large mountains and the Qilian Mountains contributed most sediments for the basin, especially for the northern, eastern and center regions; (C) During the depositional period of N_2^3 and Q_{1+2} strata, the surrounding ranges intensively uplifted and widespread shortening occurred in the western Qaidam basin. The unified paleo-Qaidam lake contracted and was then separated into several small scattered saline-brackish lakes. Sediments were derived from local sources in these mountains and the sediment routing systems returned to be restricted during this time. Red pentagrams indicate inferred section locations (YLP: Yiliping area, showing the center of the Qaidam basin). Black lines with arrows show major sediment supply directions and coverage areas. Gray areas indicate eroded regions and the blue areas show the extent of lakes. Orange curved lines in panel C indicate syn-depositional folds and crustal shortening areas. Note that the depocenters of the Qaidam basin shifted from the western area to the eastern area during the Cenozoic (Yin et al., 2008b).

Altun ranges to assess zircon fertility of the potential parent-rocks with different ages and compositions (Fig. 24). The data synthesis indicates that the element Zr contents are markedly variable (50–800 ppm) in each age group (Fig. 24A). Available data from the Paleoproterozoic crystalline rocks in the Qilian Mountains, although not numerous, demonstrate relatively high Zr contents in some samples (>300 ppm), compared with those of other age groups (Fig. 24A). This reveals that, although Paleoproterozoic rocks are less exposed in the Qilian Mountains, these old basement crystalline rocks may contribute abundant detrital zircons to the surrounding depositional systems. This provides a plausible explanation for the prominent Paleoproterozoic detrital zircon age signals in some Cenozoic samples from the northern Qaidam basin, Xining basin and the Hexi Corridor basin (Fig. 11; Figs. 12–19). In addition, even for those acid igneous rocks (e.g., granite), variable Zr contents are evident. The relationships between Zr and SiO_2 contents (Fig. 24B) show that most high-Zr igneous rocks indicate SiO_2 contents ranging ~65–70%, meaning possible high zircon fertility of these rocks. Compilation results of other orogens also indicate similar bulk-rock Zr–SiO_2 relationships (e.g., Lee et al., 2016). This can be explained as follows. In the magma crystallization and differentiation processes, mafic magmas are initially under-saturated in zircon, allowing Zr contents of fractionating magmas to rise with increasing SiO_2 until saturation conditions are reached, after which Zr contents decline by zircon fractionation (Watson and Harrison, 1983; Lee and Bachmann, 2014; Lee et al., 2016). In addition to the magma composition, temperature, oxygen fugacity and pressure of the magmas are also thought to contribute the zircon saturation (Watson and Harrison, 1983; Boehnke et al., 2013) and fertility of the crystalline forming rocks. Based on the published bulk-rock Zr data (Fig. 24), we estimate that the potential source terranes with different crystalline rock types in northern Tibet may produce two–three orders of magnitude differences in zircon fertility.

We realize that the element Zr data of course may not exactly reflect zircon fertility of the source rocks and are prone to introduce further unquantifiable bias in detrital studies. For example, fine-grained zircon too small for provenance analysis are incorporated into the fertility estimates, resulting in systematically lower zircon fertility values by measuring mineral concentrations in sediments, than those based on geochemical analyses (Malusà et al., 2016). These data at least provide referable information for better understanding the zircon fertility of the potential parent-rocks of the Cenozoic deposits in the Qaidam basin. Furthermore, lithologic erodibility (or durability) of the detrital source terranes also plays a significant role in zircon supply to sediment sinks (e.g., Capaldi et al., 2017; Spencer et al., 2018) and thus deserves more attention in detrital zircon provenance interpretations.

8.4. *Recycling of the zircon grains*

Zircon has been well known as a highly resistant accessory mineral in chemical and physical weathering and diagenetic processes (Morton and Hallsworth, 1999; Garzanti et al., 2018). The remarkable durability allows for zircon grains to survive multiple episodes of sedimentary recycling. There is a quotation from William A. Thomas (2011) about the role of detrital zircons in sedimentary provenance studies: the good news is once in the system, zircons stay in the system; and the bad news is once in the system, zircons stay in the system. Given the high closure temperature (>900 °C; Cherniak and Watson, 2001) of Pb diffusion in zircon, the U–Pb geochronological information it carries, therefore, may not relate to crystalline rocks exposed during the sedimentary cycle in question, but to the zircon-bearing sources of the parent sandstones (or metasandstones), or even to earlier sources prior to several recycling events (e.g., Andersen et al., 2016; Zotto et al., 2020). A growing number of instance studies have realized the universality of the zircon recycling regime and have emphasized that the possibility for reworking resistant zircons through multiple sedimentary cycles should always be taken into account for detrital zircon provenance interpretations (e.g., Campbell

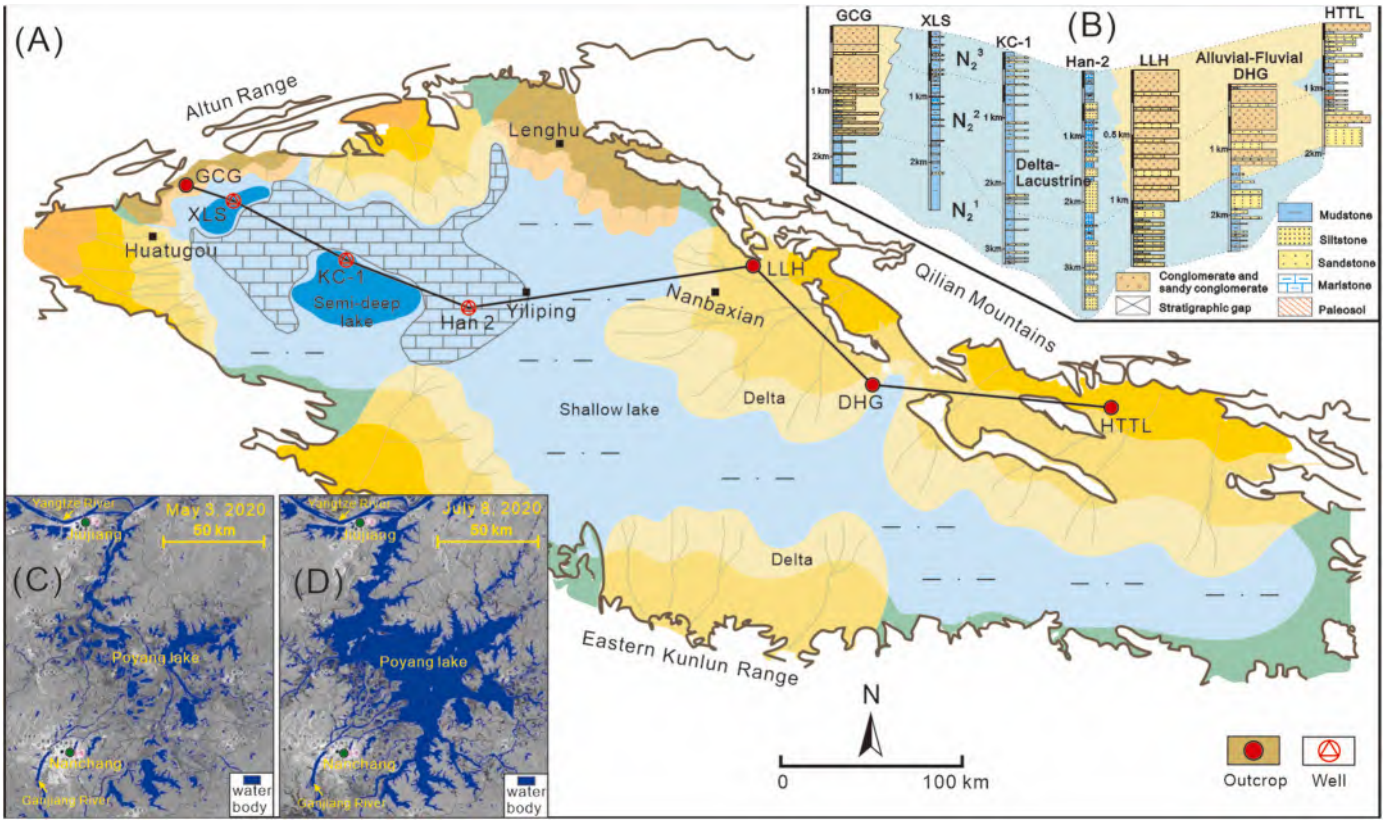

Fig. 22. (A) Paleogeography and sedimentary environments of the Miocene Qaidam basin, modified from Song et al. (2022a) and Wang et al. (2023). (B) Representative outcrop and drill well stratigraphic profiles showing N_2^1, N_2^2 and N_2^3 lithological records and the evolution of the Miocene paleo-Qaidam lake (Wang et al., 2023). (C) and (D) Remote sensing satellite images indicate significant variations in Poyang Lake distributions during periods of high water and low water levels (modified from China Water Resources & Hydropower Science Research Institute). The water body areas of the Poyang Lake were ca. 1400 km^2 (C) and 3900 km^2 (D) on May 3, 2020 and July 8, 2020, respectively. We suggest the Poyang Lake as a modern analogue for the Miocene shallow-water paleo-Qaidam lake, in which short-timescale sedimentary microenvironment variations were evident.

et al., 2005; Dickinson et al., 2009; Meinhold et al., 2011; Andersen et al., 2016, 2018; Schwartz et al., 2019; Flowerdew et al., 2020; Zotto et al., 2020; Zoleikhaei et al., 2021, 2022).

The dated detrital zircons in this study demonstrate diverse roundness features (involving subangular to well-rounded grains, Fig. 25), revealing possible occurrence of both first-cycle and multi-cycle zircon grains in these analyzed sandstone samples. Other stable, well-rounded heavy mineral grains, such as tourmaline, are also widely distributed in sandstones from the Cenozoic northern Qaidam basin (Jian et al., 2013a). We suggest that, in addition to those granitic rocks, pre-Cenozoic (meta)sedimentary strata (e.g., Proterozoic and Paleozoic metasedimentary sequences and Mesozoic sedimentary strata) which are widespread in the surrounding mountains (Fig. 1D; Gehrels et al., 2003; Jian et al., 2020; Zhang et al., 2021) also can serve as source parent-rocks for the detrital zircon grains in the Cenozoic Qaidam basin. The contribution of recycled (meta)sedimentary rocks is also supported by detrital framework composition analyses on the Cenozoic Qaidam basin record which indicate that (meta)sedimentary clasts and lithic fragments are abundant in some investigated conglomerates and sandstones (Fig. 3; Fig. 5; Jian et al., 2013a, 2022; Lu et al., 2018), respectively.

We note that Mesozoic (e.g., Jurassic coal-bearing sequences) siliciclastic sedimentary rocks in the surrounding mountains were also proposed to provide detritus for the Cenozoic Qaidam basin (Lu et al., 2018, 2022). We agree that recycling of the Mesozoic strata cannot be ignored when interpreting the Cenozoic provenance, since some Mesozoic strata within the surrounding mountains (Jian, 2013; Yu et al., 2017; Lu et al., 2018; Zhang et al., 2020; Zhao et al., 2020; Li et al., 2021a; Qian et al., 2021) indicate similar detrital zircon U–Pb age populations to the Cenozoic sedimentary rocks and the Mesozoic strata experienced deep burial, strong annealing and intensive exhumation after deposition (Jian et al., 2018). And it is possible that recycling of these Mesozoic sedimentary units may yield detrital zircons with Permian–Triassic ages for the Cenozoic strata (Lu et al., 2018). However, we suggest that the Mesozoic strata might only serve as a subordinate source for the Cenozoic sandstones in the Qaidam basin. The explanations are as follows. First, the Cenozoic sandstones are expected to be highly mature in detrital framework composition and texture if the Mesozoic siliciclastic rocks contribute largely to the Cenozoic. However, the Cenozoic sandstones (Fig. 5; Jian et al., 2013a) are much more immature than those Mesozoic (especially the Jurassic) quartz-rich sandstones (Jian et al., 2013b). Similarly, geochemical data demonstrate that Cenozoic mudstones are less weathered and more immature than Mesozoic mudstones in the northern Qaidam basin (Jian et al., 2013b). Second, sedimentary rocks generally have lower accessory mineral (such as zircon) fertility, compared to metamorphic and plutonic rocks (Malusà et al., 2016). This is reinforced by the relatively low heavy mineral concentrations of the Mesozoic sandstones from the northern Qaidam basin (Jian, 2013).

Northern and Central Qilian Mountains serve as another case where recycling of zircon grains can be applied to interpret the unpredictable Permian–Triassic zircon ages. We note that granitoid rocks in these areas indicate rare Permian–Triassic age signals (Fig. 10), whereas sedimentary rocks from the Cenozoic intermountain basins and the modern river sands therein demonstrate Permian–Triassic detrital zircon age peaks (Fig. 11; Bovet et al., 2009). Since the Permian–Cretaceous sedimentary strata in northern Qilian Mountains show extensive 200–280 Ma detrital zircon ages (Zuza et al., 2018; Li et al., 2021a), recycling of the

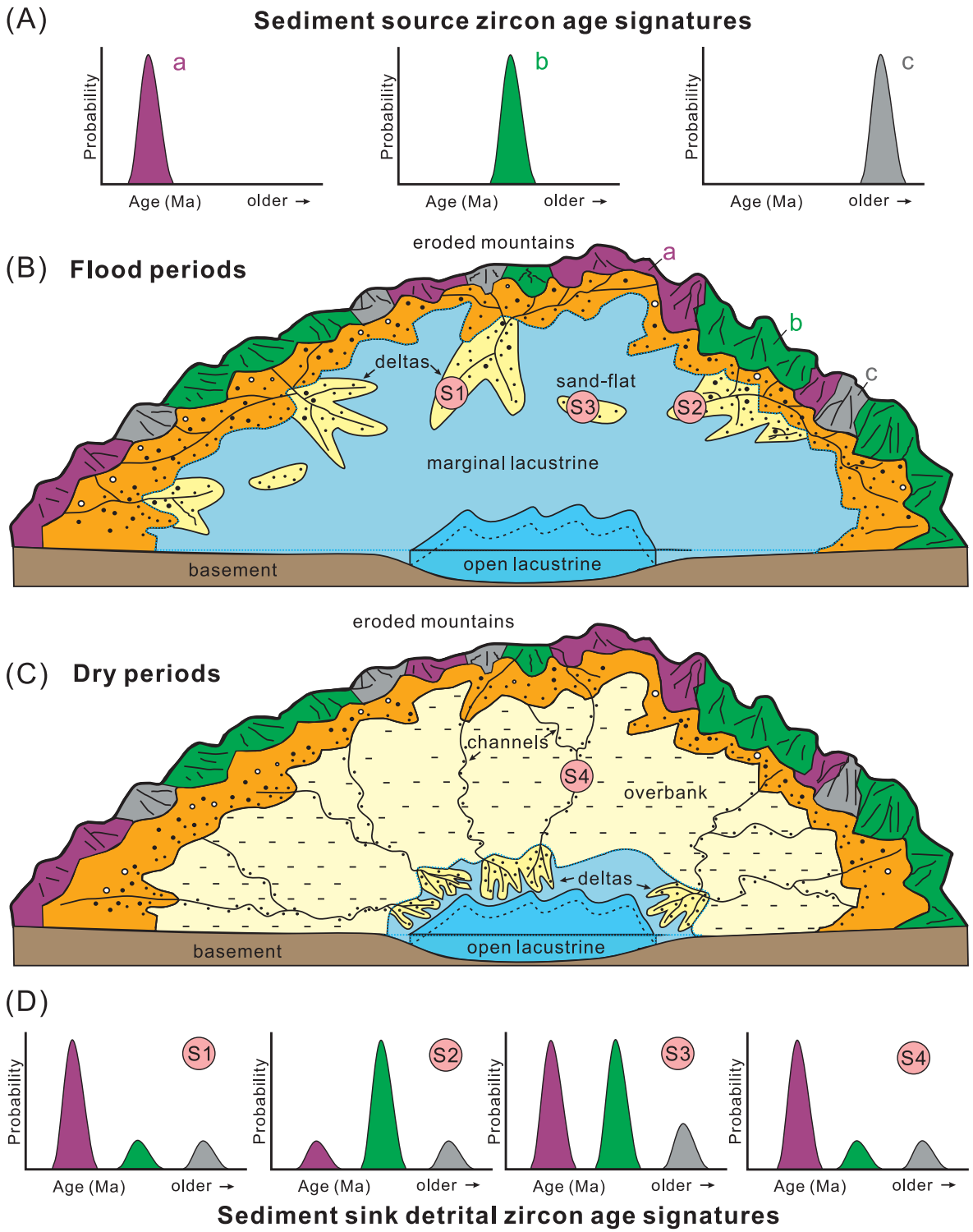

Fig. 23. Conceptual models for detrital zircon U–Pb age variations in response to lake-level fluctuations (i.e., flood-dry cycles) in low-gradient depositional systems during the lake basin expansion stage. Proportion variations in the major detrital zircon age populations to some extent can be due to sedimentary environment changes, with unchanged source regions and tectonic settings.

Permian–Cretaceous strata might play an important role in contributing detrital zircon grains of the Cenozoic basin and modern river sedimentary records.

9. Conclusions, implications and perspectives

9.1. Conclusions

Compilation of the detrital zircon age data from potential detritus source regions indicate that Permian–Triassic zircon age signals are not a distinctive indicator for distinguishing sediment contributions from

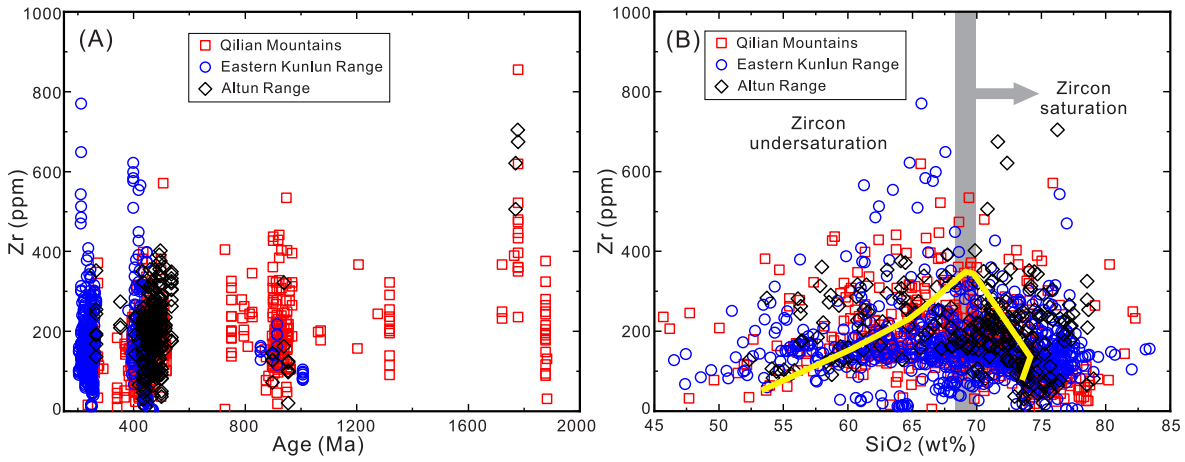

Fig. 24. Published bulk-rock Zr content data of intermediate-acid (meta) igneous rocks from the northern Tibetan Plateau. (A) Zr vs. rock age. Note that not all the geochemical samples in previous studies were dated. Thus, the formation ages of those rocks without reported age data are estimated according to statements in those literatures (see Appendix C for the reference details). (B) Zr vs. SiO_2. The yellow line in this figure shows the evolution of element Zr during closed-system crystal-liquid segregation of a hydrous (4 wt% H_2O) basaltic andesite at 3 kbar pressure (modified from Lee et al. (2016)). When magmas have low SiO_2 contents, Zr increases initially because magmas are under-saturated in zircon until the conditions of ca. 68–70 wt% SiO_2, saturation in zircon is attained, causing Zr to decrease with progressive differentiation (Lee et al., 2016). All the data are shown in Table A5. The compilation results indicate that the crystalline rocks in the Qilian, Eastern Kunlun and Altun ranges have variable Zr contents, revealing diverse zircon fertility of the potential source rocks for the Cenozoic Qaidam basin.

Fig. 25. Textural features (under plane-polarized light) of representative dated detrital zircon grains of three Cenozoic sandstone samples from the northern Qaidam basin. The zircon roundness was quantified through a mathematical method proposed by Resentini et al. (2018) based on image analysis, following the procedures given by Shen et al. (2021). Note that the roundness values of most analyzed zircon grains range from 0.2 to 0.8, revealing that the zircon grains in the Cenozoic northern Qaidam basin are subangular to well-rounded in shape (Shen et al., 2021).

the surrounding Qilian, Altun and Eastern Kunlun ranges. The Paleoproterozoic ages, i.e., 1800–2000 Ma and 2350–2500 Ma, may instead play important roles in the detrital zircon age-based provenance interpretations for the Cenozoic Qaidam basin.

Previously published and new data demonstrate remarkably spatial and temporal variations in the Cenozoic Qaidam basin detrital zircon age populations, especially for those from the northern and eastern Qaidam basin. Detrital zircons of almost all the dated Cenozoic samples from the northern and eastern Qaidam basin indicate prominent early Paleozoic (420–510 Ma) ages, whereas Paleoproterozoic (1800–2000

Ma and 2350–2500 Ma), Neoproterozoic (750–950 Ma) and Permian–-Triassic (210–290 Ma) ages only appear prominently in some samples. By contrast, most Cenozoic samples from the western and southern Qaidam basin are characterized by Phanerozoic bimodal detrital zircon age spectra (i.e., 400–480 Ma and 220–280 Ma) with minor Neoproterozoic signals. The Paleoproterozoic ages are uncommon in these samples. We advocate that the Cenozoic sandstones were mainly derived from localized, adjacent source regions rather than cross-basinal, distant mountains (Fig. 21). The detrital zircon grains in the northern and eastern Qaidam basin were mainly contributed by source terranes in the Qilian Mountains, rather than the Eastern Kunlun Range.

We note diverse detrital zircon age temporal variation trends for different regions in the basin, producing dissimilar provenance interpretations. We contend that, not only the tectonic deformation-induced source changes, but also the heterogeneity of the potential source terranes (e.g., lithologic erodibility and zircon fertility) and variable factors (e.g., hydrodynamic sorting, recycling and sedimentary microenvironments) within the transport-deposition processes, may lead to the spatiotemporal differences in detrital zircon age populations. This means that detrital zircon geochronological analysis on a single stratigraphic section or on a local area is probably not able to disclose regional tectono-sedimentary evolution history of the Cenozoic Qaidam basin and thus only provides limited information for understanding deformation mechanisms of the northern Tibetan Plateau.

9.2. Implications

9.2.1. Implications for cenozoic tectonic and climatic evolution of the northern Tibetan plateau

Provenance analysis of the Cenozoic basal coarse-grained deposits (E_{1+2}) in the Qaidam basin favors localized, spatially diverse detritus sources, small drainage networks and isolated depocenters (Fig. 21), revealing a contractional deformation regime in the early stage of the Cenozoic deposition (Jian et al., 2023). If the early Eocene onset of sediment accumulation in the Qaidam basin is reasonable, the development of the Qaidam basin and other Eocene-initiated sedimentary basins (Horton et al., 2004; Fang et al., 2019a) in northern Tibet can be considered as a far-field, fast response to the India-Eurasia collision.

We suggest that the Eastern Kunlun Range have served as a topographical barrier to restrict detritus from the Songpan-Ganzi Complex to the Qaidam basin since the Eocene initial deposition (Fig. 21). This is inconsistent with the Paleogene Paleo-Qaidam hypothesis (e.g., Yin et al., 2008b; McRivette et al., 2019) that the Qaidam and Hoh-Xil-Songpan-Ganzi basins had been parts of a single integrated basin during the early stage of the Cenozoic Tibet development. The prominent contribution of the Qilian Mountains to the northern and eastern Qaidam basin and to the adjacent wide depositional regions (Fig. 21) suggests intensive erosion and possible relatively high-relief topography during the whole Cenozoic depositional period. Although the plaeo-elevation histories of these mountains remain enigmatic, both the Qaidam basin provenance interpretations in this study and previous tectonic deformation studies on the mountains (e.g., Clark et al., 2010; Jian et al., 2018; Li et al., 2020 and references therein) reveal an early establishment of the northern boundary of the plateau. Our findings, from the perspective of clastic sedimentary record, seem to be at odds with differential growth mechanisms (Kong et al., 1997; Dayem et al., 2009; Wang et al., 2008a, 2014, 2017) but instead support models with Cenozoic synchronous deformation throughout most of the northern Tibet regions (Clark, 2012; Cheng et al., 2019a).

Although it is hard to establish relationships between detrital zircon provenance analysis results and regional paleoclimate history, it is well accepted that Cenozoic climate variations had played important roles in formation and evolution of the paleo-Qaidam lake, development of sediment routing systems and in formation of sedimentary records in the basin (Wang et al., 1999; Jian et al., 2013b, 2014; Guo et al., 2017; Cheng et al., 2019b; Sun et al., 2020; Wu et al., 2021b; Fu et al., 2022). As mentioned above, the spatiotemporal variations in detrital zircon age populations of the Cenozoic Qaidam basin can not only be attributed to tectonic deformation of the source terranes. Climate change-induced source erosion (rates and patterns) variations and depositional environment fluctuations should also be taken into account for interpreting the diversity of detrital zircon age populations (e.g., Fig. 23). Hence, detrital zircon geochronology-based provenance interpretations, especially for those high-resolution sample collections, are expected to facilitate unraveling paleoclimate issues of this region under certain conditions.

9.2.2. Implications for sedimentary provenance analysis methodology

There is no doubt that detrital zircon U–Pb geochronology is a powerful tool in sedimentary provenance research. In the Qaidam basin case study, the diverse provenance interpretations based on detrital zircon ages obtained by different research groups, however, indicate possible limitations and bias in employing this method. This means that reliable provenance interpretations might not be produced and sediment source-to-sink processes could not be exactly reconstructed depending on detrital zircon U–Pb age data alone. The following are some suggestions for reporting detrital zircon geochronological data and for addressing geological questions related to zircon records.

1) Textural parameters of the dated detrital zircon grains, including grain size, length/width ratio and roundness, are recommended to be measured and reported along with the U–Pb age data. Sedimentological analysis of the analyzed sandstone (siltstone or conglomerate in some cases) samples can be performed and depositional environment (or facies) interpretations can be provided if possible. The marked diversity of detrital zircon age populations on different spatial and temporal scales, indicated by previously reported and our new data, illustrates the need for careful consideration of sampling strategies.
2) In addition to the U–Pb ages, other data of the detrital zircon grains are suggested to be obtained if analytical conditions are available. These include trace elements, Hf, O and Zr isotopes, which can provide insightful information about origin, forming process (e.g., magmatic crystallization, temperature and crustal growth) and even tectonic regime of these single zircons (Belousova et al., 2002, 2010; Valley, 2003; Veevers et al., 2005; Grimes et al., 2007; Condie et al., 2011; McKay et al., 2018; Ibañez-Mejia and Tissot, 2019; Guo et al., 2020; Tang et al., 2021). Double-/triple-dating of single detrital zircon grains with (U–Th)/He, fission track and U–Pb systems, which does not only provide zircon crystallization ages but also deciphers cooling history during the exhumation process of the crystalline provinces, has proven as a potent tool in sediment provenance studies (Reiners et al., 2005; Saylor et al., 2012; Thomson et al., 2017; Xu et al., 2017), especially in unraveling zircon recycling puzzles (Campbell et al., 2005; Zotto et al., 2020).
3) As detrital zircons occur as accessory mineral grains (commonly <1% in volume) in clastic sedimentary rocks and might have different routings with other detrital grains in the same records, the zircon provenance may not completely represent the bulk sediment provenance (Malusà et al., 2013; Garzanti and Andò, 2019). Multi-proxy provenance approaches (e.g., petrography, geochemistry and field-based measurements) or an integrated provenance analysis involving various detritus components (e.g., detrital clay minerals, framework grains and other heavy minerals), are beneficial to better understanding source-to-sink systems of the sedimentary targets (Critelli and Reed, 1999; Greene et al., 2005; Nie et al., 2012; Jian et al., 2013b; 2022; Critelli, 2018; Critelli et al., 2021, 2023; Li et al., 2021b; Zoleikhaei et al., 2021, 2022; Fu et al., 2022; Zhang et al., 2022; Kairouani et al., 2023). Since K-feldspar is unlikely to survive more than one erosion-transport-deposition cycle and thus reveals first-cycle input from source terranes, combining Pb isotopic analysis of detrital K-feldspar is expected to help constrain the

recycling issues (e.g., Tyrrell et al., 2007; Johnson et al., 2018; Barham et al., 2021). Furthermore, integrated provenance analysis may shed light on insensitivity issues of the detrital zircon record in detecting magma-poor source terranes (O'Sullivan et al., 2016; Chew et al., 2020).

4) Potential source signatures are also important to interpreting sediment provenance and thus need to be accurately assessed. We consider that, straightforwardly synthesizing all the available zircon age data for a supposed source region, which is quite common in some case studies, is a risky business. It is a tough task to define zircon age signatures for source orogens with complex structures (Song et al., 2019; Zhang et al., 2021). We suggest that zircon age signals of terranes with different tectono-magmatic histories should be separately illustrated as clearly as possible (Figs. 10 and 11) and zircon fertility and sediment recycling issues should be concerned in detrital zircon provenance interpretations. Furthermore, deep-time paleogeographic environments, paleodrainage systems and detritus parent-rock distributions are always questionable. Thus, depositional periods or stratigraphic attributions should also be paid attention to when forming potential source signatures by using detrital zircon age data from older sedimentary strata in those source terranes.

9.3. Perspectives

There are still a number of unsolved issues and broader implications concerning detrital zircon geochronology and provenance of the Cenozoic Qaidam basin. These include but are not limited to the followings.

1) If the Qilian Mountains really contributed abundant zircon grains of Permian–Triassic U–Pb ages to the inner and surrounding Mesozoic–Cenozoic sedimentary basins (Bovet et al., 2009; Wang et al., 2016; Zhang et al., 2016; An et al., 2018; Cheng et al., 2019b; Li et al., 2021a and this study), how to explain and treat the puzzled discrepancy between igneous zircon and detrital zircon records (Figs. 10 and 11) remains an open question.
2) We note that most dated samples were collected from the current margins of the Qaidam basin (Fig. 1C). The center of the basin, where drilling wells are rare and sediment provenance has been poorly characterized, acts as a key region to better understand the sediment source-to-sink systems between the surrounding mountains and the Qaidam basin. This region is also a crucial study target to understand why the Cenozoic northern and eastern Qaidam basin is characterized by siliciclastic-dominant sequences, whereas the western Qaidam basin is filled with mixed carbonate-siliciclastic deposits (Fig. 2; Song et al., 2022a, 2022b).
3) The Qaidam basin is well known as a petroliferous basin with great hydrocarbon potentials (Zhuang et al., 2018). How the numerous detrital zircon data and provenance interpretations play roles in hydrocarbon exploration and development deserves more attention. Exploring the possible connections between sediment source-to-sink systems and hydrocarbon source-reservoir-cap rock assemblages may be an important research direction in the future.
4) Unraveling relationships between the Qaidam basin and the surrounding small–medium intermountain basins (Fig. 1C) contribute insight into better understanding Cenozoic tectonic and climatic evolution of the northern Tibetan Plateau. Since most of these basins lack well-preserved fossil records and volcaniclastic age constraints, determining accurate depositional periods and chronostratigraphic frameworks for these basins remains a challenge.
5) The Qaidam basin has been proposed as a major aeolian dust source for the Chinese Loess Plateau and the North Pacific Ocean (Pullen et al., 2011; An et al., 2012; Nie et al., 2018; Wang et al., 2020). The occurrence of enormous, characteristic yardang fields in actively folding Cenozoic sedimentary strata demonstrates severe wind erosion and voluminous sediment removal from the Qaidam basin (Kapp et al., 2011). How to treat the spatiotemporal diversity in detrital zircon age populations of the Cenozoic Qaidam basin and to generate a source signal for Asian dust provenance analysis are also a challenging work.

CRediT authorship contribution statement

Xing Jian: Conceptualization, Data curation, Funding acquisition, Investigation, Supervision, Writing – original draft. **Ping Guan:** Investigation, Resources. **Ling Fu:** Investigation, Resources. **Wei Zhang:** Investigation, Funding acquisition, Project administration. **Xiaotian Shen:** Investigation, Data curation, Visualization. **Hanjing Fu:** Investigation, Data curation. **Ling Wang:** Data curation, Visualization.

Declaration of competing interest

The authors declare that they have no known competing financial interests or personal relationships that could have appeared to influence the work reported in this paper.

Data availability

Data will be made available on request.

Acknowledgments

This research was supported by the Natural Science Foundation of Xiamen City (No. 3502Z20227006), National Natural Science Foundation of China (Nos. 41806052, 41902126) and Xiamen University Fundamental Research Funds for the Central Universities (Nos. 20720192011, 20720160114). We would like to thank Drs. Yongshu Zhang, Daowei Zhang and Suotang Fu from PetroChina for their consistent supports during the past several years. We also appreciate Hanghai Liang, Dongming Hong, Shuo Zhang, Haowei Mei, Xin Huang, Fan Feng, Yiqiu Jin and Fang Ma for their help in field work, lab analysis and data collection. Discussions with Profs. Shuguang Song, Zhong Li and Ping Wang improved the interpretations in this contribution.

Appendix A. Supplementary data

Supplementary data to this article can be found online at https://doi.org/10.1016/j.marpetgeo.2023.106566.

References

An, F., Ma, H., Wei, H., Lai, Z., 2012. Distinguishing aeolian signature from lacustrine sediments of the Qaidam Basin in northeastern Qinghai-Tibetan Plateau and its palaeoclimatic implications. Aeolian Res. 4, 17–30.

An, K., Lin, X., Wu, L., Cheng, X., Chen, H., Ding, W., Zhang, F., Gong, J., Yang, R., Zhu, K., Li, C., Zhang, Y., Gao, S., 2018. Reorganization of sediment dispersal in the jiuxi basin at~ 17 Ma and its implications for uplift of the NE Tibetan plateau. Palaeogeogr. Palaeoclimatol. Palaeoecol. 511, 558–576.

An, K., Lin, X., Wu, L., Yang, R., Chen, H., Cheng, X., Xia, Q., Zhang, F., Ding, W., Gao, S., Li, C., Zhang, Y., 2020. An immediate response to the Indian-Eurasian collision along the northeastern Tibetan Plateau: evidence from apatite fission track analysis in the Kuantan Shan-Hei Shan. Tectonophysics 774, 228278.

Anders, B., Tyrrell, S., Chew, D., Mark, C., O'Sullivan, G., Murray, J., Graham, J.R., Badenszki, E., 2022. Spatial variation in provenance signal: identifying complex sand sourcing within a Carboniferous basin using multiproxy provenance analysis. J. Geol. Soc. 179 (1).

Andersen, T., 2002. Correction of common lead in U-pb analyses that do not report 204Pb. Chem. Geol. 192, 59–79. https://doi.org/10.1016/S0009-2541(02)00195-X.

Andersen, T., Elburg, M.A., van Niekerk, H.S., Ueckermann, H., 2018. Successive sedimentary recycling regimes in southwestern Gondwana: evidence from detrital zircons in Neoproterozoic to Cambrian sedimentary rocks in southern Africa. Earth Sci. Rev. 181, 43–60.

Andersen, T., Kristoffersen, M., Elburg, M.A., 2016. How far can we trust provenance and crustal evolution information from detrital zircons? A South African case study. Gondwana Res. 34, 129–148.

Argand, E., 1922. La Tectonique de l'Asie. Proc. 13th Int. Geol. Congr. Brussels 171–372.

Armstrong-Altrin, J.S., Ramos-Vázquez, M.A., Hermenegildo-Ruiz, N.Y., Madhavaraju, J., 2021. Microtexture and U–Pb geochronology of detrital zircon

grains in the Chachalacas beach, Veracruz State, Gulf of Mexico. Geol. J. 56 (5), 2418–2438.
Avigad, D., Weissbrod, T., Gerdes, A., Zlatkin, O., Ireland, T.R., Morag, N., 2015. The detrital zircon U–Pb–Hf fingerprint of the northern Arabian–Nubian Shield as reflected by a Late Ediacaran arkosic wedge (Zenifim Formation; subsurface Israel). Precambrian Res. 266, 1–11.
Bao, J., Wang, Y., Song, C., Feng, Y., Hu, C., Zhong, S., Yang, J., 2017. Cenozoic sediment flux in the Qaidam Basin, northern Tibetan Plateau, and implications with regional tectonics and climate. Global Planet. Change 155, 56–69.
Barham, M., Kirkland, C.L., Hovikoski, J., Alsen, P., Hollis, J., Tyrrell, S., 2021. Reduce or recycle? Revealing source to sink links through integrated zircon–feldspar provenance fingerprinting. Sedimentology 68 (2), 531–556.
Belousova, E.A., Griffin, W.L., O'Reilly, S.Y., Fisher, N.L., 2002. Igneous zircon: trace element composition as an indicator of source rock type. Contrib. Mineral. Petrol. 143 (5), 602–622.
Belousova, E.A., Kostitsyn, Y.A., Griffin, W.L., Begg, G.C., O'Reilly, S.Y., Pearson, N.J., 2010. The growth of the continental crust: constraints from zircon Hf-isotope data. Lithos 119 (3–4), 457–466.
Boehnke, P., Watson, E.B., Trail, D., Harrison, T.M., Schmitt, A.K., 2013. Zircon saturation re-revisited. Chem. Geol. 351, 324–334.
Bónová, K., Pańczyk, M., Bóna, J., 2020. Surface microtextures and new U–Pb dating of detrital zircons from the Eocene Strihovce sandstones in the Magura Nappe of the External Western Carpathians: implications for their provenance. Int. J. Earth Sci. 109 (5), 1565–1587.
Bovet, P.M., Ritts, B.D., Gehrels, G., Abbink, A.O., Darby, B., Hourigan, J., 2009. Evidence of Miocene crustal shortening in the north qilian Shan from cenozoic stratigraphy of the western Hexi corridor, gansu province, China. Am. J. Sci. 309 (4), 290–329.
Bush, M.A., Saylor, J.E., Horton, B.K., Nie, J., 2016. Growth of the Qaidam Basin during Cenozoic exhumation in the northern Tibetan Plateau: inferences from depositional patterns and multiproxy detrital provenance signatures. Lithosphere 8 (1), 58–82.
Campbell, I.H., Reiners, P.W., Allen, C.M., Nicolescu, S., Upadhyay, R., 2005. He–Pb double dating of detrital zircons from the Ganges and Indus Rivers: implication for quantifying sediment recycling and provenance studies. Earth Planet Sci. Lett. 237 (3–4), 402–432.
Capaldi, T.N., Horton, B.K., McKenzie, N.R., Stockli, D.F., Odlum, M.L., 2017. Sediment provenance in contractional orogens: the detrital zircon record from modern rivers in the Andean fold-thrust belt and foreland basin of western Argentina. Earth Planet Sci. Lett. 479, 83–97.
Carrapa, B., 2010. Resolving tectonic problems by dating detrital minerals. Geology 38 (2), 191–192.
Cawood, P.A., Hawkesworth, C.J., Dhuime, B., 2012. Detrital zircon record and tectonic setting. Geology 40 (10), 875–878.
Cawood, P.A., Hawkesworth, C.J., Dhuime, B., 2013. The continental record and the generation of continental crust. Bulletin 125 (1–2), 14–32.
Chang, H., Li, L., Qiang, X., Garzione, C.N., Pullen, A., An, Z., 2015. Magnetostratigraphy of Cenozoic deposits in the western Qaidam Basin and its implication for the surface uplift of the northeastern margin of the Tibetan Plateau. Earth Planet Sci. Lett. 430, 271–283.
Chen, N., Gong, S., Sun, M., Li, X., Xia, X., Wang, Q., Wu, F., Xu, P., 2009. Precambrian evolution of the Quanji Block, northeastern margin of Tibet: insights from zircon U-Pb and Lu-Hf isotope compositions. J. Asian Earth Sci. 35, 367–376.
Chen, N., Zhang, L., Sun, M., Wang, Q., Kusky, T.M., 2012. U-Pb and Hf isotopic compositions of detrital zircons from the paragneisses of the Quanji Massif, NW China: implications for its early tectonic evolutionary history. J. Asian Earth Sci. 54, 110–130.
Chen, N.S., Liao, F.X., Wang, L., Santosh, M., Sun, M., Wang, Q.Y., 2013. Late paleoproterozoic multiple metamorphic events in the Quanji massif: links with Tarim and North China cratons and implications for assembly of the columbia supercontinent. Precambrian Res. 228, 102–116.
Cheng, F., Fu, S., Jolivet, M., Zhang, C., Guo, Z., 2016a. Source to sink relation between the eastern Kunlun range and the Qaidam basin, northern Tibetan plateau, during the cenozoic. Bulletin 128 (1–2), 258–283.
Cheng, F., Garzione, C.N., Jolivet, M., Guo, Z., Zhang, D., Zhang, C., Zhang, Q., 2019a. Initial deformation of the northern Tibetan plateau: insights from deposition of the Lulehe Formation in the Qaidam basin. Tectonics 38 (2), 741–766.
Cheng, F., Garzione, C.N., Mitra, G., Jolivet, M., Guo, Z., Lu, H., Li, X., Zhang, B., Zhang, C., Zhang, H., Wang, L., 2019b. The interplay between climate and tectonics during the upward and outward growth of the Qilian Shan orogenic wedge, northern Tibetan Plateau. Earth Sci. Rev. 198, 102945.
Cheng, F., Jolivet, M., Fu, S., Zhang, C., Zhang, Q., Guo, Z., 2016b. Large-scale displacement along the Altyn Tagh Fault (north Tibet) since its Eocene initiation: insight from detrital zircon U–Pb geochronology and subsurface data. Tectonophysics 677, 261–279.
Cheng, F., Jolivet, M., Guo, Z., Wang, L., Zhang, C., Li, X., 2021. Cenozoic evolution of the Qaidam basin and implications for the growth of the northern Tibetan plateau: a review. Earth Sci. Rev. 220, 103730.
Cheng, F., Jolivet, M., Hallot, E., Zhang, D., Zhang, C., Guo, Z., 2017. Tectono-magmatic rejuvenation of the Qaidam craton, northern Tibet. Gondwana Res. 49, 248–263.
Cherniak, D.J., Watson, E.B., 2001. Pb diffusion in zircon. Chem. Geol. 172 (1–2), 5–24.
Chew, D., O'Sullivan, G., Caracciolo, L., Mark, C., Tyrrell, S., 2020. Sourcing the sand: accessory mineral fertility, analytical and other biases in detrital U-Pb provenance analysis. Earth Sci. Rev. 202, 103093.
Clark, M.K., 2012. Continental collision slowing due to viscous mantle lithosphere rather than topography. Nature 483 (7387), 74–77.
Clark, M.K., Farley, K.A., Zheng, D., Wang, Z., Duvall, A.R., 2010. Early Cenozoic faulting of the northern Tibetan Plateau margin from apatite (U–Th)/He ages. Earth Planet Sci. Lett. 296, 78–88.
Condie, K.C., Bickford, M.E., Aster, R.C., Belousova, E., Scholl, D.W., 2011. Episodic zircon ages, Hf isotopic composition, and the preservation rate of continental crust. Bulletin 123 (5–6), 951–957.
Copeland, P., 2020. On the use of geochronology of detrital grains in determining the time of deposition of clastic sedimentary strata. Basin Res. 32 (6), 1532–1546.
Coutts, D.S., Matthews, W.A., Hubbard, S.M., 2019. Assessment of widely used methods to derive depositional ages from detrital zircon populations. Geosci. Front. 10 (4), 1421–1435.
Critelli, S., 2018. Provenance of Mesozoic to Cenozoic circum-Mediterranean sandstones in relation to tectonic setting. Earth Sci. Rev. 185, 624–648.
Critelli, S., Criniti, S., Ingersoll, R.V., Cavazza, W., 2023. Temporal and spatial significance of volcanic particles in sand (stone): implications for provenance and palaeotectonic reconstructions. Geol. Soc., London, Spec. Publ. 520 (1), 311–325.
Critelli, S., Martín-Martín, M., Capobianco, W., Perri, F., 2021. Sedimentary history and palaeogeography of the cenozoic clastic wedges of the malaguide complex, internal betic Cordillera, southern Spain. Mar. Petrol. Geol. 124, 104775.
Critelli, S., Reed, W.E., 1999. Provenance and stratigraphy of the devonian (old red sandstone) and carboniferous sandstones of spitsbergen, svalbard. Eur. J. Mineral 11 (1), 149–166.
Dayem, K.E., Molnar, P., Clark, M.K., Houseman, G.A., 2009. Far-field lithospheric deformation in Tibet during continental collision. Tectonics 28 (6).
Decelles, P.G., Kapp, P., Gehrels, G.E., Ding, L., 2014. Paleocene-Eocene foreland basin evolution in the Himalaya of southern Tibet and Nepal: implications for the age of initial India-Asia collision. Tectonics 33 (5), 824–849.
DeGraaff-Surpless, K., Mahoney, J.B., Wooden, J.L., McWilliams, M.O., 2003. Lithofacies control in detrital zircon provenance studies: insights from the Cretaceous Methow basin, southern Canadian Cordillera. Geol. Soc. Am. Bull. 115 (8), 899–915.
Dickinson, W.R., 2008. Impact of differential zircon fertility of granitoid basement rocks in North America on age populations of detrital zircons and implications for granite petrogenesis. Earth Planet Sci. Lett. 275 (1–2), 80–92.
Dickinson, W.R., Gehrels, G.E., 2009. Use of U–Pb ages of detrital zircons to infer maximum depositional ages of strata: a test against a Colorado Plateau Mesozoic database. Earth Planet Sci. Lett. 288 (1–2), 115–125.
Dickinson, W.R., Lawton, T.F., Gehrels, G.E., 2009. Recycling detrital zircons: a case study from the Cretaceous Bisbee Group of southern Arizona. Geology 37 (6), 503–506.
Ding, L., Kapp, P., Cai, F., Garzione, C.N., Xiong, Z., Wang, H., Wang, C., 2022. Timing and mechanisms of Tibetan Plateau uplift. Nat. Rev. Earth Environ. 1–16.
Ding, L., Yang, D., Cai, F.L., Pullen, A., Kapp, P., Gehrels, G.E., Zhang, L.Y., Zhang, Q.H., Lai, Q.Z., Yue, Y.H., Shi, R.D., 2013. Provenance analysis of the mesozoic hoh-xil-songpan-ganzi turbidites in northern Tibet: implications for the tectonic evolution of the eastern paleo-tethys ocean. Tectonics 32 (1), 34–48.
Dong, C., Li, C., Wan, Y., Wang, W., Wu, Y., Xie, H., Liu, D., 2011. Detrital zircon age model of Ordovician Wenquan quartzite south of Lungmuco-Shuanghu Suture in the Qiangtang area, Tibet: constraint on tectonic affinity and source regions. Sci. China Earth Sci. 54 (7), 1034–1042.
Dong, Y., Sun, S., Santosh, M., Zhao, J., Sun, J., He, D., Shi, X., Hui, B., Cheng, C., Zhang, G., 2021. Central China orogenic belt and amalgamation of east asian continents. Gondwana Res. 100, 131–194.
Dong, Y., Zhang, G., Neubauer, F., Liu, X., Genser, J., Hauzenberger, C., 2011. Tectonic evolution of the Qinling orogen, China: review and synthesis. J. Asian Earth Sci. 41 (3), 213–237.
Dröllner, M., Barham, M., Kirkland, C.L., 2022. Gaining from loss: detrital zircon source-normalized α-dose discriminates first-versus multi-cycle grain histories. Earth Planet Sci. Lett. 579, 117346.
Dröllner, M., Barham, M., Kirkland, C.L., Ware, B., 2021. Every zircon deserves a date: selection bias in detrital geochronology. Geol. Mag. 158 (6), 1135–1142.
Fang, X., Fang, Y., Zan, J., Zhang, W., Song, C., Appel, E., Meng, Q., Miao, Y., Dai, S., Lu, Y., Zhang, T., 2019a. Cenozoic magnetostratigraphy of the Xining Basin, NE Tibetan Plateau, and its constraints on paleontological, sedimentological and tectonomorphological evolution. Earth Sci. Rev. 190, 460–485.
Fang, X., Galy, A., Yang, Y., Zhang, W., Ye, C., Song, C., 2019b. Paleogene global cooling-induced temperature feedback on chemical weathering, as recorded in the northern Tibetan Plateau. Geology 47 (10), 992–996.
Fang, X., Zhang, W., Meng, Q., Gao, J., Wang, X., King, J., Song, C., Dai, S., Miao, Y., 2007. High resolution magnetostratigraphy of the Neogene Huaitoutala section in the eastern Qaidam basin on the NE Tibetan plateau, qinghai province, China and its implication on tectonic uplift of the NE Tibetan plateau. Earth Planet Sci. Lett. 258, 293–306.
Fedo, C.M., Sircombe, K.N., Rainbird, R.H., 2003. Detrital zircon analysis of the sedimentary record. Rev. Mineral. Geochem. 53 (1), 277–303.
Feng, L., Hu, C., Chen, X., Cai, X., Tian, L., Gan, W., 2012. Assessment of inundation changes of Poyang Lake using MODIS observations between 2000 and 2010. Rem. Sens. Environ. 121, 80–92.
Feng, D., Wang, C., Song, S., Xiong, L., Zhang, G., Allen, M.B., Dong, J., Su, L., 2023. Tracing tectonic processes from proto-to paleo-tethys in the east Kunlun orogen by detrital zircons. Gondwana Res. 115, 1–16.
Finzel, E.S., 2017. Detrital zircon microtextures and U-Pb geochronology of Upper Jurassic to Paleocene strata in the distal North American Cordillera foreland basin. Tectonics 36 (7), 1295–1316.
Flowerdew, M.J., Fleming, E.J., Morton, A.C., Frei, D., Chew, D.M., Daly, J.S., 2020. Assessing mineral fertility and bias in sedimentary provenance studies: examples from the Barents Shelf. Geol. Soc., London, Spec. Publ. 484 (1), 255–274.

Fornelli, A., Micheletti, F., Gallicchio, S., Tursi, F., Criniti, S., Critelli, S., 2022. Detrital zircon ages of Oligocene to Miocene sandstone suites of the Southern Apennines foreland basin system, Italy. J. Palaeogeogr. 11 (2), 222–237.
Fu, H., Jian, X., Liang, H., Zhang, W., Shen, X., Wang, L., 2022. Tectonic and climatic forcing of chemical weathering intensity in the northeastern Tibetan Plateau since the middle Miocene. Catena 208, 105785.
Garzanti, E., Andò, S., 2019. Heavy minerals for junior woodchucks. Minerals 9 (3), 148.
Garzanti, E., Andò, S., Limonta, M., Fielding, L., Najman, Y., 2018. Diagenetic control on mineralogical suites in sand, silt, and mud (Cenozoic Nile Delta): implications for provenance reconstructions. Earth Sci. Rev. 185, 122–139.
Garzanti, E., Ando, S., Vezzoli, G., 2008. Settling equivalence of detrital minerals and grain-size dependence of sediment composition. Earth Planet Sci. Lett. 273, 135–151.
Gehrels, G., 2014. Detrital zircon U-Pb geochronology applied to tectonics. Annu. Rev. Earth Planet Sci. 42, 127–149.
Gehrels, G., Kapp, P., DeCelles, P., Pullen, A., Blakey, R., Weislogel, A., Ding, L., Guynn, J., Martin, A., McQuarrie, N., Yin, A., 2011. Detrital zircon geochronology of pre-Tertiary strata in the Tibetan-Himalayan orogen. Tectonics 30, TC5016.
Gehrels, G., Valencia, V., Pullen, A., 2006. Detrital zircon geochronology by laser-ablation multicollector ICPMS at the Arizona LaserChron Center. Paleontol. Soc. Pap. 12, 67–76.
Gehrels, G., Yin, A., Wang, X., 2003. Detrital-zircon geochronology of the northeastern Tibetan Plateau. Geol. Soc. Am. Bull. 115, 881–896.
Gehrels, G.E., Yin, A., Wang, X.F., 2003. Detrital-zircon geochronology of the northeastern Tibetan plateau. Geol. Soc. Am. Bull. 115 (7), 881–896.
Gong, H., Zhao, H., Xie, W., Kang, W., Zhang, R., Yang, L., Zhang, Y., Song, J., Zhang, Y., 2017. Tectono-thermal events of the North qilian orogenic belt, NW China: constraints from detrital zircon U-Pb ages of heihe river sediments. J. Asian Earth Sci. 138, 647–656.
Greene, T.J., Carroll, A.R., Wartes, M., Graham, S.A., Wooden, J.L., 2005. Integrated provenance analysis of a complex orogenic terrane: Mesozoic uplift of the Bogda Shan and inception of the Turpan-Hami Basin, NW China. J. Sediment. Res. 75 (2), 251–267.
Griffin, W.L., Belousova, E.A., Walters, S.G., O'Reilly, S.Y., 2006. Archaean and Proterozoic crustal evolution in the Eastern Succession of the Mt Isa district, Australia: U–Pb and Hf-isotope studies of detrital zircons. Aust. J. Earth Sci. 53 (1), 125–149.
Grimes, C.B., John, B.E., Kelemen, P.B., Mazdab, F.K., Wooden, J.L., Cheadle, M.J., Hanghøj, K., Schwartz, J.J., 2007. Trace element chemistry of zircons from oceanic crust: a method for distinguishing detrital zircon provenance. Geology 35 (7), 643–646.
Guan, P., Jian, X., 2013. The Cenozoic sedimentary record in Qaidam basin and its implications for tectonic evolution of the northern Tibetan plateau (In Chinese with English Abstract). Acta Sedimentol. Sin. 31, 824–833.
Guo, J.L., Wang, Z., Zhang, W., Moynier, F., Cui, D., Hu, Z., Ducea, M.N., 2020. Significant Zr isotope variations in single zircon grains recording magma evolution history. Proc. Natl. Acad. Sci. USA 117 (35), 21125–21131.
Guo, P., Liu, C., Huang, L., Wang, P., Wang, K., Yuan, H., Xu, C., Zhang, Y., 2017. Genesis of the late Eocene bedded halite in the Qaidam basin and its implication for paleoclimate in east Asia. Palaeogeogr. Palaeoclimatol. Palaeoecol. 487, 364–380.
He, P., Song, C., Wang, Y., Wang, D., Chen, L., Meng, Q., Fang, X., 2021. Early Cenozoic activated deformation in the Qilian Shan, northeastern Tibetan Plateau: insights from detrital apatite fission-track analysis. Basin Res. 33 (3), 1731–1748.
Heermance, R.V., Pullen, A., Kapp, P., Garzione, C.N., Bogue, S., Ding, L., Song, P., 2013. Climatic and tectonic controls on sedimentation and erosion during the pliocene–quaternary in the Qaidam basin (China). Bulletin 125 (5–6), 833–856.
Hong, D., Jian, X., Fu, L., Zhang, W., 2020. Garnet trace element geochemistry as a sediment provenance indicator: an example from the Qaidam basin, northern Tibet. Mar. Petrol. Geol. 116, 104316.
Horton, B.K., Dupont-Nivet, G., Zhou, J., Waanders, G.L., Butler, R.F., Wang, J., 2004. Mesozoic-Cenozoic evolution of the Xining-Minhe and Dangchang basins, northeastern Tibetan Plateau: magnetostratigraphic and biostratigraphic results. J. Geophys. Res. Solid Earth 109 (B4).
Houseman, G., England, P., 1993. Crustal thickening versus lateral expulsion in the Indian-Asian continental collision. J. Geophys. Res. Solid Earth 98 (B7), 12233–12249.
Ibañez-Mejia, M., Pullen, A., Pepper, M., Urbani, F., Ghoshal, G., Ibañez-Mejia, J.C., 2018. Use and abuse of detrital zircon U-Pb geochronology—a case from the Río Orinoco delta, eastern Venezuela. Geology 46 (11), 1019–1022.
Ibañez-Mejia, M., Tissot, F.L., 2019. Extreme Zr stable isotope fractionation during magmatic fractional crystallization. Sci. Adv. 5 (12), eaax8648.
Ireland, T.R., Williams, I.S., 2003. Considerations in zircon geochronology by SIMS. Rev. Mineral. Geochem. 53 (1), 215–241.
Ji, J., Zhang, K., Clift, P.D., Zhuang, G., Song, B., Ke, X., Xu, Y., 2017. High-resolution magnetostratigraphic study of the paleogene-neogene strata in the northern Qaidam basin: implications for the growth of the northeastern Tibetan plateau. Gondwana Res. 46, 141–155.
Jian, X., 2013. Controls on Mesozoic and Cenozoic sedimentary evolution of the northern Qaidam basin: tectonic and climatic implications. In: Chinese with English Abstract). Unpub. Ph.D. Dissertation. Peking University.
Jian, X., Fu, L., Wang, P., Guan, P., Zhang, W., Fu, H., Mei, H., 2023. Sediment provenance of the Lulehe Formation in the Qaidam basin: insight to initial cenozoic deposition and deformation in northern Tibetan plateau. Basin Res. 35 (1), 271–294.
Jian, X., Guan, P., Fu, S.T., Zhang, D.W., Zhang, W., Zhang, Y.S., 2014. Miocene sedimentary environment and climate change in the northwestern Qaidam basin, northeastern Tibetan Plateau: facies, biomarker and stable isotopic evidences. Palaeogeogr. Palaeoclimatol. Palaeoecol. 414, 320–331.
Jian, X., Guan, P., Zhang, D.W., Zhang, W., Feng, F., Liu, R.J., Lin, S.D., 2013a. Provenance of Tertiary sandstone in the northern Qaidam basin, northeastern Tibetan Plateau: integration of framework petrography, heavy mineral analysis and mineral chemistry. Sediment. Geol. 290, 109–125.
Jian, X., Guan, P., Zhang, W., Feng, F., 2013b. Geochemistry of Mesozoic and Cenozoic sediments in the northern Qaidam basin, northeastern Tibetan Plateau: implications for provenance and weathering. Chem. Geol. 360, 74–88.
Jian, X., Guan, P., Zhang, W., Liang, H., Feng, F., Fu, L., 2018. Late Cretaceous to early Eocene deformation in the northern Tibetan Plateau: detrital apatite fission track evidence from northern Qaidam basin. Gondwana Res. 60, 94–104.
Jian, X., Weislogel, A., Pullen, A., 2019a. Triassic sedimentary filling and closure of the eastern paleo-tethys ocean: new insights from detrital zircon geochronology of songpan-ganzi, yidun, and West Qinling flysch in eastern Tibet. Tectonics 38 (2), 767–787.
Jian, X., Weislogel, A., Pullen, A., Shang, F., 2020. Formation and evolution of the Eastern Kunlun Range, northern Tibet: evidence from detrital zircon U-Pb geochronology and Hf isotopes. Gondwana Res. 83, 63–79.
Jian, X., Zhang, W., Liang, H., Guan, P., Fu, L., 2019b. Mineralogy, petrography and geochemistry of an early Eocene weathering profile on basement granodiorite of Qaidam basin, northern Tibet: tectonic and paleoclimatic implications. Catena 172, 54–64.
Johnson, S.P., Kirkland, C.L., Evans, N.J., McDonald, B.J., Cutten, H.N., 2018. The complexity of sediment recycling as revealed by common Pb isotopes in K-feldspar. Geosci. Front. 9 (5), 1515–1527.
Kairouani, H., Zaghloul, M.N., Abbassi, A., Micheletti, F., Fornelli, A., El Mourabet, M., Piccoli, F., Criniti, S., Critelli, S., 2023. Provenance and source-to-sink of lower-middle Jurassic sediments from hinterland mounts to NW-Gondwana hyper-extended passive margin (Prerif sub-domain, External Rif, Morocco): first evidence from sedimentary petrology and detrital Zircon geochronology. Mar. Petrol. Geol. 157, 106492.
Kang, H., Chen, Y., Li, D., 2020. The nature and history of the South Qilian orogenic belt: constraints from compositions of rivers' sediments and their detrital zircon U–Pb geochronology, Lu-Hf isotopic compositions. Geol. J. 55 (1), 712–727.
Kang, H., Chen, Y., Li, D., Bao, C., Chen, Y., Xue, H., 2019. Detrital zircon record of rivers' sediments in the North Qilian Orogenic Belt: implications of the tectonic evolution of the northeastern Tibetan Plateau. Geol. J. 54 (4), 2208–2228.
Kang, H., Chen, Y.L., Li, D.P., Bao, C., Zhang, H.Z., 2018. Zircon U-Pb ages and Hf isotopic compositions of fluvial sediments from the Huangshui, Beichuan, and Xichuan rivers, Northwest China: constraints on the formation and evolution history of the Central Qilian Block. Geochem. J. 52 (1), 37–57.
Kapp, P., DeCelles, P.G., 2019. Mesozoic–Cenozoic geological evolution of the Himalayan-Tibetan orogen and working tectonic hypotheses. Am. J. Sci. 319 (3), 159–254.
Kapp, P., DeCelles, P.G., Gehrels, G.E., Heizler, M., Ding, L., 2007. Geological records of the lhasa-qiangtang and indo-asian collisions in the nima area of central Tibet. Geol. Soc. Am. Bull. 119 (7–8), 917–933.
Kapp, P., Pelletier, J.D., Rohrmann, A., Heermance, R., Russell, J., Ding, L., 2011. Wind erosion in the Qaidam basin, central Asia: implications for tectonics, paleoclimate, and the source of the Loess Plateau. GSA Today (Geol. Soc. Am.) 21 (4/5), 4–10.
Kong, X., Yin, A., Harrison, T.M., 1997. Evaluating the role of preexisting weaknesses and topographic distributions in the Indo-Asian collision by use of a thin-shell numerical model. Geology 25 (6), 527–530.
Košler, J., Fonneland, H., Sylvester, P., Tubrett, M., Pedersen, R.B., 2002. U–Pb dating of detrital zircons for sediment provenance studies—a comparison of laser ablation ICPMS and SIMS techniques. Chem. Geol. 182 (2–4), 605–618.
Lancaster, P.J., Storey, C.D., Hawkesworth, C.J., Dhuime, B., 2011. Understanding the roles of crustal growth and preservation in the detrital zircon record. Earth Planet Sci. Lett. 305 (3–4), 405–412.
Lawrence, R.L., Cox, R., Mapes, R.W., Coleman, D.S., 2011. Hydrodynamic fractionation of zircon age populations. Bulletin 123 (1–2), 295–305.
Leary, R.J., Smith, M.E., Umhoefer, P., 2020. Grain-size control on detrital zircon cycloprovenance in the late Paleozoic Paradox and Eagle basins, USA. J. Geophys. Res. Solid Earth 125 (7), e2019JB019226.
Lease, R.O., Burbank, D.W., Gehrels, G.E., Wang, Z., Yuan, D., 2007. Signatures of mountain building: detrital zircon U/Pb ages from northeastern Tibet. Geology 35 (3), 239–242.
Lee, C.-T.A., Bachmann, O., 2014. How important is the role of crystal fractionation in making intermediate magmas? Insights from Zr and P systematics. Earth Planet Sci. Lett. 393, 266–274.
Lee, C.T.A., Yeung, L.Y., McKenzie, N.R., Yokoyama, Y., Ozaki, K., Lenardic, A., 2016. Two-step rise of atmospheric oxygen linked to the growth of continents. Nat. Geosci. 9 (6), 417–424.
Leier, A.L., Kapp, P., Gehrels, G.E., DeCelles, P.G., 2007. Detrital zircon geochronology of carboniferous–cretaceous strata in the lhasa terrane, southern Tibet. Basin Res. 19 (3), 361–378.
Li, B., Zuza, A.V., Chen, X., Hu, D., Shao, Z., Qi, B., Wang, Z., Levy, D.A., Xiong, X., 2020. Cenozoic multi-phase deformation in the Qilian Shan and out-of-sequence development of the northern Tibetan Plateau. Tectonophysics 782, 228423.
Li, B., Zuza, A.V., Chen, X., Wang, Z.Z., Shao, Z., Levy, D.A., Wu, C., Xu, S., Sun, Y., 2021a. Pre-Cenozoic evolution of the northern Qilian Orogen from zircon geochronology: framework for early growth of the northern Tibetan Plateau. Palaeogeogr. Palaeoclimatol. Palaeoecol. 562, 110091.
Li, C., Zheng, D., Zhou, R., Wang, W., Yu, J., Liu, C., Wang, Y., Pang, J., Ma, Y., Hao, Y., Li, Y., Wang, X., 2021b. Topographic growth of the northeastern Tibetan Plateau

during the middle–late Miocene: insights from integrated provenance analysis in the NE Qaidam Basin. Basin Res. 33 (6), 3212–3230.
Li, J., Zhang, Z., Tang, W., Li, K., Luo, Z., Li, J., 2014. Provenance of Oligocene–Miocene sediments in the Subei area, eastern Altyn Tagh fault and its geological implications: evidence from detrital zircons LA-ICP-MS U–Pb chronology. J. Asian Earth Sci. 87, 130–140.
Li, L., Meng, Q., Pullen, A., Garzione, C.N., Wu, G., Wang, Y., Ma, S., Duan, L., 2014. Late permian–early middle triassic back-arc basin development in West Qinling, China. J. Asian Earth Sci. 87, 116–129.
Li, W., Neubauer, F., Liu, Y., Genser, J., Ren, S., Han, G., Liang, C., 2013. Paleozoic evolution of the Qimantagh magmatic arcs, Eastern Kunlun Mountains: constraints from zircon dating of granitoids and modern river sands. J. Asian Earth Sci. 77, 183–202.
Liang, Y., Zhang, B., Zhang, Y., Zhang, Y., Wang, J., Liu, Z., 2021. Evolution of the Miocene megalake in the western Qaidam basin, northwestern China. Palaeogeogr. Palaeoclimatol. Palaeoecol. 571, 110384.
Liu, Y., Neubauer, F., Li, W., Genser, J., Li, W., 2012. Tectono-thermal events of the northern Qaidam margin-southern Qilian area, western China (in Chinese with English abstract). J. Jilin Univ. (Earth Sci. Ed.) 42, 1317–1329.
Lu, H., Xiong, S., 2009. Magnetostratigraphy of the Dahonggou section, northern Qaidam basin and its bearing on cenozoic tectonic evolution of the qilian Shan and Altyn Tagh Fault. Earth Planet Sci. Lett. 288, 539–550.
Lu, H., Ye, J., Guo, L., Pan, J., Xiong, S., Li, H., 2018. Towards a clarification of the provenance of Cenozoic sediments in the northern Qaidam Basin. Lithosphere 11 (2), 252–272.
Lu, H., Sang, S., Wang, P., Zhang, Z., Pan, J., Li, H., 2022. Initial uplift of the Qilian Shan, northern Tibet since ca. 25 Ma: implications for regional tectonics and origin of eolian deposition in Asia. GSA Bulletin 134 (9–10), 2531–2547.
Makuluni, P., Kirkland, C.L., Barham, M., 2019. Zircon grain shape holds provenance information: a case study from southwestern Australia. Geol. J. 54 (3), 1279–1293.
Malusà, M.G., Resentini, A., Garzanti, E., 2016. Hydraulic sorting and mineral fertility bias in detrital geochronology. Gondwana Res. 31, 1–19.
Malusà, M.G., Carter, A., Limoncelli, M., Villa, I.M., Garzanti, E., 2013. Bias in detrital zircon geochronology and thermochronometry. Chem. Geol. 359, 90–107.
McKay, M.P., Jackson Jr., W.T., Hessler, A.M., 2018. Tectonic stress regime recorded by zircon Th/U. Gondwana Res. 57, 1–9.
McKenzie, N.R., Horton, B.K., Loomis, S.E., Stockli, D.F., Planavsky, N.J., Lee, C.T.A., 2016. Continental arc volcanism as the principal driver of icehouse-greenhouse variability. Science 352 (6284), 444–447.
McRivette, M.W., Yin, A., Chen, X., Gehrels, G.E., 2019. Cenozoic basin evolution of the central Tibetan plateau as constrained by U-Pb detrital zircon geochronology, sandstone petrology, and fission-track thermochronology. Tectonophysics 751, 150–179.
Meinhold, G., Morton, A.C., Fanning, C.M., Frei, D., Howard, J.P., Phillips, R.J., Strogen, D., Whitham, A.G., 2011. Evidence from detrital zircons for recycling of Mesoproterozoic and Neoproterozoic crust recorded in Paleozoic and Mesozoic sandstones of southern Libya. Earth Planet Sci. Lett. 312 (1–2), 164–175.
Miao, Y., Wu, F., Warny, S., Fang, X., Lu, H., Fu, B., Song, C., Yan, X., Escarguel, G., Yang, Y., Meng, Q., Shi, P., 2019. Miocene fire intensification linked to continuous aridification on the Tibetan Plateau. Geology 47 (4), 303–307.
Moecher, D.P., Samson, S.D., 2006. Differential zircon fertility of source terranes and natural bias in the detrital zircon record: implications for sedimentary provenance analysis. Earth Planet Sci. Lett. 247 (3–4), 252–266.
Molnar, P., England, P., Joseph, M., 1993. Mantle dynamics, uplift of the Tibetan plateau and the Indian monsoon. Rev. Geophys. 31, 357–396.
Morton, A.C., Hallsworth, C.R., 1999. Processes controlling the composition of heavy mineral assemblages in sandstones. Sediment. Geol. 124 (1–4), 3–29.
Muhlbauer, J.G., Fedo, C.M., Farmer, G.L., 2017. Influence of textural parameters on detrital-zircon age spectra with application to provenance and paleogeography during the Ediacaran–Terreneuvian of southwestern Laurentia. GSA Bulletin 129 (11–12), 1585–1601.
Nie, J., Horton, B.K., Saylor, J.E., Mora, A., Mange, M., Garzione, C.N., Basu, A., Moreno, C.J., Caballero, V., Parra, M., 2012. Integrated provenance analysis of a convergent retroarc foreland system: U–Pb ages, heavy minerals, Nd isotopes, and sandstone compositions of the Middle Magdalena Valley basin, northern Andes, Colombia. Earth Sci. Rev. 110 (1–4), 111–126.
Nie, J., Pullen, A., Garzione, C.N., Peng, W., Wang, Z., 2018. Pre-Quaternary decoupling between Asian aridification and high dust accumulation rates. Sci. Adv. 4 (2), eaao6977.
Nie, J., Ren, X., Saylor, J.E., Su, Q., Horton, B.K., Bush, M.A., Chen, W., Pfaff, K., 2020. Magnetic polarity stratigraphy, provenance, and paleoclimate analysis of Cenozoic strata in the Qaidam Basin, NE Tibetan Plateau. Bulletin 132 (1–2), 310–320.
Nie, J., Stevens, T., Rittner, M., Stockli, D., Garzanti, E., Limonta, M., Bird, A., Ando, S., Vermeesch, P., Saylor, J., Lu, H., Breecker, D., Hu, X., Liu, S., Resentini, A., Vezzoli, G., Peng, W., Carter, A., Ji, S., Pan, B., 2015. Loess plateau storage of northeastern Tibetan plateau-derived Yellow River sediment. Nat. Commun. 6 (1), 1–10.
O'Sullivan, G.J., Chew, D.M., Samson, S.D., 2016. Detecting magma-poor orogens in the detrital record. Geology 44 (10), 871–874.
Orme, D.A., Carrapa, B., Kapp, P., 2015. Sedimentology, provenance and geochronology of the upper Cretaceous–lower Eocene western Xigaze forearc basin, southern Tibet. Basin Res. 27 (4), 387–411.
Owen, L.A., Finkel, R.C., Haizhou, M., Barnard, P.L., 2006. Late Quaternary landscape evolution in the Kunlun Mountains and Qaidam Basin, Northern Tibet: a framework for examining the links between glaciation, lake level changes and alluvial fan formation. Quat. Int. 154, 73–86.
Perri, F., Rizzo, G., Mongelli, G., Critelli, S., Perrone, V., 2008. Zircon compositions of lower Mesozoic redbeds of the Tethyan margins, West-Central mediterranean area. Int. Geol. Rev. 50 (11), 1022–1039.
Pullen, A., Kapp, P., Gehrels, G.E., Vervoort, J.D., Ding, L., 2008. Triassic continental subduction in central Tibet and mediterranean-style closure of the paleo-tethys ocean. Geology 36 (5), 351–354.
Pullen, A., Kapp, P., McCallister, A.T., Chang, H., Gehrels, G.E., Garzione, C.N., Heermance, R.V., Ding, L., 2011. Qaidam Basin and northern Tibetan Plateau as dust sources for the Chinese Loess Plateau and paleoclimatic implications. Geology 39 (11), 1031–1034.
Qian, T., Wang, Z., Wang, Y., Liu, S., Gao, W., Li, W., 2021. Jurassic evolution of the Qaidam Basin in western China: constrained by stratigraphic succession, detrital zircon U-Pb geochronology and Hf isotope analysis. Bulletin 133 (11–12), 2291–2318.
Reiners, P.W., Campbell, I.H., Nicolescu, S., Allen, C.M., Hourigan, J.K., Garver, J.I., Mattinson, J.M., Cowan, D.S., 2005. U-Th)/(He-Pb) double dating of detrital zircons. Am. J. Sci. 305 (4), 259–311.
Resentini, A., AndÒ, S., Garzanti, E., 2018. Quantifying roundness of detrital minerals by image analysis: sediment transport, shape effects, and provenance implications. J. Sediment. Res. 88 (2), 276–289.
Royden, L.H., Burchfiel, B.C., King, R.W., Wang, E., Chen, Z., Shen, F., Liu, Y., 1997. Surface deformation and lower crustal flow in eastern Tibet. Science 276 (5313), 788–790.
Saylor, J.E., Stockli, D.F., Horton, B.K., Nie, J., Mora, A., 2012. Discriminating rapid exhumation from syndepositional volcanism using detrital zircon double dating: implications for the tectonic history of the Eastern Cordillera, Colombia. Bulletin 124 (5–6), 762–779.
Schwartz, T.M., Schwartz, R.K., Weislogel, A.L., 2019. Orogenic recycling of detrital zircons characterizes age distributions of North American Cordilleran strata. Tectonics 38 (12), 4320–4334.
Sharman, G.R., Graham, S.A., Grove, M., Kimbrough, D.L., Wright, J.E., 2015. Detrital zircon provenance of the Late Cretaceous–Eocene California forearc: influence of Laramide low-angle subduction on sediment dispersal and paleogeography. GSA Bulletin 127 (1–2), 38–60.
Shen, X., Jian, X., Li, C., Liu, J.T., Chang, Y.P., Zhang, S., Mei, H., Fu, H., Zhang, W., 2021. Submarine topography-related spatial variability of the southern Taiwan Strait sands (East Asia). Mar. Geol. 436, 106495.
Sircombe, K.N., Stern, R.A., 2002. An investigation of artificial biasing in detrital zircon U-Pb geochronology due to magnetic separation in sample preparation. Geochem. Cosmochim. Acta 66 (13), 2379–2397.
Sláma, J., Košler, J., 2012. Effects of sampling and mineral separation on accuracy of detrital zircon studies. G-cubed 13 (5).
Song, B., Zhang, K., Hou, Y., Ji, J., Wang, J., Yang, Y., Yang, T., Wang, C., Shen, T., 2019. New insights into the provenance of Cenozoic strata in the Qaidam Basin, northern Tibet: constraints from combined U-Pb dating of detrital zircons in recent and ancient fluvial sediments. Palaeogeogr. Palaeoclimatol. Palaeoecol. 533, 109254.
Song, S., Huang, L., Zhang, Q., Li, X., Liu, C., 2022a. New insights for origin of fine-grained sediments from the early Neogene Qaidam Basin: wind and fluvial–lacustrine source-to-sink processes. Mar. Petrol. Geol., 105853
Song, S., Huang, L., Zhang, Y., Zhang, Q., Zhou, F., Liu, C., Chen, Y., Wu, Y., Zhang, Y., 2022b. Middle Miocene climate transition in the Tibetan Plateau: identification and significance. Geol. Mag. 159 (1), 153–172.
Song, S., Su, L., Li, X.H., Niu, Y., Zhang, L., 2012. Grenville-age orogenesis in the qaidam-qilian block: the link between south China and Tarim. Precambrian Res. 220, 9–22.
Soreghan, M.J., Soreghan, G.S., Hamilton, M.A., 2002. Paleowinds inferred from detrital-zircon geochronology of upper Paleozoic loessite, western equatorial Pangea. Geology 30 (8), 695–698.
Spencer, C.J., Kirkland, C.L., Roberts, N.M., 2018. Implications of erosion and bedrock composition on zircon fertility: examples from South America and Western Australia. Terra. Nova 30 (4), 289–295.
Stalder, N.F., Fellin, M.G., Caracciolo, L., Guillong, M., Winkler, W., Milli, S., Moscatelli, M., Critelli, S., 2018. Dispersal pathways in the early messinian adriatic foreland and provenance of the laga formation (central apennines, Italy). Sediment. Geol. 375, 289–308.
Sun, X., Wang, P., 2005. How old is the Asian monsoon system?—palaeobotanical records from China. Palaeogeogr. Palaeoclimatol. Palaeoecol. 222, 181–222.
Sun, Y., Liu, J., Liang, Y., Ji, J., Liu, W., Aitchison, J.C., Sun, J., Lu, J., Song, B., Xu, Y., Zhang, K., Liu, Z., 2020. Cenozoic moisture fluctuations on the northeastern Tibetan Plateau and association with global climatic conditions. J. Asian Earth Sci. 200, 104490.
Sun, Z., Yang, Z., Pei, J., Ge, X., Wang, X., Yang, T., Li, W., Yuan, S., 2005. Magnetostratigraphy of Paleogene sediments from northern Qaidam Basin, China: implications for tectonic uplift and block rotation in northern Tibetan plateau. Earth Planet Sci. Lett. 237, 635–646.
Sylvester, P.J., Souders, A.K., Liu, R., 2022. Significance of U-Pb detrital zircon geochronology for mudstone provenance. Geology 50 (6), 670–675.
Tang, M., Ji, W.Q., Chu, X., Wu, A., Chen, C., 2021. Reconstructing crustal thickness evolution from europium anomalies in detrital zircons. Geology 49 (1), 76–80.
Tapponnier, P., Xu, Z., Roger, F., Meyer, B., Arnaud, N., Wittlinger, G., Yang, J., 2001. Oblique stepwise rise and growth of the Tibet Plateau. Science 294, 1671–1677.
Thomas, W.A., 2011. Detrital-zircon geochronology and sedimentary provenance. Lithosphere 3 (4), 304–308.
Thomson, K.D., Stockli, D.F., Clark, J.D., Puigdefàbregas, C., Fildani, A., 2017. Detrital zircon (U-Th)/(He-Pb) double-dating constraints on provenance and foreland basin evolution of the Ainsa Basin, south-central Pyrenees, Spain. Tectonics 36 (7), 1352–1375.

Tyrrell, S., Haughton, P.D., Daly, J.S., 2007. Drainage reorganization during breakup of Pangea revealed by in-situ Pb isotopic analysis of detrital K-feldspar. Geology 35 (11), 971–974.
Valley, J.W., 2003. Oxygen isotopes in zircon. Rev. Mineral. Geochem. 53 (1), 343–385.
Veevers, J.J., Saeed, A., Belousova, E.A., Griffin, W.L., 2005. U–Pb ages and source composition by Hf-isotope and trace-element analysis of detrital zircons in Permian sandstone and modern sand from southwestern Australia and a review of the paleogeographical and denudational history of the Yilgarn Craton. Earth Sci. Rev. 68 (3–4), 245–279.
Vermeesch, P., 2012. On the visualization of detrital age distributions. Chem. Geol. 312–313, 190–194.
Wang, C., Dai, J., Zhao, X., Li, Y., Graham, S.A., He, D., Ran, B., Meng, J., 2014. Outward-growth of the Tibetan plateau during the cenozoic: a review. Tectonophysics 621, 1–43.
Wang, C., Zhao, X., Liu, Z., Lippert, P.C., Graham, S.A., Coe, R.S., Yi, H., Zhu, L., Liu, S., Li, Y., 2008a. Constraints on the early uplift history of the Tibetan Plateau. Proc. Natl. Acad. Sci. USA 105, 4987–4992.
Wang, J., Wang, Y.J., Liu, Z.C., Li, J.Q., Xi, P., 1999. Cenozoic environmental evolution of the Qaidam Basin and its implications for the uplift of the Tibetan Plateau and the drying of central Asia. Palaeogeogr. Palaeoclimatol. Palaeoecol. 152, 37–47.
Wang, L., Jian, X., Fu, H., Zhang, W., Shang, F., Fu, L., 2023. Decoupled local climate and chemical weathering intensity of fine-grained siliciclastic sediments from a paleo-megalake: an example from the Qaidam basin, northern Tibetan Plateau. Sediment. Geol. 454, 106462.
Wang, L., MacLennan, S.A., Cheng, F., 2020. From a proximal-deposition-dominated basin sink to a significant sediment source to the Chinese Loess Plateau: insight from the quantitative provenance analysis on the Cenozoic sediments in the Qaidam basin, northern Tibetan Plateau. Palaeogeogr. Palaeoclimatol. Palaeoecol. 556, 109883.
Wang, Q., Chen, N., Li, X., Hao, S., Chen, H., 2008b. LA-ICPMS zircon U-Pb geochronological constraints on the tectonothermal evolution of the early paleoproterozoic dakendaban group in the Quanji block, NW China. Chin. Sci. Bull. 53, 2849–2858.
Wang, W., Zhang, P., Garzione, C.N., Liu, C., Zhang, Z., Pang, J., Wang, Y., Zheng, D., Zheng, W., Zhang, H., 2022. Pulsed rise and growth of the Tibetan Plateau to its northern margin since ca. 30 Ma. Proc. Natl. Acad. Sci. USA 119 (8), e2120364119.
Wang, W., Zhang, P., Yu, J., Wang, Y., Zheng, D., Zheng, W., Zhang, H., Pang, J., 2016. Constraints on mountain building in the northeastern Tibet: detrital zircon records from synorogenic deposits in the Yumen Basin. Sci. Rep. 6 (1), 1–8.
Wang, W., Zheng, W., Zhang, P., Li, Q., Kirby, E., Yuan, D., Zheng, D., Liu, C., Wang, Z., Zhang, H., Pang, J., 2017. Expansion of the Tibetan plateau during the Neogene. Nat. Commun. 8 (1), 1–12.
Watson, E.B., Harrison, T.M., 1983. Zircon saturation revisited: temperature and composition effects in a variety of crustal magma types. Earth Planet Sci. Lett. 64, 295–304.
Weislogel, A.L., Graham, S.A., Chang, E.Z., Wooden, J.L., Gehrels, G.E., 2010. Detrital zircon provenance from three turbidite depocenters of the Middle–Upper Triassic Songpan-Ganzi complex, central China: record of collisional tectonics, erosional exhumation, and sediment production. Bulletin 122 (11–12), 2041–2062.
Weislogel, A.L., Graham, S.A., Chang, E.Z., Wooden, J.L., Gehrels, G.E., Yang, H., 2006. Detrital zircon provenance of the late triassic songpan-ganzi complex: sedimentary record of collision of the North and South China blocks. Geology 34 (2), 97–100.
Wu, C., Yin, A., Zuza, A.V., Zhang, J., Liu, W., Ding, L., 2016. Pre-Cenozoic geologic history of the central and northern Tibetan Plateau and the role of Wilson cycles in constructing the Tethyan orogenic system. Lithosphere 8 (3), 254–292.
Wu, C., Zuza, A.V., Chen, X., Ding, L., Levy, D.A., Liu, C., Liu, W., Jiang, T., Stockli, D.F., 2019a. Tectonics of the eastern Kunlun range: cenozoic reactivation of a paleozoic-early mesozoic orogen. Tectonics 38 (5), 1609–1650.
Wu, C., Zuza, A.V., Li, J., Haproff, P.J., Yin, A., Chen, X., Ding, L., Li, B., 2021a. Late Mesozoic−Cenozoic cooling history of the northeastern Tibetan Plateau and its foreland derived from low-temperature thermochronology. GSA Bulletin 133 (11–12), 2393–2417.
Wu, C., Zuza, A.V., Zhou, Z., Yin, A., McRivette, M.W., Chen, X., Ding, L., Geng, J., 2019b. Mesozoic-Cenozoic evolution of the Eastern Kunlun Range, central Tibet, and implications for basin evolution during the Indo-Asian collision. Lithosphere 11, 524–550.
Wu, M., Zhuang, G., Hou, M., Liu, Z., 2021b. Expanded lacustrine sedimentation in the Qaidam Basin on the northern Tibetan Plateau: manifestation of climatic wetting during the Oligocene icehouse. Earth Planet Sci. Lett. 565, 116935.
Xia, G., Wu, C., Li, G., Li, G., Yi, H., Wagreich, M., 2021. Cenozoic growth of the eastern Kunlun range (northern Tibetan plateau): evidence from sedimentary records in the southwest Qaidam basin. Int. Geol. Rev. 63 (6), 769–786.
Xu, J., Stockli, D.F., Snedden, J.W., 2017. Enhanced provenance interpretation using combined U–Pb and (U–Th)/He double dating of detrital zircon grains from lower Miocene strata, proximal Gulf of Mexico Basin, North America. Earth Planet Sci. Lett. 475, 44–57.
Xu, W.C., Zhang, H.F., Liu, X.M., 2007. U–Pb zircon dating constraints on formation time of Qilian high-grade metamorphic rock and its tectonic implications. Chin. Sci. Bull. 52, 531–538.
Yang, S., Zhang, F., Wang, Z., 2012. Grain size distribution and age population of detrital zircons from the Changjiang (Yangtze) River system, China. Chem. Geol. 296, 26–38.
Yin, A., Dang, Y.Q., Zhang, M., Chen, X.H., McRivette, M.W., 2008b. Cenozoic tectonic evolution of the Qaidam basin and its surrounding regions (Part 3): structural geology, sedimentation, and regional tectonic reconstruction. Geol. Soc. Am. Bull. 120 (7–8), 847–876.
Yin, A., Harrison, T.M., 2000. Geologic evolution of the Himalayan-Tibetan orogen. Annu. Rev. Earth Planet Sci. 28, 211–280.
Yu, L., Xiao, A., Wu, L., Tian, Y., Rittner, M., Lou, Q., Pan, X., 2017. Provenance evolution of the Jurassic northern Qaidam Basin (West China) and its geological implications: evidence from detrital zircon geochronology. Int. J. Earth Sci. 106 (8), 2713–2726.
Yu, S., Zhang, J., del Real, P.G., Zhao, X., Hou, K., Gong, J., Li, Y., 2013. The Grenvillian orogeny in the Altun–Qilian–North Qaidam mountain belts of northern Tibet Plateau: constraints from geochemical and zircon U–Pb age and Hf isotopic study of magmatic rocks. J. Asian Earth Sci. 73, 372–395.
Yu, X., Fu, S., Wang, Z., Li, Q., Guo, Z., 2017. The discovery of early Paleoproterozoic high-Na trondhjemite in the northeastern Qaidam basin: evidence from the drilling core samples. Precambrian Res. 298, 615–628.
Yu, X., Guo, Z., Guan, S., Du, W., Wang, Z., Bian, Q., Li, L., 2019. Landscape and tectonic evolution of Bayin River watershed, northeastern Qaidam basin, northern Tibetan Plateau: implications for the role of river morphology in source analysis and low-temperature thermochronology. J. Geophys. Res.: Earth Surf. 124 (7), 1701–1719.
Yuan, D.-Y., Ge, W.-P., Chen, Z.-W., Li, C.-Y., Wang, Z.-C., Zhang, H.-P., Zhang, P.-Z., Zheng, D.-W., Zheng, W.-J., Craddock, W.H., Dayem, K.E., Duvall, A.R., Hough, B.G., Lease, R.O., Champagnac, J.-D., Burbank, D.W., Clark, M.K., Farley, K.A., Garzione, C.N., Kirby, E., Molnar, P., Roe, G.H., 2013. The growth of northeastern Tibet and its relevance to large-scale continental geodynamics: a review of recent studies. Tectonics 32, 1358–1370.
Yue, Y., Ritts, B.D., Graham, S.A., Wooden, J.L., Gehrels, G.E., Zhang, Z., 2004. Slowing extrusion tectonics: lowered estimate of post-Early Miocene slip rate for the Altyn Tagh fault. Earth Planet Sci. Lett. 217 (1–2), 111–122.
Zeh, A., Cabral, A.R., 2021. Combining detrital zircon shape and U–Pb–Hf isotope analyses for provenance studies–An example from the Aquiri region, Amazon Craton, Brazil. Precambrian Res. 364, 106343.
Zhang, C., Wu, L., Chen, W., Zhang, Y., Xiao, A., Zhang, J., Chen, S., Chen, H., 2020. Early Cretaceous foreland-like Northeastern Qaidam Basin, Tibetan Plateau and its tectonic implications: insights from sedimentary investigations, detrital zircon U–Pb analyses and seismic profiling. Palaeogeogr. Palaeoclimatol. Palaeoecol. 557, 109912.
Zhang, J., Wang, Y., Zhang, B., Zhang, Y., 2016. Tectonics of the Xining basin in NW China and its implications for the evolution of the NE qinghai-Tibetan plateau. Basin Res. 28 (2), 159–182.
Zhang, S., Jian, X., Liu, J.T., Wang, P., Chang, Y.P., Zhang, W., 2022. Climate-driven drainage reorganization of small mountainous rivers in Taiwan (East Asia) since the last glaciation: the Zhuoshui River example. Palaeogeogr. Palaeoclimatol. Palaeoecol. 586, 110759.
Zhang, S., Jian, X., Pullen, A., Fu, L., Liang, H., Hong, D., Zhang, W., 2021. Tectono-magmatic events of the Qilian orogenic belt in northern Tibet: new insights from detrital zircon geochronology of river sands. Int. Geol. Rev. 63 (8), 917–940.
Zhang, Z., Nie, J., Fang, X., 2017. Provenance analysis reveals mountain uplift in the midsection of the Altyn Tagh Fault during the middle Miocene. Can. J. Earth Sci. 54 (3), 278–289.
Zhang, X., Song, B., Yang, T., Hou, Y., Yang, Y., Ai, K., Wang, J., Zhang, K., (in press), Source-to-sink relationships between the Qaidam Basin and its surrounding mountain ranges: new insights from detrital zircon U–Pb ages in modern river sediments. J. Earth Sci.. .
Zhao, J., Zeng, X., Tian, J., Hu, C., Wang, D., Yan, Z., Wang, K., Zhao, X., 2020. Provenance and paleogeography of the Jurassic Northwestern Qaidam Basin (NW China): evidence from sedimentary records and detrital zircon geochronology. J. Asian Earth Sci. 190, 104060.
Zhou, H., Chen, L., Diwu, C., Lei, C., 2018. Cenozoic uplift of the qimantage mountains, northeastern Tibet: contraints from provenance analysis of cenozoic sediments in Qaidam basin. Geol. J. 53 (6), 2613–2632.
Zhu, D.C., Zhao, Z.D., Niu, Y., Dilek, Y., Mo, X.X., 2011. Lhasa terrane in southern Tibet came from Australia. Geology 39 (8), 727–730.
Zhu, W., Wu, C., Wang, J., Zhou, T., Li, J., Zhang, C., Li, L., 2017. Heavy mineral compositions and zircon U-Pb ages of Cenozoic sandstones in the SW Qaidam basin, northern Tibetan Plateau: implications for provenance and tectonic setting. J. Asian Earth Sci. 146, 233–250.
Zhuang, G., Hourigan, J.K., Ritts, B.D., Kent-Corson, M.L., 2011. Cenozoic multiple-phase tectonic evolution of the northern Tibetan plateau: constraints from sedimentary records from Qaidam basin, Hexi corridor, and Subei basin, northwest China. Am. J. Sci. 311, 116–152.
Zhuang, G., Johnstone, S.A., Hourigan, J., Ritts, B., Robinson, A., Sobel, E.R., 2018. Understanding the geologic evolution of Northern Tibetan Plateau with multiple thermochronometers. Gondwana Res. 58, 195–210.
Zhuang, G., Zhang, Y.G., Hourigan, J., Ritts, B., Hren, M., Hou, M., Wu, M., Kim, B., 2019. Microbial and geochronologic constraints on the Neogene paleotopography of northern Tibetan Plateau. Geophys. Res. Lett. 46 (3), 1312–1319.
Zimmermann, U., Andersen, T., Madland, M.V., Larsen, I.S., 2015. The role of U-Pb ages of detrital zircons in sedimentology—an alarming case study for the impact of sampling for provenance interpretation. Sediment. Geol. 320, 38–50.
Zoleikhaei, Y., Mulder, J.A., Cawood, P.A., 2021. Integrated detrital rutile and zircon provenance reveals multiple sources for Cambrian sandstones in North Gondwana. Earth Sci. Rev. 213, 103462.
Zoleikhaei, Y., Mulder, J.A., Cawood, P.A., 2022. Evaluating sediment recycling through combining inherited petrogenic and acquired sedimentary features of multiple detrital minerals. Basin Res. 34 (3), 1055–1083.
Zotto, S.C., Moecher, D.P., Niemi, N.A., Thigpen, J.R., Samson, S.D., 2020. Persistence of Grenvillian dominance in Laurentian detrital zircon age systematics explained by

sedimentary recycling: evidence from detrital zircon double dating and detrital monazite textures and geochronology. Geology 48 (8), 792–797.
Zutterkirch, I.C., Kirkland, C.L., Barham, M., Elders, C., 2022. Thin-section detrital zircon geochronology mitigates bias in provenance investigations. J. Geol. Soc. 179 (2).
Zuza, A.V., Wu, C., Reith, R.C., Yin, A., Li, J., Zhang, J., Zhang, Y., Wu, L., Liu, W., 2018. Tectonic evolution of the Qilian Shan: an early Paleozoic orogen reactivated in the Cenozoic. GSA Bulletin 130 (5–6), 881–925.
Zuza, A.V., Wu, C., Wang, Z., Levy, D.A., Li, B., Xiong, X., Chen, X., 2019. Underthrusting and duplexing beneath the northern Tibetan Plateau and the evolution of the Himalayan-Tibetan orogen. Lithosphere 11 (2), 209–231.